VIENTO FORMATION: A SYNDEPOSITIONAL DELTAIC SYSTEM RECORDING ADJACENT PASSIVE SALT DIAPIR RISE, LA POPA BASIN, NORTHEAST MEXICO

by

CONSTANTIN PANTILIMON PLATON

AMY WEISLOGEL, COMMITTEE CHAIR
KATHERINE GILES
IBRAHIM CEMEN
ALBERTO PEREZ-HUERTA

A THESIS

Submitted in partial fulfillment of the requirements
for the degree of Master of Science in the
Department of Geological Sciences
in the Graduate School of
The University of Alabama

TUSCALOOSA, ALABAMA

2011

Copyright Constantin Pantilimon Platon 2011
ALL RIGHTS RESERVED

ABSTRACT

The Paleocene/Eocene Viento Formation, the youngest shallow marine unit in La Popa mini-basin, Mexico, is exposed adjacent to a surface outcropping salt diapir that is partially welded. Viento Formation offers a rare insight into the facies distribution and stacking pattern of siliciclastic strata exposed adjacent to the welded salt diapir in the margin of La Popa mini-basin, and are analogous for subsurface hydrocarbon-bearing reservoirs. The depositional facies distribution, structural geometry and stratigraphic architecture of the Viento Formation was influenced by Hidalgoan shortening across the basin, on-going passive rise of La Popa salt diapir and eustatic sea level changes.

Viento Formation strata are exposed along a ~5 km belt adjacent to La Popa salt weld, which consists of discontinuously outcropping remnant gypsum. The Viento Formation displays thinning from SE toward NW over ~900 m to pinch-out. Viento strata form a series of five stacked sequence stratigraphic wedges ranging 25-200 m thick. Beds dip vertically at the weld but dip orientations decrease to ~30° basinward. Sharp, subaqueous erosional surfaces and abundant, low-angle unconformities that becomes conformable within tens of meters distance from the diapir characterize wedge halokinetic sequence boundaries. Seventeen identified sand-prone lithofacies indicate deposition in a tide-influenced delta system and include prodelta, delta front and platform, and fluvio-deltaic facies assemblages. Overall shallowing upward depositional facies successions are comprised of shale, or rarely limestone buildup, oyster facies, horizontal heterolithic stratification, inclined heterolithic bedding, bioturbated sandstone with *Ophiomorpha* and oyster-shells, mud-draped ripple-laminated sandstone, spheroidal weathering sandstone, trough-cross bedded sandstone, herringbone sandstone, sandstone with wood fragments and mud ripped-up clasts, and conglomerate and conglomeratic sandstone.

Conglomerate and conglomeratic sandstone contain abundant well-rounded and well-sorted black chert and diapir-derived detritus – Jurassic metaigneous boulders that decrease in abundance, size, and angularity in a basinward direction.

Cyclical tectonic compressional events coeval with continuous sediment loading controlled La Popa salt diapir rise and drove episodic diapir extrusion. Viento stratal composition, distribution, and distinct geometry of halokinetic drape folding forms a tapered composite halokinetic sequence that reflects an overall increase in local third-order net sediment accumulation rates relative to salt rise rates.

DEDICATION

To Iancu, Mirela and my parents.

LIST OF ABBREVIATIONS AND SYMBOLS

~	Approximately
≤	Less than or equal to
≥	Greater than or equal to
<	Less than
>	Greater than
cm	Centimeters
Formation	Formation
km	kilometer
m	meter
Ma	Million years
SB	Depositional Sequence Boundary
FS	Flooding Surface
HS	Halokinetic Sequence
HST	Hightstand system tract
TST	Transgressive system tract
Kpa	Cretaceous Parras Shale
Ksj	Cretaceous San Jose carbonate lentil
Pa	Palaeogene Adjuntas Formation
Pv	Palaeogene Viento Formation
Pc	Palaeogene Carroza Formation
R_{net}	Net vertical salt rise
A_{sed}	Sediment Accumulation rate of siliciclastics

ACKNOWLEDGMENTS

I am grateful to my advisor, Dr. Amy L. Weislogel, currently with Department of Geology and Geography, University of West Virginia, Morgantown, WV, for the “boot camp” training in La Popa basin, her patience, exceptional guidance, and mentorship throughout my master studies. Her pertinent comments and objective criticism helped me become a better scientist.

Sincere thanks to my committee members for their careful and thoughtful reviews and supervision that conducted to the completion of this project: Dr. Ibrahim Cemen, Dr. Alberto Perez-Huerta, Dr. Delores Robinson, Dr. Ernest Mancini, Emeritus Professor of UA, currently with the Department of Geology and Geophysics, Texas A&M, College Station, TX, and Dr. Katherine Giles from Institute of Tectonic Studies, New Mexico State University, Las Cruces, NM. Thanks to Dr. Ibrahim Cemen, Chair of the Department of Geological Sciences and Dr. Andrew Goodliffe, Director of Graduate Program Director, for closely watching me progress.

Thanks to Dr. Tim Lawton from Institute of Tectonic Studies, New Mexico State University, Las Cruces, NM, and Dr. Mark Rowan, Rowan Structural Consulting, Boulder, CO, for helpful discussions in and out of the field and constant supervision. Thanks to Nila Mastler from Institute of Tectonic Studies, New Mexico State University, Las Cruces, NM, for logistical support preparing fieldwork trips in La Popa, Mexico and my participation at the Institute of Tectonic Studies Annual Industry Consortium.

I acknowledge Bryan Hunt from the Department of Geological Sciences at The University of Alabama, and Giovanni Romero, Breanna Hennessy, and Joe Andrie from the Institute of Tectonic Studies at New Mexico State University, for their valuable time and

assistance with my fieldwork in Mexico. Thanks to Jenny Rothfuss, Bryan Hunt, and Joe Andrie for their friendship and for proofreading parts of this manuscript.

I express my gratitude toward all the colleagues, faculty, and staff of the Department of Geological Sciences at The University of Alabama that overlapped their presence here with mine: thanks to each one of you for creating such a warm and supportive climate benefic for both personal grow and scientific progress! Because of you, I enjoyed my time here very much!

Thanks to Dr. Ibrahim Cemen, Debbie Frank, Betty Fagen, Darlene Capps, Diane Norris, and Jim Donahoe for being kind and anytime ready to assist me, from printing posters to registering for classes. Thanks to Denise Cox, Geological Sciences Advisory Board and Storm Energy, for her contagious enthusiasm and mentorship during my job search.

I thank Dr. Andrew Goodliffe and Dr. Harold Stowell for believing in me from the very beginning when I approached the Department of Geological Sciences and for offering me the chance to join its master program. Thanks to Dr. Paul Aahron for encouragements inside and outside the classroom and for showing interest in my research progress through the years.

Thanks to my graduate student colleagues who facilitated my integration with the American Geoscience Culture: Jennifer Rothfuss, Tommy Lovell, Grayson Ridgway, Ryan Alexander, Robert Holler, Matt Gatewood, Lance Wilson, Jeffrey Fuchs, Hunter Phillips, Erika Rentschler, Jason Harvell, Brittany Hollon, Matt McKay, David Aldridge, Jessa Moser, Emeka Nwafor, Karen Parker, Rachael Rutter, David Slavic, Marco Bianchi, Milo Cameron, Tom Creech, Rajesh Dhungana, Jaydeep Ghosh, Whitney Harris, Subodha Khanal, Joe Lambert, Subhadip Mandal, and Miguel Etayo.

I deeply thank my friend and spouse Mirela Maxim for unrelenting love and encouragements and for taking care of our son Iancu Platon while I was repeatedly gone, often for weeks long, during geologic fieldtrips or participating in scientific conferences. I thank a few very close family friends that helped and encouraged me and my family during this endeavor: Claudiu and Anca Lungu, Gary and Patricia Falls, and Roberto and Celina Caslaru. I also thank my parents and parents in laws that pray to God for ours wellbeing.

Thanks to the supporters behind the following organizations that contributed financially to the completion of this field based project (four trips to Mexico totalizing seven weeks in the field):

- 2010 Geological Sciences Advisory Board Summer Scholar Award ($3,000);
- 2009 American Association of Petroleum Geologists Grants-In-Aid Frederick A. Sutton Memorial Grant ($3,000);
- 2009 Gulf Coast Association of Geological Societies Research Grant ($1,500);
- 2008 – 2011 University of Alabama Graduate School Travel and Research Fund and the Department of Geological Sciences Johnson Travel and Research Grant (over $2,000);
- 2008 – 2010 Institute of Tectonic Studies of New Mexico State University (over $15,000)

CONTENTS

ABSTRACT ……...……ii

DEDICATION ……...iv

LIST OF ABBREVIATIONS AND SYMBOLS ……..…….…….……..v

ACKNOWLEDGMENTS ..…….……...….……..vi

LIST OF FIGURES ……...……xi

CHAPTER 1 – INTRODUCTION

1.1. Goal and motivation …….……1

1.2. Salt tectonics and halokinetic sequence stratigraphy background ……...…8

CHAPTER 2 – GEOLOGIC HYSTORY OF LA POPA BASIN

2.1. Structural evolution ……14

2.2. Stratigraphy ……17

CHAPTER 3 – METHODOLOGY

3.1. Tools and approach ……28

3.2. Study area …….……..29

CHAPTER 4 – LITHOLOGIC FACIES DESCRIPTION AND INTERPRETATION

4.1. Conglomerate and conglomeratic sandstone facies ……...……32

4.1.1. Sandstone with metaigneous clasts facies ……..…….32

4.1.2. Conglomerate with chert pebbles facies …….37

4.1.3. Oyster bearing sandstone facies ……..……43

4.1.4. Sandstone with lag facies …….…….……..47

4.1.5. Sandstone with mud chips and mud intraclast facies ……..……51

4.1.6. Sandstone with wood fragments facies ……..……54

4.1.7. Limestone clast-bearing conglomeratic sandstone facies ……...……58

4.2. Sandstone facies ……...…..62

4.2.1. Trough cross-bedded sandstone facies ……62

4.2.2. Ripple laminated sandstone facies ……..65

4.2.3. Inclined heterolithic stratification facies …….……69

4.2.4. Spheroidal weathering sandstone facies ……...……..72

4.2.5. Bioturbated sandstone facies ……...……75

4.2.6. Oyster facies ……..……..81

4.2.7. Horizontal heterolithic stratification facies …….……84

4.2.8. Tan fissile shale facies ……...…….89

4.2.9. Purple mudstone with paleosols facies …….……92

4.3. Limestone facies ……..……...……95

4.3.1. Massive limestone facies ……95

CHAPTER 5 – VIENTO FORMATION STRUCTURE AND COMPOSITE HALOKINETIC SEQUENCE STRATIGRAPHY CLASSIFICATION

5.1. Framework ……..…….……..99

5.2. Subdivisions within the study area …….…….100

5.3. Viento Formation stratigraphic contacts ……..……103

5.4. Datum ……..……106

5.5. The southeastern diapir-distal area ……..106

5.5.1. Position of La Popa salt weld in the southeastern diapir-distal area …….……111

5.6. The northwestern diapir-proximal area ……...…….117

5.7. Metaigneous-bearing conglomeratic sandstone beds prevalence and distribution ..125

5.8. Comparison of the SE diapir-distal and the NW diapir-proximal areas ……..….127

5.9. Parasequence development ……..127

5.10. T-R cycles and Sequence Boundaries ……..……..128

5.11. Composite halokinetic sequence stratigraphy ……...…….128

5.12. Processes of halokinetic sequence development ……...…….129

5.12.1. Hidalgoan shortening vs. local downbuilding ……130

5.12.2. Contrast between Giles et al. wedge halokinetic sequence model vs. Viento Formation model …….131

CHAPTER 6 – DISCUSSIONS

6.1. La Popa minibasin paleogeography and the Viento Formation deposition system .134

6.2. Active diapirism during the Viento Formation deposition time ……..……136

6.3. Distinguishing delta from estuary deposits ……..……137

6.4. Comparison between wedge-forming units outcropping in La Popa basin ….……139

6.5. Comparison of the Viento Formation with the Muerto Formation ……..139

6.6. Comparison of the Viento Formation with the Delgado Sandstone Member ……..141

6.7. Comparison between the Viento Formation and the Upper Sandstone Member ….141

6.8. Lateral compression influence on generating wedge-geometries halokinesis …….143

CHAPTER 7 – CONCLUSIONS ……...144

REFERENCES …….....145

APPENDIX 1 – Fence diagram of measured sections and correlations interpretation of the Viento Formation halokinetic sequence stratigraphy

LIST OF FIGURES

Figure 1. Geologic map and location of La Popa basin .....……..……...3

Figure 2. Geologic cross-section within the bend of La Popa salt weld and geologic cross-section across La Popa basin showing other outcropping salt structures ..…….5

Figure 3. Controls on and attributes of hook versus wedge and Tabular – CHS versus Tapered – CHS ……..……...12

Figure 4. Stratigraphic column of deposits cropping in La Popa basin along the weld ...18

Figure 5. Field photomosaic showing the topography and the main elements within the northwestern sector of the study area ……22

Figure 6. View from the contact zone of Carroza and Viento formations, toward La Popa weld …….……..……23

Figure 7. Sitting at the weld, view toward Carroza syncline ……....25

Figure 8. Google based aerial image showing the location of the measured sections within the Viento Formation …….……...29

Figure 9. Field photographs of the sandstone with metaigneous clasts facies ...……..….34

Figure 10. Field photographs of conglomerate with chert pebble facies ……..……..…..38

Figure 11. Field photographs of oyster-bearing sandstone facies …….……44

Figure 12. Field photographs of sandstone with lag facies ……..…….47

Figure 13. Field photographs of sandstone with mud chips and mud intraclasts facies.…….……51

Figure 14. Field photographs of the sandstone with wood fragment facies ……..…54

Figure 15. Field photographs of the limestone clast-bearing conglomeratic sandstone facies …….……59

Figure 16. Field photographs of the trough cross-bedded sandstone facies ……..…..….62

Figure 17. Field photographs of the ripple laminated sandstone facies …….…...……65

Figure 18. Field photographs of the inclined heterolithic stratification facies in cross-sectional view ……69

Figure 19. Field photographs of the spheroidal weathering sandstone facies ….....…72

Figure 20. Field photographs of the bioturbated sandstone facies ……..…..76

Figure 21. Field photographs of the oyster facies ……...……..81

Figure 22. Field photographs of horizontal heterolithic stratification facies ……..…..85

Figure 23. Field photographs of the tan fissile shale facies …….…….89

Figure 24. Field photographs of the purple mudstone with paleosols facies ……..……..92

Figure 25. Field photographs of the massive limestone facies …….95

Figure 26. Field photograph of steeply dipping beds in the lowermost Viento Formation adjacent to La Popa salt wall …….…….101

Figure 27. Field photographs of the contact between Viento Formation with the overlying Carroza Formation ……..……...…..103

Figure 28. Field photographs of the La Popa weld deformed zone exposed in the southeastern diapir distal area ……....…….108

Figure 29. Field photograph of an angular unconformity with 13° of discordance located in the uppermost part of the Viento Formation (section 1W at meter 485) ……..……..109

Figure 30. Stratigraphy of the basal Viento Formation at section 1SE …….…….112

Figure 31. Field photographs illustrating the stratal relationship and lithologies present in the basal part of section 1SE …….…..114

Figure 32. Field photographs of the contact between the lowermost strata of Viento Formation and pods of remnant gypsum of La Popa salt wall in the northwestern diapir-proximal area. ……..…….…..119

Figure 33. Field photographs of Viento Formation beds crosscut by veins within ~50 m from La Popa salt wall ……..……..……121

Figure 34. Field photographs of the Viento Formation strata exposed in the northwestern diapir-proximal area ……..……..…….123

Figure 35. Drawing depicting schematically the processes that accompanied and modeled the stratigraphic architecture of the Viento Formation deposits …….130

CHAPTER 1 – INTRODUCTION

1.1. Goal and motivation

Sedimentary basins in which salt-influenced structures are well exposed and easily accessible are rare (e.g. Paradox Basin, USA, Lawton and Buck, 2006; Flinders Ranges, Australia, Rowan and Vendeville, 2006). One of the few places in the world where such feature as salt diapirs, growth faults, and salt welds are well-exposed is La Popa Basin, Nuevo Leon, northeastern Mexico (Fig. 1; Giles and Lawton, 1999; Weislogel and Lawton, 2000; Lawton et al., 2001; Giles and Lawton, 2002; Rowan et al., 2003; Aschoff and Giles, 2005; Buck et al., 2009; Lawton et al., 2009; Rowan et al., in press). Commonly, such features are identified in the subsurface during exploration for hydrocarbons using seismic reflection technology. However, seismic reflection methods applied to near-salt reservoirs generate imperfect images due to steeply dipping strata and the high velocity contrast between the salt and the adjacent sediment (Jackson et al., 1994; Rowan et al., 2003; Rowan and Vendeville, 2006). Advanced 3-D technology is available to image near-salt strata, but the cost of acquisition and processing limits its use to specific, rigorously selected targets (Jackson et al., 1994). Therefore, detailed field investigations of well-exposed and preserved salt structures provides information about the relationship between passive salt movement and sedimentation patterns and can offer an affordable predictive analog model for facies architecture of structures buried deep in the subsurface (Giles and Lawton, 1999; Weislogel and Lawton, 2000; Lawton et al., 2001; Giles and Lawton, 2002; Aschoff and Giles, 2005; Shelley and Lawton, 2005).

The Paleogene Viento Formation is a shallow marine siliciclastic unit in the upper Difunta Group exposed in the Parras and La Popa basins of northeastern Mexico (McBride et al., 1974; Lawton et al., 2001; Soegaard et al., 2003; Lawton et al., 2009). This work represents the

first detailed facies analysis of the Viento Formation exposed in La Popa Basin. The Viento Formation depositional system was investigated in a halokinetic sequence stratigraphic context in order to assess the influence of the adjacent La Popa salt wall/diapir, which is now a secondary salt weld (Giles and Lawton, 1999). A salt weld is a surface or zone that joins strata originally separated by autochthonous or allochthonous salt (Jackson and Talbot, 1991; Jackson et al., 1994), and might contain brecciated, insoluble residue or evaporite pseudomorphs as remnants of the evaporite body that once occupied the area between the two sides of the salt wall (Rowan et al, in press). Primary salt welds are typically buried in the subsurface and defined on seismic data as horizontal-subhorizontal surfaces formed by the removal of autochthonous salt, whereas a secondary salt weld is a vertical-subvertical surface developed from an evacuated vertical diapir. The site of the present La Popa weld was formerly occupied by a steep-sided evaporite wall that evolved from a squeezed vertical and elongate diapir (Fig. 2; Rowan et al., in press).

The purpose of this work is to analyze the Viento Formation sediment accumulation in relationship with the passive evolution of the adjacent La Popa salt wall. The first objective is to reconstruct the depositional environment and stratal geometries of the Viento Formation as exposed adjacent to the La Popa weld. This is accomplished by describing facies in detail, interpreting their depositional environments, and correlating halokinetic stratigraphic sequences (e.g. Giles and Rowan, in press). This framework is then used to carry out the second objective, which is to interpret interaction of the Viento Formation with La Popa salt wall that formerly occupied the site of the present-day La Popa salt weld. Therefore, the Viento Formation is used as a proxy to infer the evolution of the salt wall as triggered by downbuilding (differential sediment loading) and/or tectonic shortening.

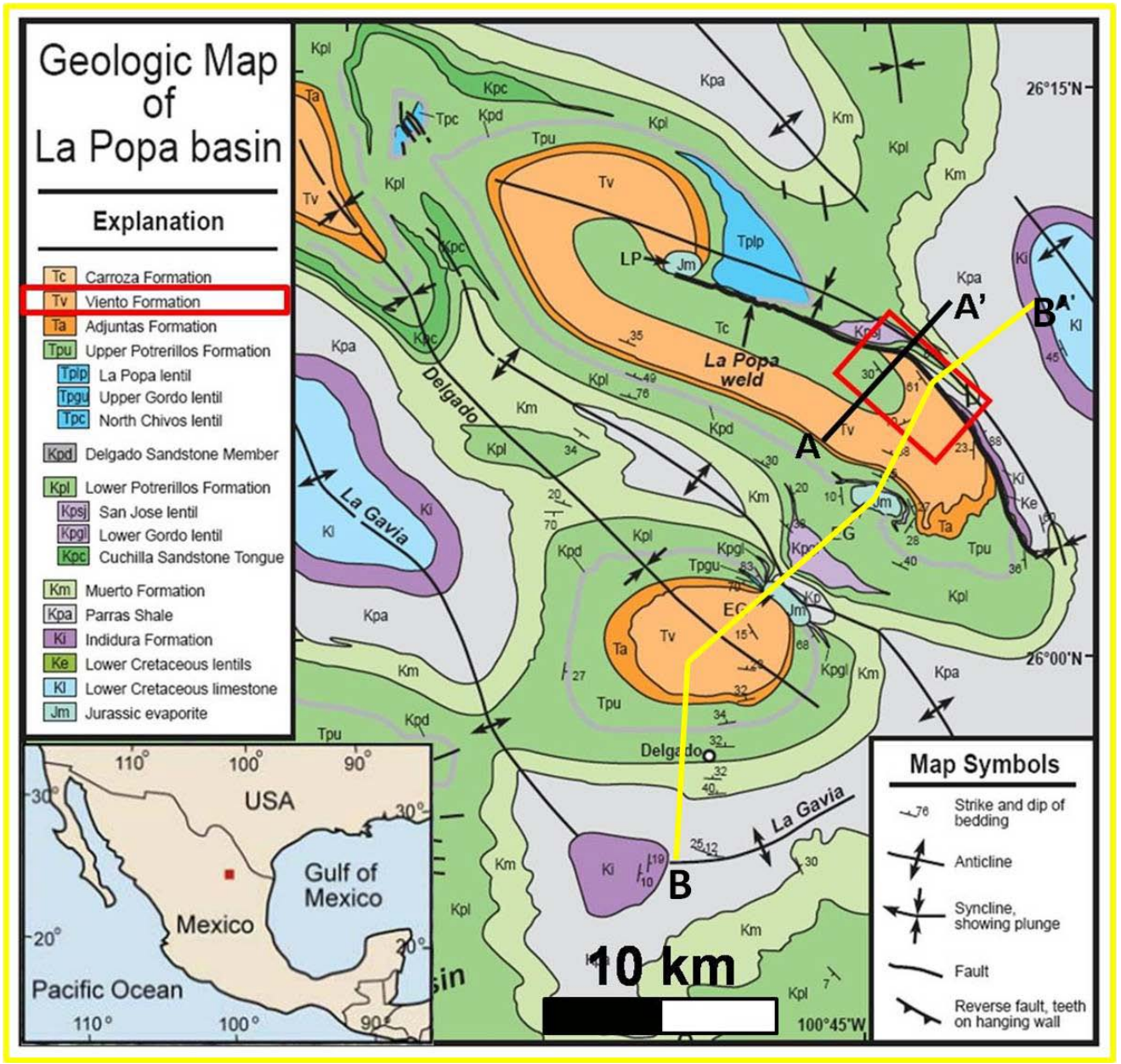
Geologic Map of La Popa basin
Explanation
Tc Carroza Formation
Tv Viento Formation
Ta Adjuntas Formation
Tpu Upper Potrerillos Formation
Tplp La Popa lentil
Tpgu Upper Gordo lentil
Tpc North Chivos lentil
Kpd Delgado Sandstone Member
Kpl Lower Potrerillos Formation
Kpsj San Jose lentil
Kpgl Lower Gordo lentil
Kpc Cuchilla Sandstone Tongue
Km Muerto Formation
Kpa Parras Shale
Ki Indidura Formation
Ke Lower Cretaceous lentils
Kl Lower Cretaceous limestone
Jm Jurassic evaporite
USA
Gulf of Mexico
Mexico
Pacific Ocean
La Popa weld
Delgado
La Gavia
LP
EG
A
A'
B
B'
26°15'N
26°00'N
100°45'W
10 km
Map Symbols
Strike and dip of bedding
Anticline
Syncline, showing plunge
Fault
Reverse fault, teeth on hanging wall

Figure 1. Geologic map of the La Popa Basin, and inset geographic map of Mexico with red dot signifying the location of La Popa Basin in northeastern Mexico (modified after Lawton et al., 2001). Note the ~25 km long, northwest-southeast curvilinear surface trace of the La Popa salt weld and the two outcropping diapirs El Gordo and El Papalote. The red box indicates the study area within the Viento Formation and the bend of La Popa salt weld. The black line A-A' and the yellow line B-B' are two cross-sections shown in Figure 2.

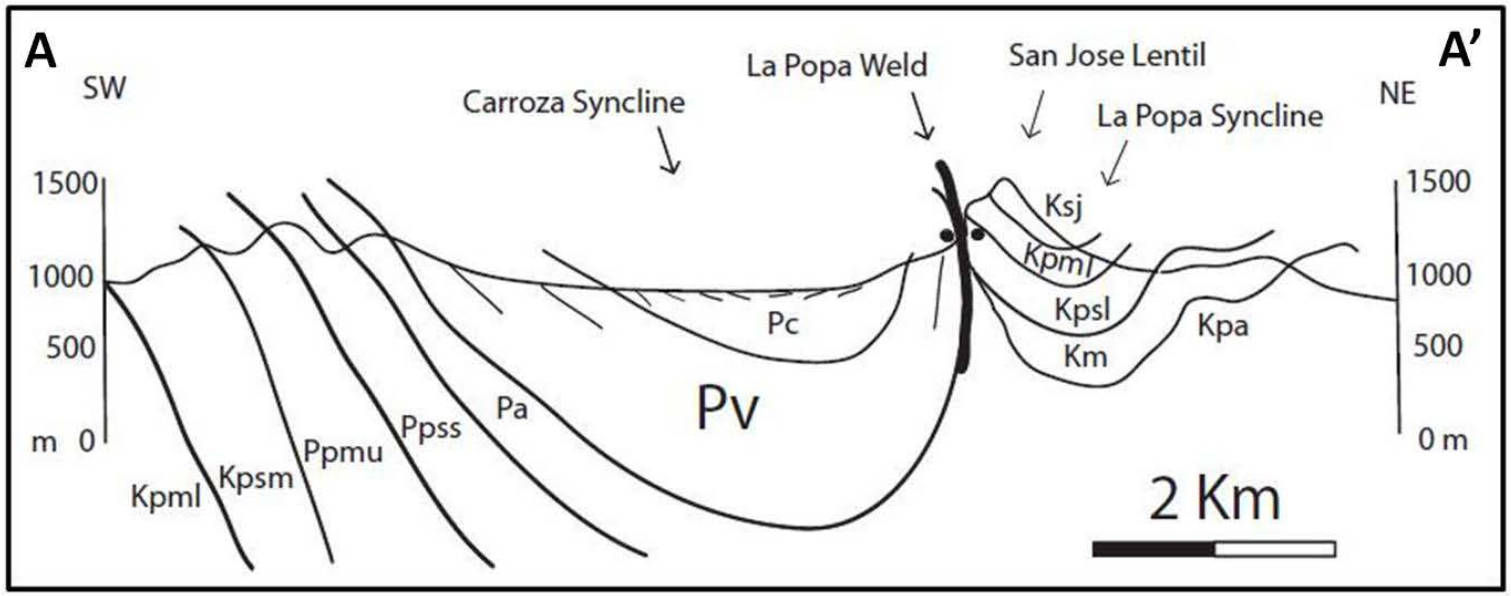
A
A'
SW
NE
Carroza Syncline
La Popa Weld
San Jose Lentil
La Popa Syncline
1500
1000
500
m 0
0 m
Ksj
Kpml
Kpsl
Km
Kpa
Pc
Pv
Pa
Ppss
Ppmu
Kpsm
Kpml
2 Km

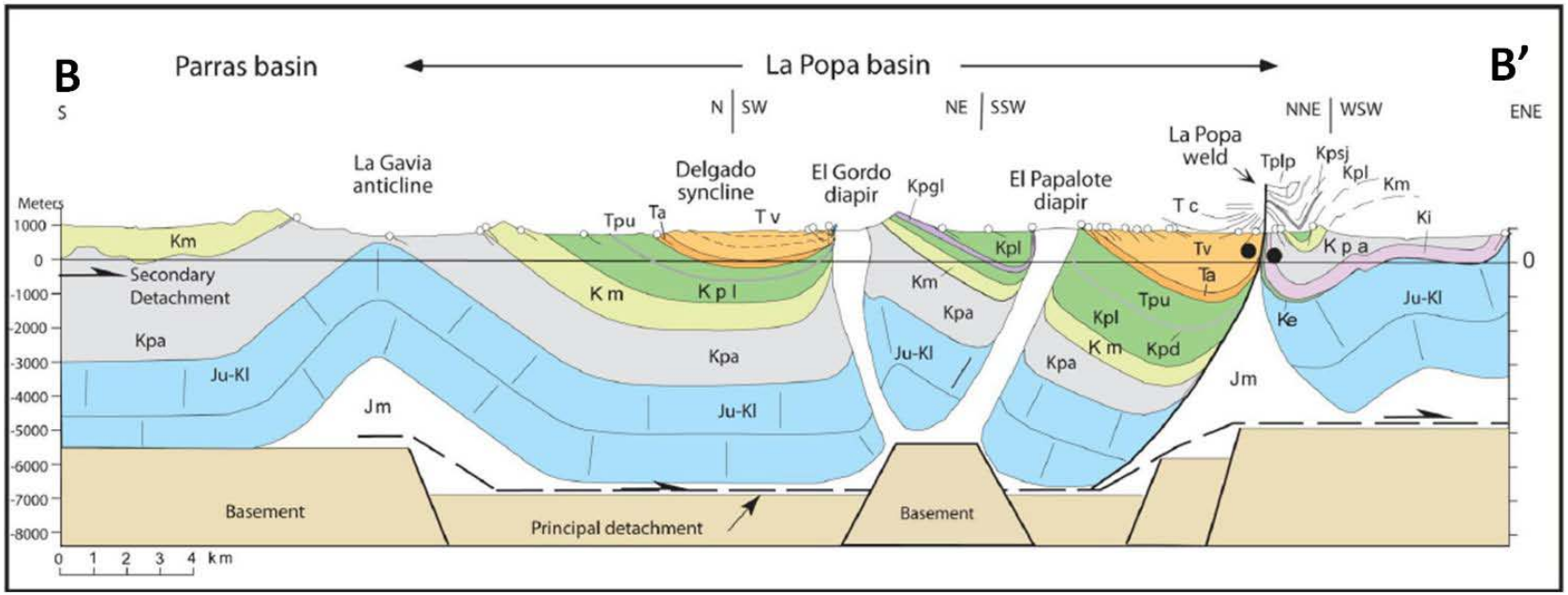
B
B'
Parras basin
La Popa basin
S
N SW
NE SSW
NNE WSW
ENE
La Gavia anticline
Delgado syncline
El Gordo diapir
El Papalote diapir
La Popa weld
Meters
1000
0
-1000
-2000
-3000
-4000
-5000
-6000
-7000
-8000
Km
Secondary Detachment
Kpa
Ju-Kl
Jm
Tpu
Ta
Tv
K m
K p l
Kpgl
Kpl
Tc
Tplp
Kpsj
Km
Ki
K p a
Ke
Kpd
Basement
Principal detachment
0 1 2 3 4 km

Figure 2. Geologic cross-section across the bend of La Popa salt weld (black line A-A') and across La Popa basin including the El Papalote and the El Gordo diapirs (yellow line B-B'). Location of line A-A' and line B-B' are shown on Figure 1. Cross-section A-A' is redrawn from Rowan et al., (*in press*). Vertical exaggeration approximately 2:1. Units explained from older to younger: Kpa – Parras Shale; Km – Muerto Formation; Potrerillos Formation subdivided into members: Kpsl – Lower Siltstone; Kpml – Lower Mudstone; Kpms – Middle Siltstone; Kpd – Delgado Sandstone; Ppmu – Upper Mudstone; Ppss – Upper Sandstone; intercalated with Kpsl and Ppmu are two limestone lentils, Ksj – San Jose, Ppl – La Popa; Pa – Paleocene Adjuntas; Pv – Paleogene Viento; Pc – Paleogene Carroza. Pv – Paleogene Viento Formation is the unit of interest for this research. Short lines within Pv and Pc show bedding dips. Cross-section B-B' was originally created by Millan, (2004) and modified by Giles et al. (2008). Units explained are listed as in the stratigraphic column in Figure 1.

Although thrust loading is the dominant control of salt-influenced foreland basin subsidence in La Popa basin (Verges et al., 2002; Rowan and Vendeville, 2006; Hudec and Jackson, 2006; Latta and Anastasio, 2007), episodic tectonic pulses of shortening overlapped in time and space with progressive halokinetic downbuilding during Viento Formation deposition. This study tests the models of halokinetic sequence development caused by passive diapirism (Giles and Lawton, 2002; Rowan et al., 2003; Giles and Rowan, *in press*). Passive diapirism occurs in response to sedimentary differential loading and is quantified as the syndepositional rise of an evaporite stock (Rowan et al., in press). According to these models, halokinetic sequences that form due to passive diapir rise occur only locally and develop in response to variations between salt rise rates and sediment accumulation rates (Aschoff and Giles, 2005; Shelley and Lawton, 2005; Giles and Rowan, in press). Results from this study can be potentially applied to other types of data (seismic, core log, etc.) to enhance the geometry prediction of hydrocarbon reservoirs in producing provinces where the targets are adjacent to secondary salt welds or vertical diapirs, particularly those that have undergone compression.

1.2. Salt tectonics and halokinetic sequence stratigraphy background

Studies related to salt tectonics focus on the process known as *halokinesis*, the subsurface movement of evaporite minerals under low temperature and pressure conditions (Jackson, 1991). Salt maintain constant ~2.15 g/cm^3 density virtually independent of burial depth, which is not true for other sediments that become denser upon burial. In addition, in contrast to other sediment rock type, the salt is much weaker under both compression and tension, and over common geological time-scales will deform as a viscous fluid (Warren, 2006). Therefore, because of these physical properties, salt does not drive salt tectonics but reacts passively to external forces (e.g., passive diapirism).

Halokinesis can result in *passive diapirism* (Rowan et al., 2003) and *downbuilding*, the vertical rise of an evaporite body that is constantly near the sea floor or land surface, coeval with strata being deposited in the adjacent minibasin. Differential sediment loading of an autochthonous evaporite layer produces lateral variations in overburden thickness, density, and strength, which initiates halokinesis. The process of downbuilding occurs as the evaporite structure grows upward while the surrounding strata deposited in the minibasin subside downward (Rowan et al., 2003; Rowan and Vendeville, 2006). Due to slightly higher topographic relief, the crest of the diapir will generally be covered only by a thin layer of sediments and will remain at or near the sea floor or land surface (Giles and Lawton, 2002). Passive diapirism ceases when the rate of evaporite rise is less than the sediment accumulation rate or when the salt layer supplying the salt to the growing diapir is depleted, causing the diapir to become buried. In this study, the terms evaporite and salt are used interchangeably to refer to mechanically weak minerals including anhydrate, gypsum, halite, and barite (Jackson and Talbot, 1991; Warren, 2010).

Passive diapirism (Rowan et al., 2003) produces halokinetic sequences (Giles and Lawton, 2002; Giles and Rowan, in press), which are defined as “relatively conformable successions of growth strata genetically influenced by near-surface extrusive salt movement and are locally bounded at the top and base by angular unconformities that become disconformable to conformable with increasing distance from the diapiric structure”. Typical depositional parasequences (*sensu* Vail et al., 1977, Posamentier et al., 1992; Posamentier and Allen, 1999; Catuneanu, 2002; Catuneanu et al., 2010) can be correlated basin-wide, usually maintain relatively constant thickness, and reflect the rate of sediment accumulation relative to the rate of accommodation space development. In contrast, halokinetic sequences develop only locally within 1-2 km extent from the salt structure and reflect the rate of net vertical evaporite rise relative to the rate of local sediment accumulation (Giles and Lawton, 2002; Giles and Rowan, in press).

Two end-member types of halokinetic sequences (Fig. 3) are recognized based on structural orientation, angular unconformities, lithofacies distribution, and structural geometry (Giles and Lawton, 2002; Giles et al, 2005; Giles and Rowan, in press). Hook halokinetic sequences are typically associated with low sediment accumulation rates relative to salt rise rates and exhibit high degree of internal folding, forming “J hook” unconformities with 90° truncation angles. Debris flow facies typically overlie unconformities and are composed of diapir-derived material. In La Popa Basin, autochthonous lenticular carbonate buildups that cap diapir-generated topographic highs, referred to as lentils, are reworked as debris flow deposits (McBride et al., 1974; Giles and Lawton, 2002). The lentils and associated debris flow deposits are onlapped by outer shelf black shale, which shallows upward into lower shoreface siliciclastics (Giles et al., 2002). Hook-type sequences also display evidence of brittle shear

along the unconformity, with the sense-of-shear indicators showing that the older beds have rotated away from the diapir (Rowan et al., 2003; Rowan et al., in press). In contrast, wedge halokinetic sequences are associated with relatively high sediment accumulation rates relative to salt rise rates. Wedge halokinetic sequences exhibit minimal or no shearing and display angular unconformities with discordance of less than 30° that become conformable within 100 m from the diapiric structure (Giles and Lawton, 2002; Giles and Rowan, in press).

Stacks of individual halokinetic sequences form composite halokinetic sequences (CHS) (Giles and Rowan, in press). A stack of hook halokinetic sequences forms a tabular composite halokinetic sequence (Tabular-CHS) (Fig. 3). Tabular-CHS contain subparallel base and top boundaries, a narrow zone of thinning near the diapir, and the stacked monocline axial trace are parallel to the diapir. Tabular-CHS form when the relative ratio between average 3rd-order sediment accumulation rate and diapiric salt rise rate is low. Topographic relief is created by the diapir because accommodation space created by diapir rise and salt withdrawal outpaces sediment accumulation. Erosion or failure of the topographically-expressed diapir creates the halokinetic sequence boundary and sedimentation above this surface creates the next halokinetic sequence (Giles and Rowan, in press). Since the panel of sediment over the diapir is relatively thin, this causes the zone of halokinetic deformation to be narrow.

A stack of wedge halokinetic sequences forms a tapered composite halokinetic sequence (Tapered-CHS) (Fig. 3). Tapered-CHS exhibits convergent base and top boundaries, a broad zone of thinning toward the diapir, and the axial trace of the drape fold monocline is inclined away from the diapir margin. Tapered-CHS form when the relative ratio between average 3rd-order sediment accumulation rate and diapiric salt rise rate is high. Topographic relief over the diapir during deposition of Tapered-CHS is minimal because overall sediment accumulation

keeps pace with the accommodation space created by salt withdrawal and diapir rise. However, during shorter periods of time where sediment accumulation rates decrease, the rising diapir creates a minor topographic expression and becomes either eroded or bypassed. This creates the CHS boundary, and resumed high sediment accumulation forms the next Tapered-CHS (Giles and Rowan, in press). Since the panel of sediment over the diapir is relatively thick, the zone of halokinetic deformation is wide.

Boundaries between CHS are marked by erosional unconformities with stratal onlap above, a shift in syncline hinge zones, termed "jumping synclines" by Giles and Rowan (in press), and a pronounced salt cusp where the unconformity intersects the diapir. Jumping synclines are particularly easily recognized in Tapered-CHS, as the upper part of the axial plane from the older Tapered-CHS terminates >500 m from the diapir and the lower part of the axial trace from the youngest Tapered-CHS jumps back to a point closer to the diapir.

Understanding the process of salt-sediment interaction is significant to science and is critical to petroleum exploration for several reasons. Salt stocks with topographic expression, which form when the salt stock rise rate outpaces the sediment accumulation rate, will result in a narrow zone of thinning near diapir with abrupt facies changes, drape folding 50 – 200 m from the diapir and ≤90° angular unconformities that form J-hook halokinetic sequences (Fig. 3). On the other hand, if the salt stock rise rate is equivalent to the sediment accumulation rate, this will result in a broad zone of thinning with gradational facies change, drape folding 300 – 1000 m from the diapir and <30° angular unconformities that form wedge halokinetic sequences (Giles and Rowan, in press). Moreover, because salt is an excellent heat-conductor it impacts the timing of hydrocarbon maturation and when salt acts as a seal it impacts hydrocarbon migration pathways. Therefore, salt-related stratal geometries and depofacies, such as those within the

Viento Formation exposed adjacent to La Popa salt weld in La Popa basin, provide an opportunity to document on outcrop the distribution and quality of sedimentary deposits that can be analogous to subsurface hydrocarbon-bearing rock-reservoirs developed adjacent to vertical evaporite stocks.

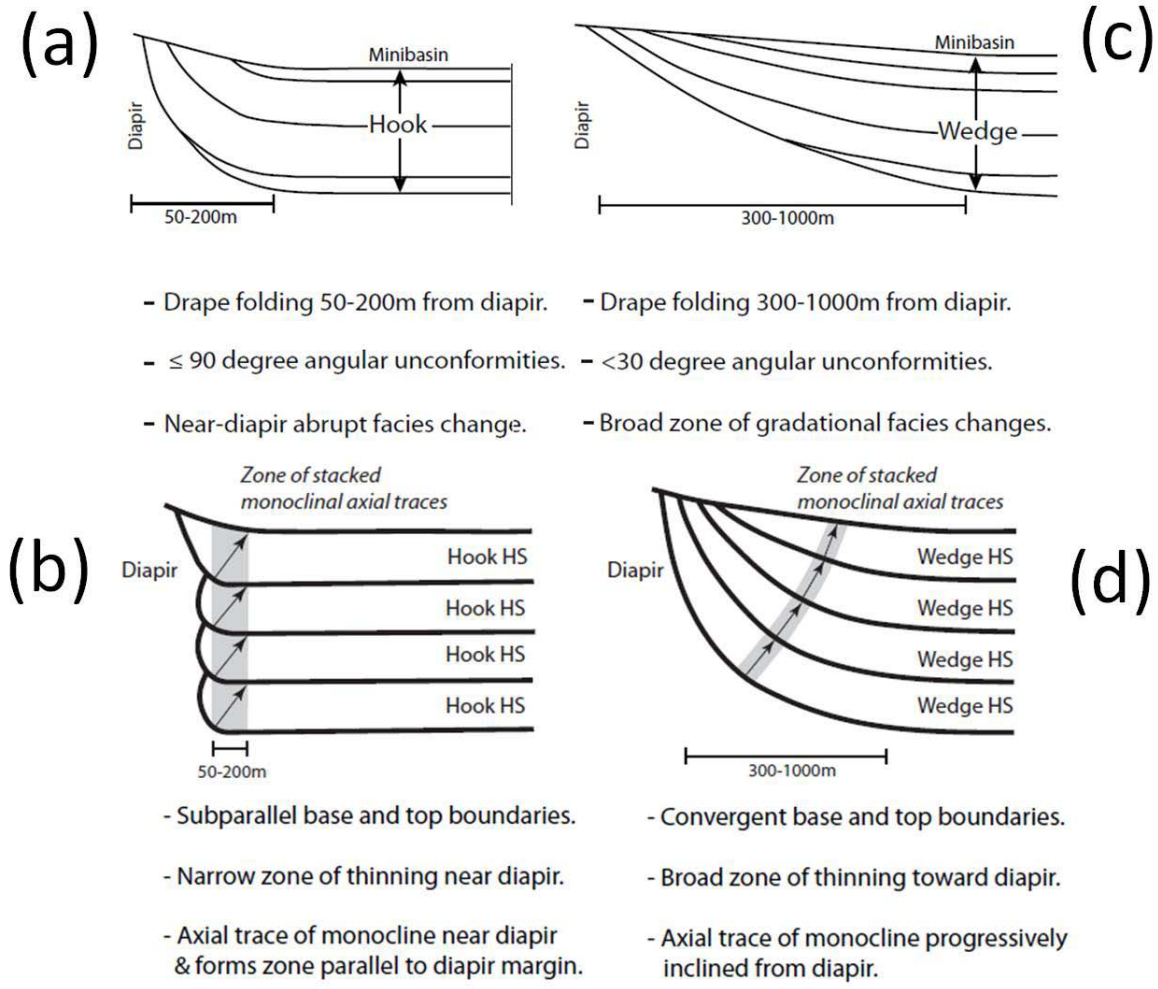

Figure 3. Controls and attributes of two end member types of halokinetic sequences and composite halokinetic sequences (CHS). (a) Hook halokinetic sequences that stack to form Tabular-CHS shown in figure (b). (c) Wedge halokinetic sequences that stack to form Tapered-CHS shown in figure (d). See text for explanation. Figure taken from Giles and Rowan (in press).

CHAPTER 2 – GEOLOGIC HYSTORY OF LA POPA BASIN

2.1. Structural evolution

La Popa basin is located in northeastern Mexico in the states of Coahuila and Nuevo Leon, approximately 75 km northwest of the city of Monterrey. The basin is approximately 60 km wide and occupies an area of approximately 2,000 km^2. The Sierra Madre Oriental fold-thrust belt to the south and Coahuila fold belt to the north bound La Popa basin structurally and topographically (Fig. 1; McBride et al., 1974; Lawton et al., 2001; Soegard et al., 2003; Lawton et al., 2009).

The La Popa region evolved as an isolated rift or pull-apart basin during Middle to Late Jurassic crustal extension approximately coeval with the opening of the Gulf of Mexico and the rollback of the Mescalera Plate (Dickinson and Lawton, 2001), at which time evaporites of the Minas Viejas Formation were deposited. Flexural subsidence that records development of the Sierra Madre fold belt began in the Late Cretaceous (Campanian). Folding in La Popa basin began to form in Mid-Maastrichtian time and continued through the Middle Eocene, which is the age of youngest preserved strata in the foreland (Lawton and Rowan, 2008). Shortening initiated during the Late Cretaceous Hidalgoan orogeny (ca. 65-35 Ma) ultimately inverted the La Popa foreland basin due to rise of the adjacent Sierra Madre Oriental to the south (Lawton et al., 2001; Soegaard et al., 2003; Lawton and Rowan, 2008; Lawton et al., 2009). The deformation style of La Popa basin was strongly pre-conditioned by steep basement faults, pre-Mesozoic sedimentary deposits (Lawton and Rowan, 2008; Rowan et al., *in press*), and by several kilometers thick evaporite deposits (Kroeger and Stinnesbeck, 2003). The basin forms a structural low between detachment folds that expose Lower Cretaceous limestone. Basement flanking the basin may be at significantly shallower depth than in the basin center, permitting preservation of the thick

Cretaceous-Paleogene sedimentary section. La Popa basin deformation was dominated by thin-skinned deformation that produced NW-SE-trending, large-scale, salt-detachment folds and faults (Lawton et al., 2001; Rowan et al., 2003; Millan-Garrido, 2004; Latta and Anastasio, 2007; Lawton and Rowan, 2008; Rowan et al., *in press*). The deformation style of La Popa basin is somewhat different from the deformation style of the Laramide orogen to the northwest, in that deformation did not reactivate basement structures and shortening was accommodated primarily by low-angle thin-skinned faults (Vergez et al., 2002; Soegaard et al., 2003), whereas generally the Laramide orogeny was accompanied by thick-skinned/basement-involved deformation. Hidalgoan detachment folds affected all the formations of the Difunta Group, indicating that shortening continued beyond the Middle Eocene (Lawton et al., 2001).

In La Popa basin, outcrop exposures of the Minas Viejas Formation consist of roughly circular salt stocks that are approximately 4–6 km^2 in outcrop area (McBride et al., 1974; Laudon, 1984; Weislogel and Lawton, 2000; Lawton et al., 2001; Giles and Lawton, 2002; Aschoff and Giles, 2005; Shelley and Lawton, 2005) and small, isolated pods of evaporite exposed within the sub-vertical La Popa weld (Fig.1; Giles and Lawton, 1999; Lawton et al., 2001; Rowan et. al., 2003; Rowan et al., *in press*). In addition to gypsum, these salt stocks contain allochthonous blocks of metamorphosed mafic-intermediate, igneous rocks and Jurassic carbonate (Laudon, 1984; Lawton et al., 2001; Giles and Lawton, 2002; Rowan et al., *in press*). A well drilled 15 km southeast of La Popa basin on the crest of a detachment anticline encountered 600 m of gypsum, 900 m of interbedded gypsum and halite, 2100 m of halite, several meters of olivine basalt, 520 m of interbedded halite and black carbonaceous limestone and ended in 370 m of black carbonaceous limestone (Lawton et al., 2001). This massive thickness of evaporite is not primary but is structural due to ductile flow of evaporite into the

hinge of an anticline. Nevertheless, the subsurface data suggests that much of the abundant deformed gypsum and the lack of halite in exposures of La Popa basin salt structures probably represent a residuum caprock, a result of halite dissolution from the diapir during interaction with seawater (Lawton et al., 2001). The current interpretation of the exotic sedimentary and meta-igneous blocks within the Minas Viejas Formation is that they were depositionaly intercalated with the evaporite sequence (Garrison et al., 1999; Lawton et al., 2001) and moved with the evaporite as it becomes diapiric.

Evaporite deposition of the Minas Viejas Formation began in an internally drained Jurassic saltpan isolated from the global ocean, accompanied by eruption and shallow intrusion of mafic magma (Lawton et al., 2009). These igneous rocks formed from partial melts of the continental mantle during Upper Jurassic rifting and were subsequently deposited as lava flows in a hypersaline setting (Lawton et al., 2001) approximately 146 Ma based on ^{40}Ar-^{39}Ar on biotite and potassium feldspar (Garrison and McMillan, 1999). These rocks have been thoroughly recrystallized (thermally metamorphosed) to chlorite-epidote and preserve remnant igneous texture but without metamorphic foliation fabrics, and are referred to as metaigneous rocks. As rifting proceeded, halite deposition gradually gave way to gypsum deposition in a sabkha setting. Widespread flooding of northern Mexico resulted in limestone deposition by the early Kimmeridgian. Halokinesis of the Minas Viejas Formation initiated during subsequent burial by younger sedimentary deposits (Rowan et al., 2003). Evaporite mobilization broke up the intercalated blocks and carried them upward in diapiric structures from which they were periodically expelled at seafloor, reworked and redeposited (Garrison and McMillan, 1999; Lawton et al., 2001; Giles and Lawton, 2002).

The origin of La Popa salt weld has been a subject of controversy. It was initially mapped as a reverse fault (McBride et al., 1974; Laudon et al., 1984; Millan-Garrido, 2004). Giles and Lawton (1999) and Rowan et al. (2003; *in press*) reinterpreted it as a secondary salt weld that developed over a two-phase history. During the first phase (Late Jurassic and Early Cretaceous), the salt wall rose as a passive diapiric structure probably initiated over a basement fault in response to continuous sediment-accumulation loading (probably the salt diapir started as an elongate wall, therefore not due to shortening). Cretaceous to Eocene Hidalgoan compressional forces repeatedly squeezed the structure causing it to become narrower (Lawton et al., 2001; Rowan et al., *in press*). These combined forces caused extrusion of evaporite minerals from the salt wall along with exotic blocks preserved within Late Cretaceous to Eocene units. The evaporite minerals dissolved and the exotic blocks were reworked into gravel clasts. Reverse offset during halokinesis along the weld caused sedimentary strata on both sides of the weld to become juxtaposed.

The weld exhibits a ~25 km long curvilinear SE-to NW map trace (Fig.1) with zero stratigraphic displacement apparent at either end; however, stratigraphic offset increases due to halokinesis to approximately 5 km at the midpoint along the trace of the weld (Giles and Lawton, 1999; Rowan et al., *in press*). Exposures of the Parras Shale and overlying Difunta Group are present along the weld. Wedges of gypsum containing meta-igneous clasts and barite crop-out discontinuously along the trace of the weld zone. Growth strata on both sides of the weld suggest long-term subsidence adjacent to the weld due to evaporite withdrawal.

2.2. Stratigraphy

La Popa basin developed as a foreland basin from Cretaceous until Paleocene/Eocene time (Dickinson and Lawton, 2001; Lawton et al., 2001; Lawton et al., 2009). Maximum

subsidence occurred by 50-45 Ma, and was followed by uplift that resulted in erosion of as much as 5-7 km of strata from the basin by the latest Eocene (~ 34 Ma; Gray et al., 2001; Hudson and Hanson, 2010). McBride et al. (1974) and Lawton et al. (2009) attribute the origin of the sediments in La Popa basin to derivation from the Sierra Madre orogen including several arc terrains in southwestern United States and western Mexico. The strata contained within the basin are primarily marginal marine, tidal, and deltaic deposits, which show throughout the basin history an overall progradation from outer shelf to terrestrial deposition (Fig. 4).

Early Cretaceous to Middle Eocene deposits are exposed at the surface in La Popa basin (Fig. 4; McBride et al., 1974; Lawton et al., 2001; Gray et al., 2001). The Early Cretaceous strata in La Popa basin are approximately 100 m thick and consist of mostly limestone interbedded with subordinate shale. The Upper Cretaceous deposits exposed in La Popa basin include the Indidura Formation, the Parras Shale, and the lower part of the Difunta Group (Fig. 3). The Difunta Group (Fig. 4) is composed of 4,500 m of Maastrichtian to Middle Eocene siliciclastic deposits that are divided into five formations, which are in ascending order Muerto, Potrerillos, Adjuntas, Viento, and Carroza (McBride et. al., 1974; Lawton et al., 2001). The Difunta Group is composed primarily of shallow marine to marginal marine, fine-grained, siliciclastic units in its lower part and, non-marine, coarse-grained sandstone, and conglomerate units in its upper part. Shallow-marine carbonate build-ups developed locally within the Difunta Group adjacent to salt structures in La Popa basin (McBride et. al., 1974; Giles and Lawton, 1999; Lawton et al., 2001).

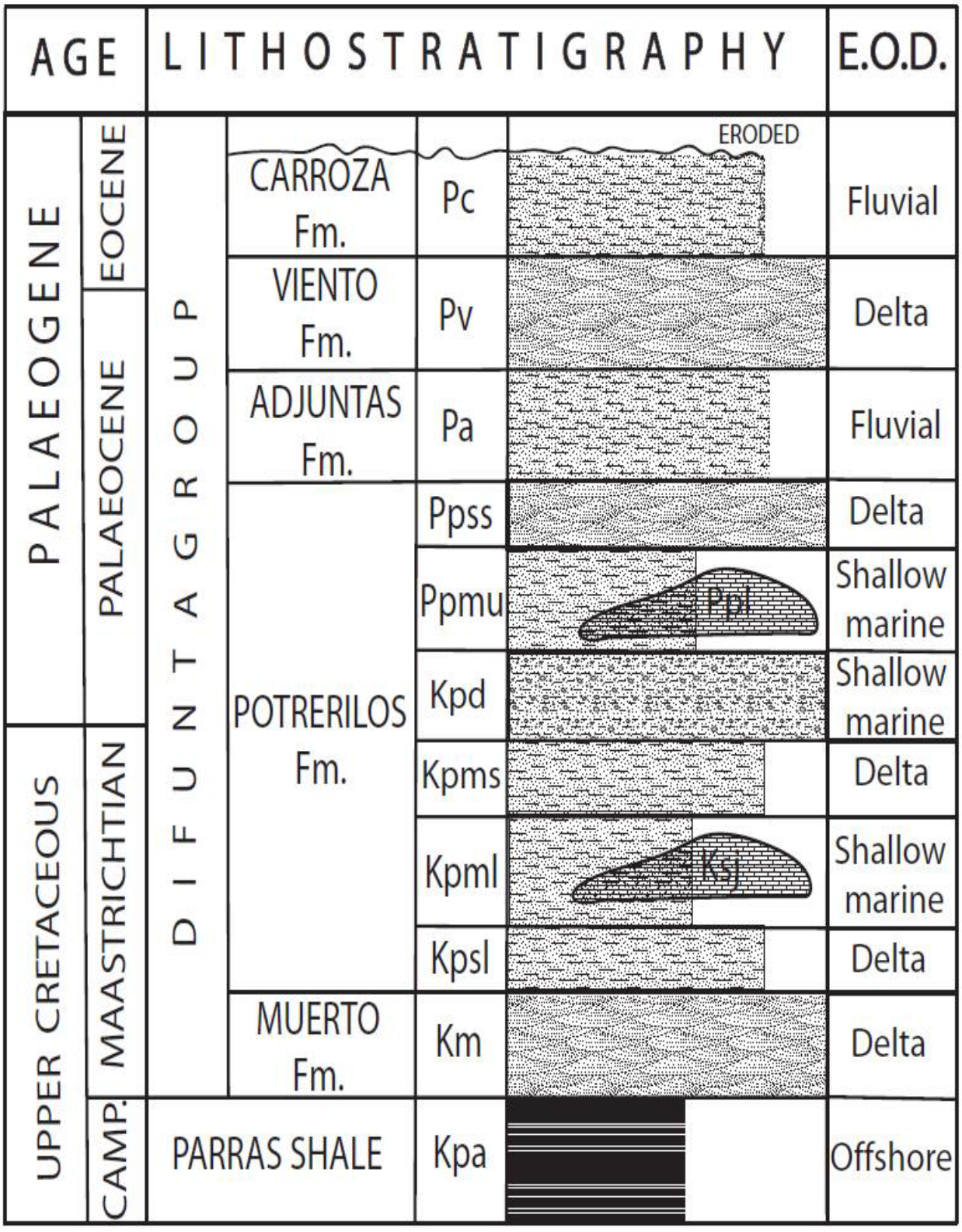
AGE
LITHOSTRATIGRAPHY
E.O.D.
PALAEOGENE
EOCENE
PALAEOCENE
UPPER CRETACEOUS
MAASTRICHTIAN
CAMP.
DIFUNTA GROUP
CARROZA Fm.
VIENTO Fm.
ADJUNTAS Fm.
POTRERILOS Fm.
MUERTO Fm.
PARRAS SHALE
Pc
Pv
Pa
Ppss
Ppmu
Kpd
Kpms
Kpml
Kpsl
Km
Kpa
ERODED
Pp
Ks
Fluvial
Delta
Fluvial
Delta
Shallow marine
Shallow marine
Delta
Shallow marine
Delta
Delta
Offshore

Figure 4. Chronostratigraphic column showing the units that crop out along the La Popa salt weld in La Popa basin. Environment of deposition (E.O.D) interpretation is compiled from Lawton et al. (2001); Shelley and Lawton (2005); Aschoff and Giles (2005); Rowan et al. (*in press*), and this study. Units are labeled as in Figure 2 black line A-A'. Note that the Viento Formation occurs between terrestrial deposits of the Adjuntas Formation below and the Carroza Formation above.

The Potrerillos Formation is the thickest unit in the Difunta Group (2,300 m) (McBride, 1974), and is composed of six members that consist primarily of bioturbated shale, siltstone and sandstone that represent delta platform deposits (McBride et al., 1974; Lawton et al., 2001). The Delgado Sandstone measures up to 500 m thick at El Papalote and Gordo diapirs, and is interpreted to represent a shoreface system (McBride et al., 1974; Lawton et al., 2001). In the study area, within the Lower Mudstone and the Upper Mudstone members of the Potrerillos Formation are two carbonate build-ups, referred to as the San Jose and La Popa lentils, which form topographically high cliffs and thicken toward salt diapirs (Fig. 3 and Fig. 4). A number of angular unconformities adjacent to La Popa weld indicate that salt diapirism was active during the time of Potrerillos Formation deposition (McBride et al., 1974; Lawton et al., 2001).

The Adjuntas Formation is approximately 260 m thick at its type locality, gradationally overlies the Potrerillos Formation, and consists of non-marine red siltstone and sandstone strata that include freshwater gastropods and crocodile fossils of early Eocene age (McBride et al., 1974; Lawton et al., 2001). The Viento Formation (Fig. 4, Fig. 5, and Fig. 6) is a thick sandstone-rich unit that contains chert pebbles, metaigneous clasts, oysters, and bundled heterolithic bedsets. The Viento Formation measures 730 m at its type locality, lies in sharp contact with the overlying Adjuntas Formation (McBride et al., 1974; Lawton et al., 2001), and formed in a shallow marine, coastal complex setting (McBride et al., 1974; Lawton et al., 2001). The age of the Viento Formation is poorly constrained. Based on Ypresian (55.8 to 48.6 Ma) mollusks collected from the Adjuntas Formation (Vega and Perrilliat, 1989a; Vega and Perrilliat, 1989b; Vega and Perrilliat, 1992; Vega et al., 2007; Perrilliat et al., 2008), the overlying Viento Formation is inferred to be Middle Eocene 49 Ma to 45 Ma (Lawton et al., 2009). The Carroza Formation overlies the Viento Formation and is the youngest unit of the Difunta Group in La

Popa basin. Although the top is truncated by erosion, it measures 620 m thick at its type location (McBride et al., 1974; Lawton et al., 2001). It consists of non-marine red and purple weathering mudstone, siltstone, and sandstone, which are interpreted as fluvial and overbank deposits (McBride et al., 1974; Lawton et al., 2001; Andrie, 2011). Both the Viento and Carroza formations are undated, but they are inferred to be Middle Eocene and younger in age based on constraints from the underlying Adjuntas Formation (Soegaard et al., 2003).

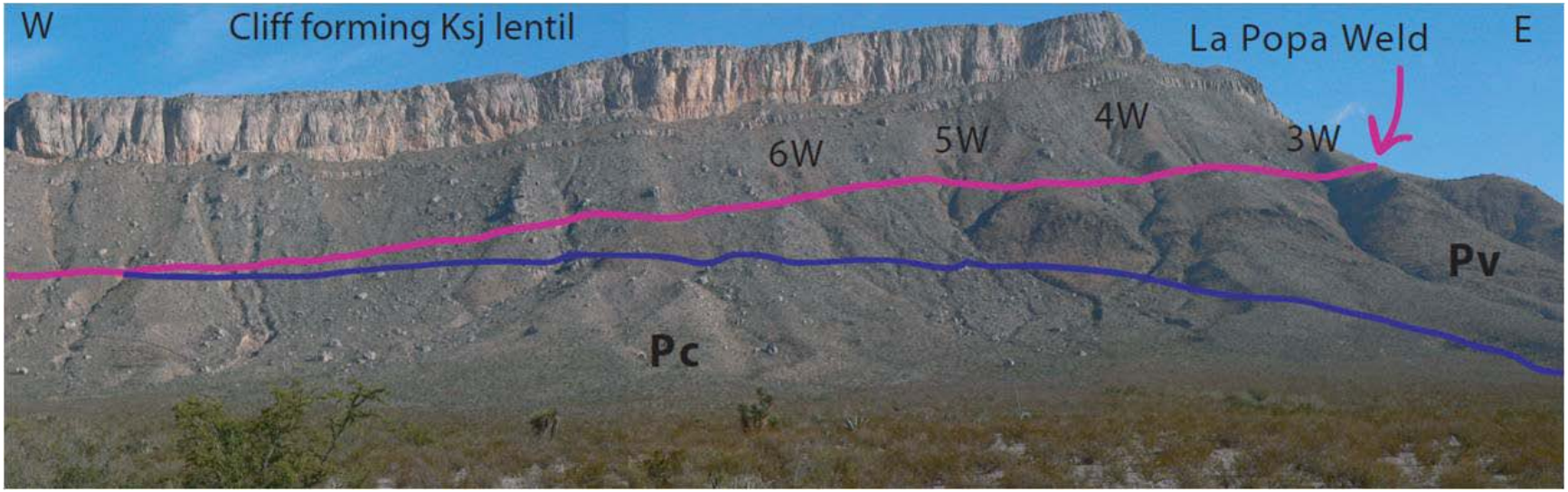

Figure 5. Field photograph showing the topography and the main elements within the northwestern part of the study area: carbonate cliff forming Cretaceous San Jose Lentil (Ksj); Palaeogene Viento (Pv) and Palaeogene Carroza (Pc) formations. Pink line below the cliff represents the trace of La Popa salt weld, and the blue line below represents the contact between Pv and Pc. The contact between the two lines represents the place where Pv pinches out. The notations 3W, 4W, 5W, and 6W point to the drainages where Viento stratigraphic sections were measured. The view is to the north and field of view is ~4 km wide. The carbonate cliff (Ksj) is ~30 m high. The difference in elevation is ~400 m, from ~1300 m elevation at the cliff top to ~900 m elevation on the valley floor.

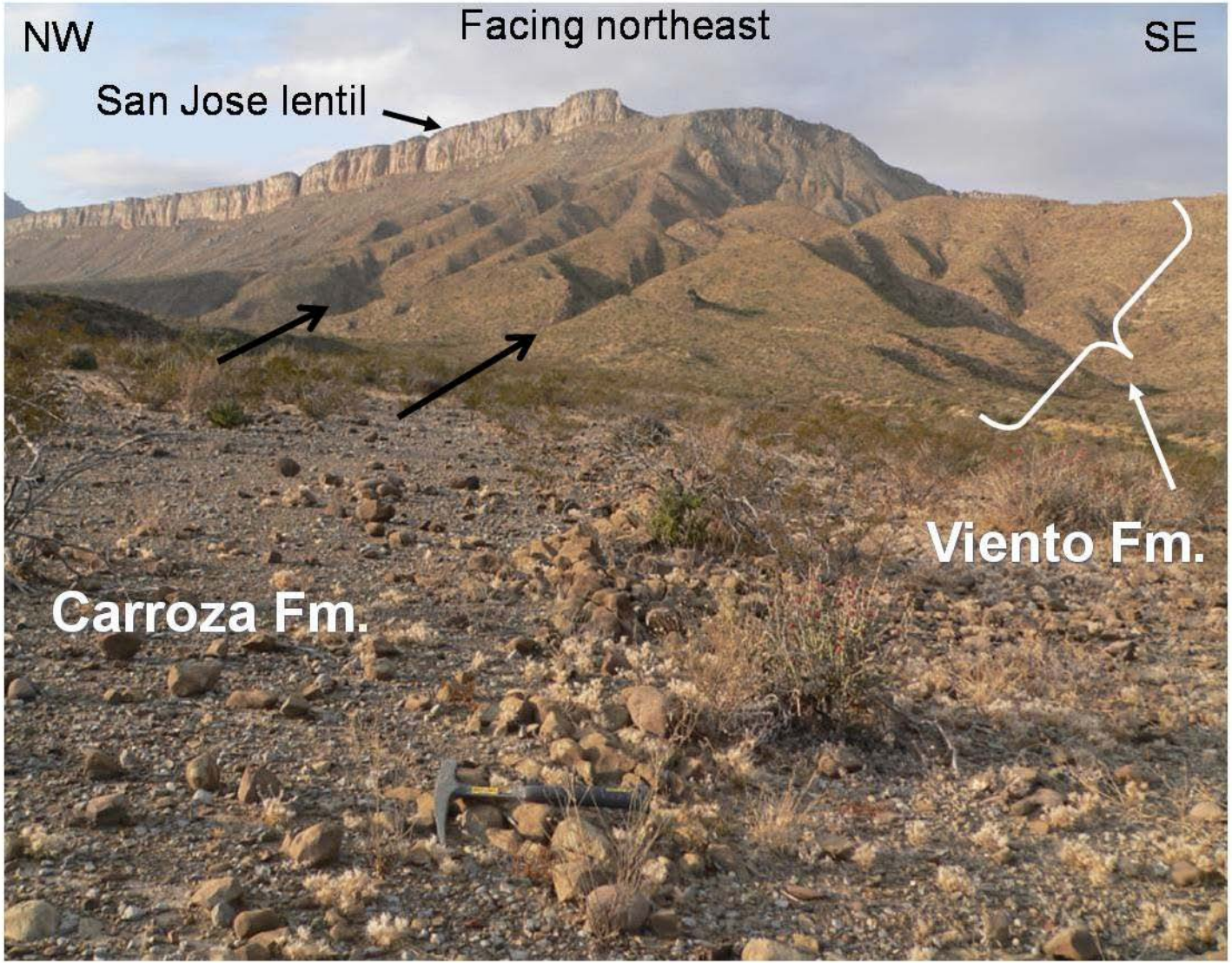
NW
Facing northeast
SE
San Jose lentil
Viento Fm.
Carroza Fm.

Figure 6. View from the contact zone of Carroza and Viento formations, toward La Popa weld located approximately at the base of the San Jose Lentil, showing the topography in the study area. Most of the hill side is Viento Formation deposits that thin toward NW. Note the strike of ridge-forming Viento sandstone beds. Black arrows pointing SE indicate arroyos where were measured stratigraphic sections.

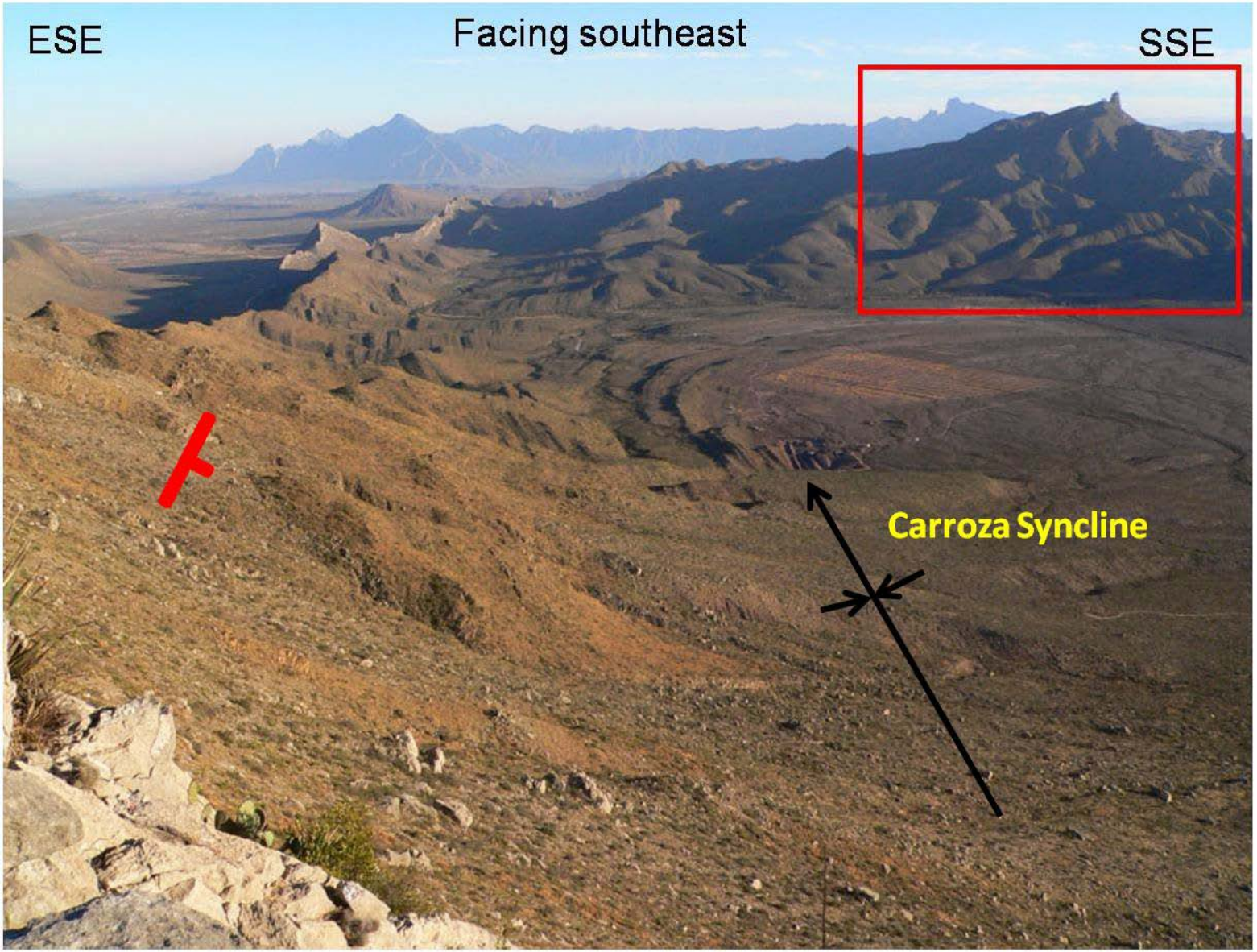
ESE
Facing southeast
SSE
Carroza Syncline

Figure 7. View from the La Popa weld facing the bowl shape interior of the Carroza syncline. The aproximate location of the Carroza syncline is indicated by the black arrow, with the point of the arrow indicating the plunge direction. Note topography and bedding attitudes (red symbol represents strike and dip) of ridge-forming Viento Formation sandstone beds. In rectangle, Viento beds outside the study area and on the other side of the basin, Viento beds were uplifted to 1500 m elevation due to Hidalgoan shortening and the overlying Carroza deposits were entirely removed. In contrast, in the study area (foreground), Viento beds are at an elevation ranging from 900 m to 1200 m and the younger Carroza deposits are preserved and exposed in the valley below.

CHAPTER 3 – METHODS

3.1. Tools and approach

A 1.5 m Jacob staff and Brunton compass were used to measure seven stratigraphic sections. A Brunton compass was used to measure bedding attitudes, and a San Jose De La Popa quadrangle (scale 1:50,000) and Garmin GPS (average 5 m accuracy) were used to record relevant locations. Lithofacies were identified and depositional environments were interpreted based on lithologies, grain size, shape, sorting, color, sedimentary structures, ichnofauna, internal bedding organization and geometries, and vertical and lateral facies associations. Hydrochloric acid, rock hammer, hand lens (10X), and grain-size card and scale were used to aid with lithologic identification and classification during fieldwork.

In the study area, sandstone beds exhibit vertical and overturned dip angles near the La Popa salt weld, but dip decreases to ~30° toward the Carroza syncline axis. Ridge-forming beds within the Viento Formation were walked across drainages in order to observe lateral relationships between lithofacies and to correlate stratal units. The contact surfaces between the Viento Formation and adjacent formations within the study area were walked out: La Popa weld, the Potrerillos Formation, the Parras Formation, the San Jose Lentil, and the Carroza Formation. Halokinetic sequence stratigraphic interpretations were based on criteria set forth in Giles and Rowan, *in press* and time correlations (sequence stratigraphy) based on the T-R model of Embry (1992; 2002).

3.2. Study area

The study area covers approximately 8 km^2 and is delineated to the north by the San Jose Lentil and the surface trace of La Popa salt weld. La Popo salt weld extends for ~25 km long and exhibits a prominent bend in its surface trace. The Viento Formation was investigated to the south of, and for ~5 km along the surface trace of the La Popa salt weld. Stratigraphic sections were measured perpendicular to the surface strike of the salt weld along drainages and arroyos with continuous exposure (Fig. 7). Conveniently, the position of these sections allowed for field correlation of the Viento strata exposed adjacent to the surface trace of the weld for approximately 4 km. Only sections 1SE, 1W, 2W, 3W, 4W, 5W, and 6W were investigated and facies described in detail. Sections 7W through 13W are located in poorly developed arroyos where the bedrock is mostly covered. The contact with La Popa salt wall is clearly marked by pods of gypsum and the contact with younger Carroza Formation is recognized easily due by the distinctive purple weathering color of the Carroza deposits. The Viento Formation strata in arroyos 7W through 13W are highly weathered and deformed and depositional facies could not be determined. However, the section thickness was deduced with the aid of GPS and aerial images. All sections are conveniently located within a few hundreds of meters or less distance from each other and spread over a total distance of ~4 km alongside the salt weld. Except section 1SE, which is located ~2 km to the southeast, from section 6W toward the northwest over a distance of less than 2 km, the deposits of the Viento Formation thin and ultimately pinch out in section 13W (Fig. 5 and Fig. 8).

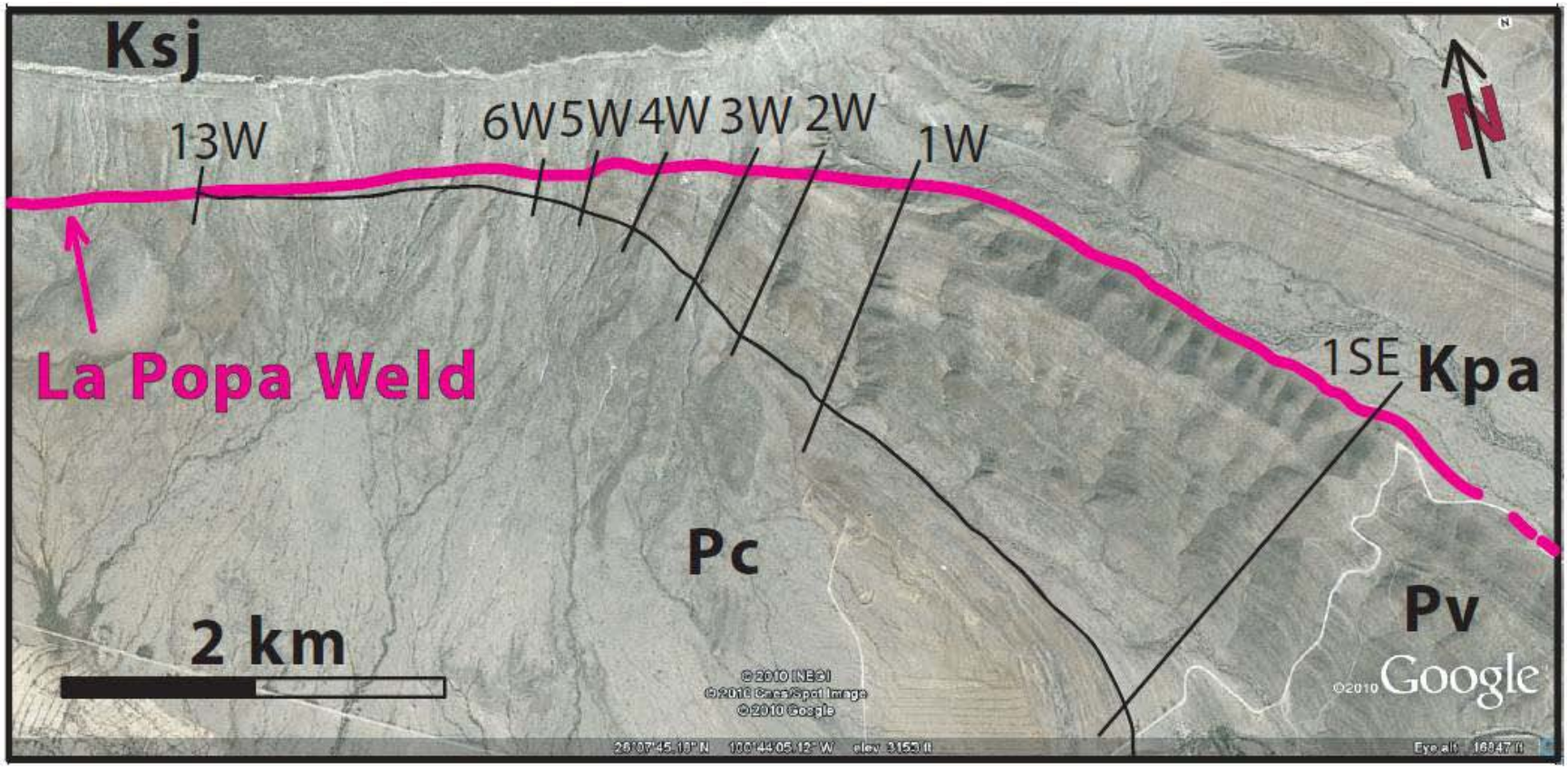
Ksj
13W
6W
5W
4W
3W
2W
1W
1SE
Kpa
La Popa Weld
Pc
Pv
2 km
©2010 Google

Figure 8. Aerial image showing the location of the measured sections within the Viento Formation (Pv), notated 1SE, 1W, 2W, 3W, 4W, 5W, 6W and 13W. Other sections where Viento Formation partially crops out were recorded along the weld and noted from 6W to 13W, location shown in Appendix 1 to the point where Viento deposits pinch out to zero thickness (line 13W). For the purposes of this study, Viento Formation is formally subdivided into a southeastern diapir-distal area from line 1SE to line 1W, and into a northwestern diapir-proximal area from line 1W to pinchout in line 13W. Units of interest within the study area: Cretaceous San Jose lentil (Ksj); Cretaceous Parras Shale (Kpa); Viento Formation (Pv) and Carroza Formation (Pv). La Popa weld is indicated by the arrow and is colored in purple.

CHAPTER 4 – LITHOLOGIC FACIES DESCRIPTION AND INTERPRETATION

Viento Formation strata exposed to the southeast of La Popa weld consists of high sand to-mud ratio deposits that represent a repetitive and complex distribution of depositional environments with significant fluvial, tidal, and marine influence. Seventeen lithofacies, which vary slightly between outcrops, were recognized and are described below in order from most landward to most basinward facies.

4.1. Conglomerate and conglomeratic sandstone facies

The conglomeratic sandstone facies is the most common and prevalent lithofacies within the study area and is composed of six different facies. These facies exhibits great variability in clast composition, including metaigneous clasts, chert and limestone clasts, mudstone intraclast, oyster and gastropod shells, wood fragments, and mud chips. All six facies are composed of medium- to coarse-grained, subangular- to angular, poorly sorted sandstone matrix. The essential characteristic these facies share in common is the content in metaigneous clasts. This facies group represents the coarsest grained facies within the study area. In general, conglomeratic sandstone facies lack primary sedimentary structures other than low-angle trough cross-stratification, and beds form black to dark-brown semi-continuous ridges, which can be traced laterally in the field and across drainages for ≥300 m. In Appendix 1, conglomerate and conglomeratic sandstone beds are colored “Mediterranean” (turquoise/aqua marine).

4.1.1. Sandstone with metaigneous clasts facies

4.1.1.1. Description

This facies contains rare, rounded to angular, pebble- to cobble-sized (30 cm) porphyritic metaigneous clasts that range from felsic to mafic in composition, with intermediate- to mafic-clasts being more common. The metaigneous clasts are friable, occur as rounded pebbles, and

weather white, brown, or green. Clast-size and angularity both increase with increasing proximity to the weld. Matrix is composed of medium- to coarse-grained, poorly sorted sandstone that weathers orange- to tan. Primary sedimentary structures are rare and exhibit low-angle trough cross-stratification. Beds are 1.5-5 m thick, extend laterally for tens of meters, have erosional bases, and display a lenticular- to channel shaped geometry (Fig. 9).

4.1.1.2. Interpretation

Sandstone with metaigneous clasts facies represents thalweg of fluvio-deltaic distributary channel deposits (Shanley and Hettinger, 1992; Willis, 2005; Fielding et al., 2005a). The morphology of modern fluvio-deltaic distributary channels and systems exhibit commonly gentle slope inclined at 1-14° (Choi et al., 2004), which makes it unlikely to transport pebble- to cobble-sized clasts from highland source areas. However, modern fluvio-deltaic distributary channels systems record deep bathymetries and high-energy bottom currents, which creates reasonable conditions to transport pebble- to cobble-sized clasts as bedload. Bedload processes transported metaigneous pebbles and cobbles only tens of meters distance from the salt wall. Increase in size and angularity of the metaigneous clasts with proximity to the weld indicates that clasts were reworked by transportation mechanisms at the channel bottom floor. The high degree of weathering and friability of the metaigneous clasts may suggest: a) reaction aureoles due of abrupt pressure and temperature conditions change while transported up to the surface within the squeezed evaporite wall (Garrison and McMillan, 1999; Fischer et al., 2009), and b) after reworking (rounding), prolonged subaerial exposure before being incorporated within the Viento deposits (Lawton et al., 2009; Hudson and Hanson, 2010), or c) prolong subaerial exposure of the outcrops during Quaternary (Lawton et al., 2009; Hudson and Hanson, 2010).

The metaigneous clasts are evidence of evaporite rise and extrusion at the surface and were sourced by the rising La Popa salt wall (Lawton et al, 2001; Lawton et al., 2009; Garrison et al., 1999). The sandstone with metaigneous clasts facies is very significant with respect to the history and evolution of La Popa salt wall. The metaigneous clasts originated from syn-rift volcanic rocks that were initially interbedded with the Jurassic evaporite Minas Viejas Formation. Massive input of sand continuously discharged by the Viento system overlaying the ~8,000-10,000 m of Cretaceous-Tertiary rock, in conjunction with episodic Laramide compression events drove evaporite diapir rise. The syn-rift volcanic blocks were transported upward during diapir rise, exhumed, and exposed subaerially and/or subaqueously. Reworking in shallow waters caused mechanical breakdown of larger blocks into pebbles and cobbles, and angularity decreased during transport within the Viento depositional system. La Popa diapir is the only source available in the minibasin that could provide the metaigneous clasts.

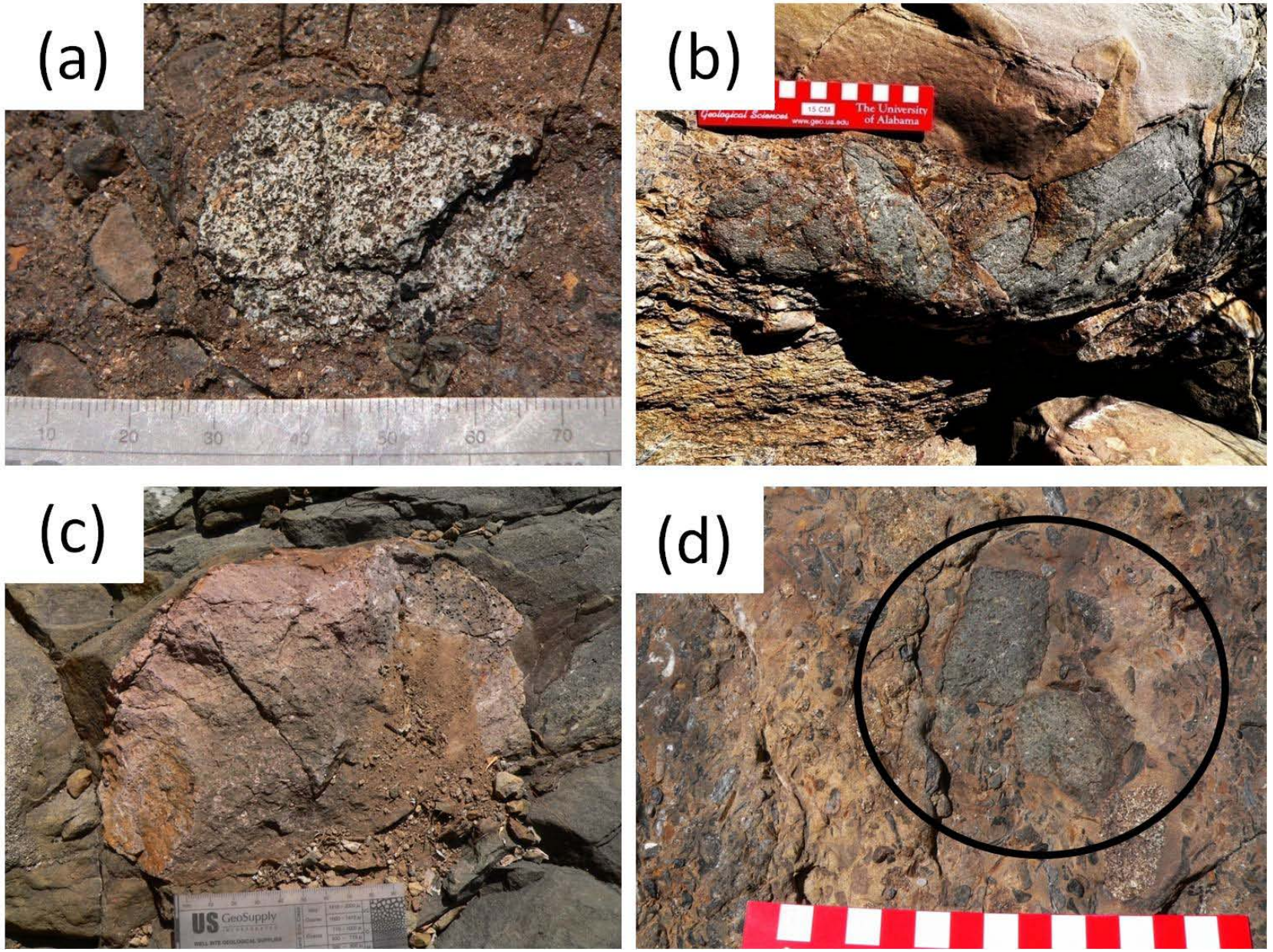
(a)
(b)
(c)
(d)
15 CM
The University of Alabama
US GeoSupply

Figure 9. Field photographs of the sandstone with metaigneous clasts facies. (a) Subrounded, felsic, metaigneous clast 4 cm in diameter surrounded by smaller intermediate to mafic clasts in a coarse-grained sandstone matrix. Scale in cm along bottom of the photograph; (b) Subangular green-blue metaigneous clasts imbedded in medium-grained well-sorted sandstone matrix. The largest clast is to the right and is 17 cm in diameter. Scale is 15 cm long. (c) Imbedded is a 20 cm across, rounded, friable, felsic- to intermediate metaigneous boulder. Card is 10 cm long. (d) Angular metaigneous clasts 7 cm across imbedded in poorly sorted sandstone matrix. Card is 15 cm long.

4.1.2. Conglomerate with chert pebbles facies

4.1.2.1. Description

This facies consists of abundant, very well-sorted, very well-rounded, indurated, black- to brown chert pebbles 2-4 cm in diameter encased in a poorly sorted, coarse-grained sandstone matrix. In addition, conglomerate with chert pebbles facies contains rare metaigneous clasts similar in size and shape to the chert pebbles. Oyster and gastropod shell fragments, mudstone intaclasts, and wood chips are also common. In general, beds lack primary sedimentary structures and appear massive, however, occasionally some beds are graded, and clasts arrangement indicates slight imbrications. The conglomerate with chert pebbles are clast-supported and bed geometry is mainly laterally extensive sheets ranging 0.20-3 m thick, which can be traced over a distance of several hundred meters. Beds exhibit erosional bases with concave geometries and overlie finer-grained bioturbated and/or mud-draped sandstone facies (Fig. 10).

4.1.2.2. Interpretation

Conglomerate with chert pebbles beds were formed by a high-energy fluvial system perhaps associated with flooding seasons and high discharge rates that formed massive, laterally continuous and fairly thin sheet deposits. However, clast imbrications indicate bedload transport, also the erosional bases suggests bedload erosion followed by bedload deposition. Chert consistency in size and roundness, beds exhibiting imbrications and sharp, erosional bases accounts for high-velocity water-flow transport conditions. The Viento deltaic system transported chert clasts, along with metaigneous clasts of similar size and coarse sand through distributary fluvial channels (Shanley et al., 1992; Olariu and Bhattacharya, 2006; Dalrymple and Choi, 2007; Leleu et al., 2009).

Unlike the metaigneous clasts sourced by La Popa salt wall, the abundant chert pebbles were sourced by the Sierra Madre Oriental fold and thrust belt and Coahuila platform to the southwest of La Popa basin, which contains thick and abundant Cretaceous chert beds (Lawton et al., 2001; Lawton et al., 2009). The Coahuila platform was a basement high throughout the Mesozoic (Goldhammer, 1999; Gray et al., 2001; Dickinson and Lawton, 2001). The chert pebbles consistent color, sphericity, hardness and weathering, strongly indicates that they originated from the same source area. The chert pebbles are very well sorted and have high sphericity indicating long distance transport, which is consistent with location of the Sierra Madre Oriental fold and thrust belt and Coahuila platform 100 km to the southwest of La Popa basin as a source area.

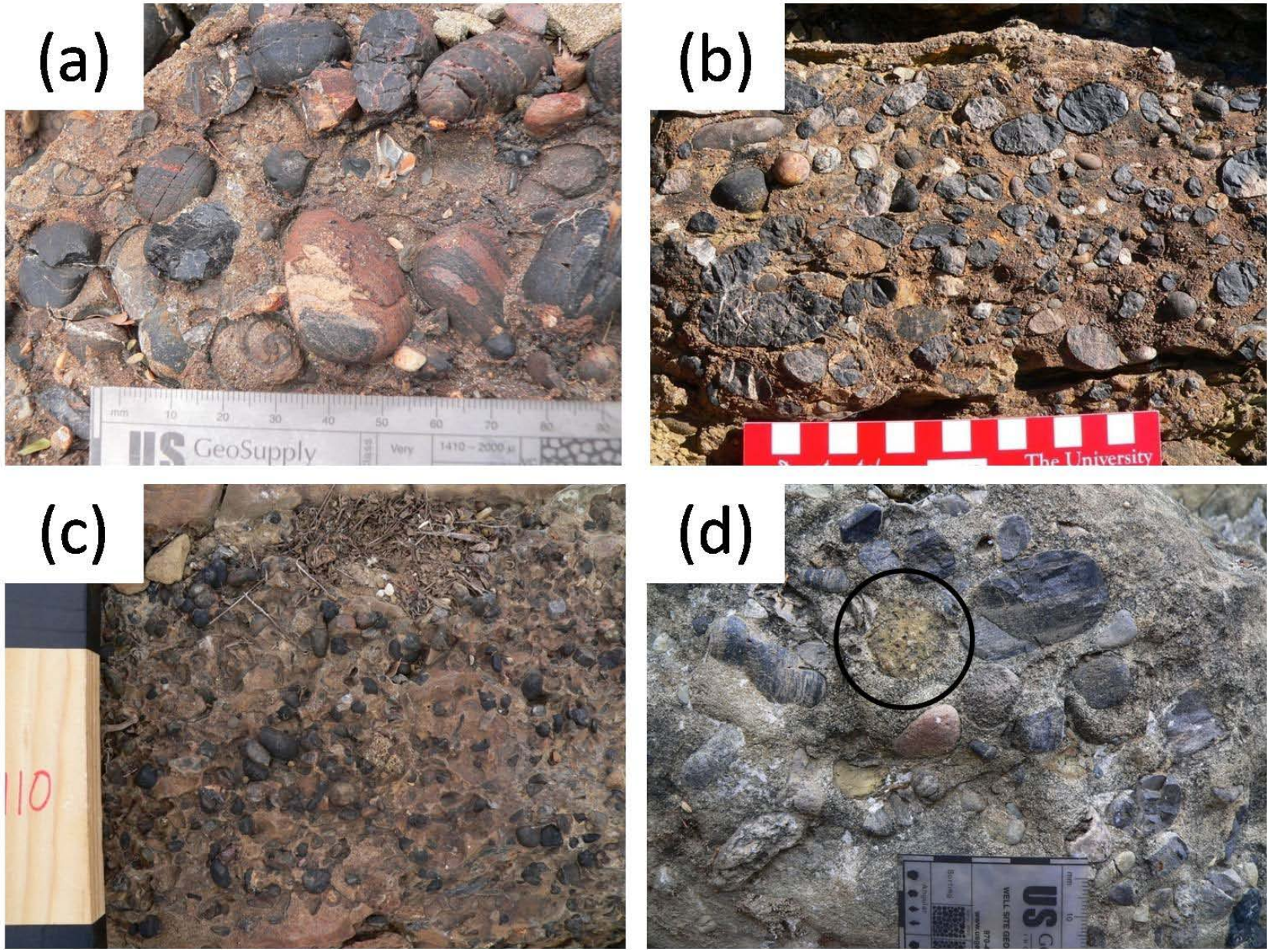
(a)
(b)
(c)
(d)
US GeoSupply
The University

(e)

(f)

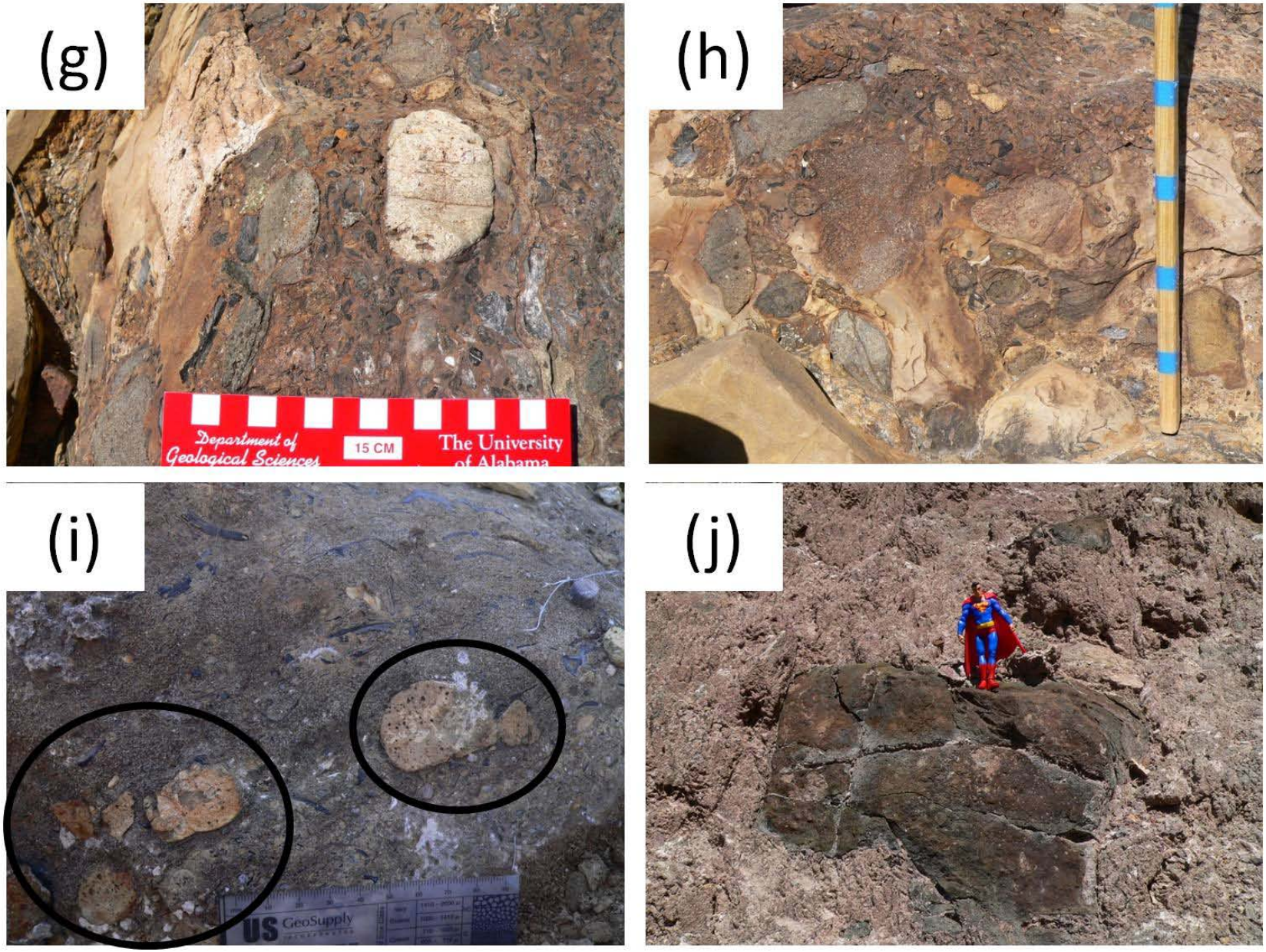
(g)
Department of Geological Sciences
15 CM
The University of Alabama
(h)
(i)
US GeoSupply
(j)

Figure 10. Field photographs of conglomerate with chert pebble facies. (a) Abundant, black and brown chert 2-4 cm in diameter and gastropod shell within coarse-grained sandstone matrix. Grain-size card for scale is 10 cm. (b) Cross-sectional view of sharp-based, 20 cm thick conglomerate bed with well rounded- to subangular chert pebbles exhibiting slight imbrications. Scale is 15 cm long. (c) Abundant very well sorted and rounded 1-3 cm black chert pebbles. Divisions on the Jacob staff are 10 cm long. (d) Black, blue and red chert pebbles and a single green metaigneous clast circled. Card for scale is 5 cm wide. (e) Sharp, erosional contact between fine and well sorted, mud-draped, trough cross-bedded sandstone capped by conglomerate with chert pebble facies. Circled is a metaigneous pebble next to oyster shell fragments. Card for scale to the left is 10 cm long. (f) Erosional contact of conglomerate with chert pebble facies over silty, bioturbated sandstone facies. Divisions on Jacob staff are 10 cm long. (g) Well rounded, 5 cm metaigneous clasts with chert clasts and oyster shells within very coarse-grained, poorly sorted sandstone matrix; scale is 15 cm long. (h) Coarse-grained sandstone matrix display abundant, subrounded, 10 – 30 cm metaigneous clasts, chert pebbles, and oyster fragments. Divisions on Jacob staff are 10 cm long. (i) Rounded metaigneous clasts 5 cm across within poorly sorted coarse-grained sandstone matrix that contains oyster shells and chert pebbles 2-6 cm. Card is 10 cm long. (j) Metaigneous cobble encased within exposed gypsum and anhydrite of La Popo weld located in bottom section 4W. Note the angularity and size. Figurine for scale is 10 cm tall.

4.1.3. Oyster-bearing sandstone facies

4.1.3.1. Description

This facies consists of abundant, 5-15 cm long, disarticulated oyster shells, and rare 1-4 cm gastropod fragments, within well-cemented, poorly sorted, silt- to medium-grained sand matrix that weathers tan- to brown in color. Oyster-bearing sandstone beds exhibit massive appearance, gradational basal contact, lenticular geometry, range 1-3 m thick and continue laterally for >150 m. Rarely, when metaigneous clasts, chert pebbles, and wood fragments are present together, beds may exhibit sharp basal contacts, low angle trough cross-bedding and bioturbation (Fig. 11).

4.1.3.2. Interpretation

Oyster-bearing sandstone facies were deposited in high velocity water environment characterized by rapid sediment accumulations as indicated by massive appearance and clast composition assortment. The low-angle trough cross bedding suggests deposition and lateral migration of large-scale, low-relief bedforms within high flow water conditions. Abundant oyster fauna is a strong indicator of a relatively persistent, stressed, brackish water environment (MacEachern et al., 2005; Ponten and Plink-Bjorklund, 2007; MacEachern and Gingras, 2008). Brackish environment may have been related to a combination of slow and inconsistent salt dissolution associated with La Popa salt wall, which also sourced the metaigneous clasts, mixed with marine waters carried inland by tides, such that salinity maintained below seawater salinity. Saline incursions may extend upstream for long distances (over 100 km) into deltaic distributary channels and bayou under tidal processes and slack water conditions may persist (Shanley et al., 1992; Willis, 2005). Oyster shells commonly live in lagoonal/bayou environments (Buatois et al., 2008; MacEachern and Gingras, 2008; Carmona et al., 2009). The large size and the

disarticulated but relatively intact nature of the oyster shells suggest relatively short transport distance from the living habitat environment. Together, these elements of the oyster-bearing sandstone facies indicate deposition in fluvio-deltaic distributary channels that were part of the upper delta plain.

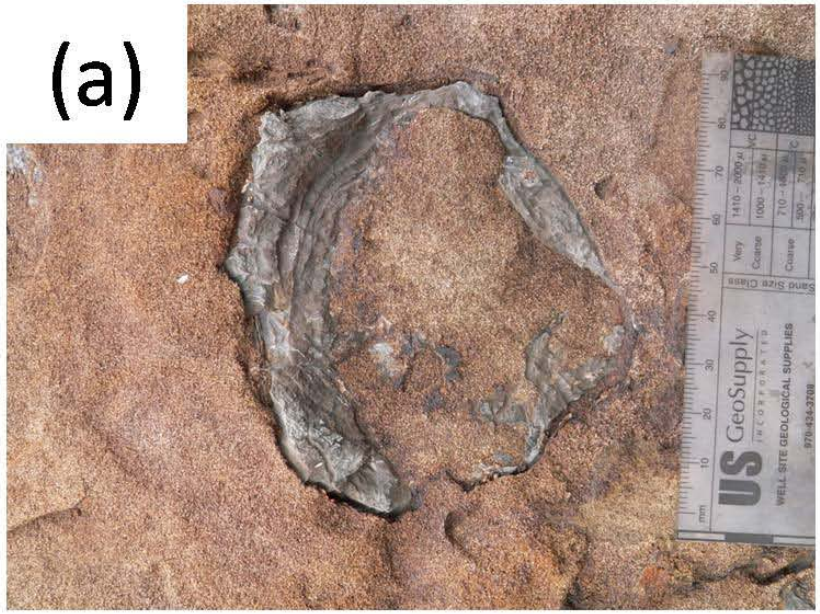
(a)
US GeoSupply
WELL SITE GEOLOGICAL SUPPLIES

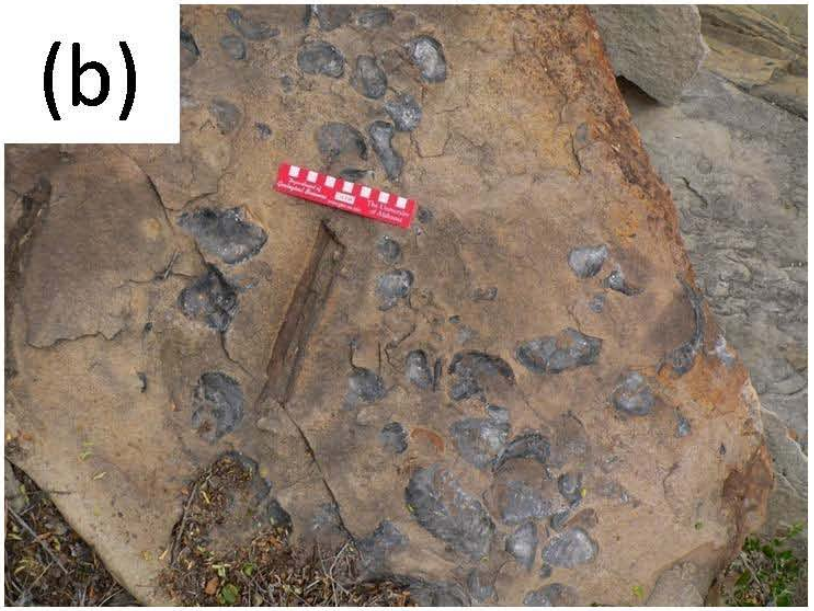
(b)

(c)

Figure 11. Field photographs of oyster-bearing sandstone facies. (a) Close-up of a well exposed and well preserved disarticulated oyster shell within a coarse-grained, brown sandstone matrix. Grain-size card is 10 cm long; (b) Abundant 5-12 cm wide, disarticulated oyster shells exposed on a bedding plane within silt to medium-grained sandstone matrix and 20 cm long wood fragment. Card is 15 cm long; (c) Abundant, 10 cm disarticulated oyster shells within coarse-grained brown sandstone matrix. Rock hammer is 33 cm long.

4.1.4. Sandstone with lag facies

4.1.4.1. Description

This facies is rare and contains poorly sorted sandstone with a pebble lag composed of clasts of variable composition. Commonly lags are rich in oyster and gastropod shell fragments that may display borings, along with well-rounded and well sorted chert pebbles 0.5-5 cm in diameter, rare metaigneous clasts 2-3 cm in diameter, and very coarse-grained sand and pisolites. Sandstone with lag occurs as 5-15 cm thick tabular sheets and rarely may preserve plane lamination. When sandstone with lag is sand-supported, it tends to exhibit imbrications, and top and basal bedding contacts are sharp but non-erosive. Sandstone with lag facies is normally graded and typically is capped by finer-grained sandstone. Individual lag horizons are discontinuous and extend laterally for only tens of meters (Fig. 12).

4.1.4.2. Interpretation

Sandstone with lag deposits facies represents relatively short-lived, poorly developed deposits that accumulated within low-relief scours within fluvio-deltaic distributary channels in lower delta plain. The normal grading and the finer-grained sandstone facies capping lag deposits indicate waning, decelerating flow conditions over time. The variable composition of clasts within sandstone lag deposits is dependent upon debris composition transported by flow in basinward direction, or in landward direction under tidal conditions. Pisolites form by the precipitation of calcium carbonate around nuclei trapped in sediment within the vadose zone of soils or marine tidal flats. Oyster and gastropod shells and boreholes indicate brackish (hyposaline) and *in situ* deposition. Narrowly sized and horizontally arranged oyster shells suggest small distance transport from the growing habitat. Sandstone with lag facies are the common result of stream processes (Miall, 1985; Pattison, 1995; Willis, 2005).

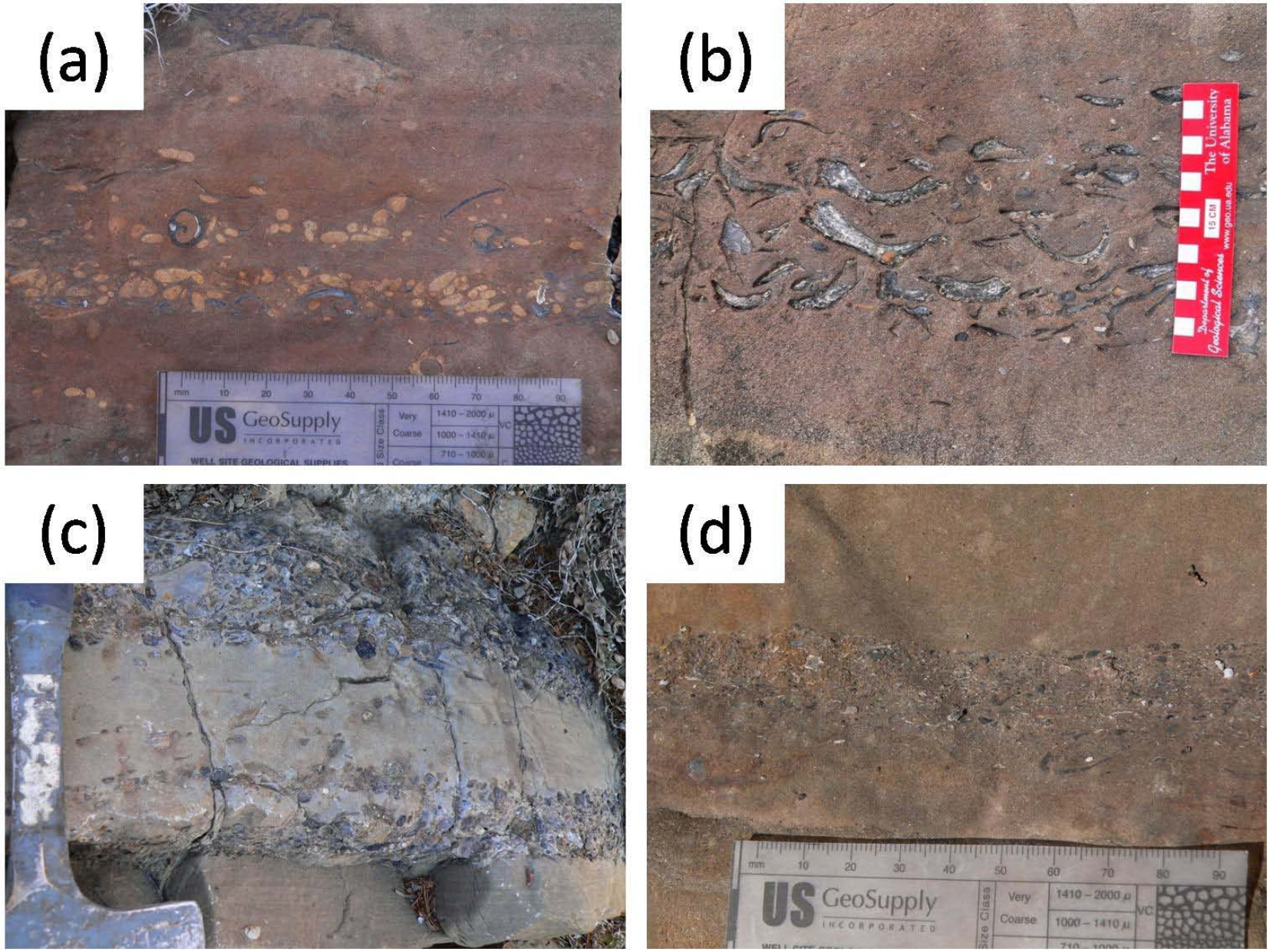
(a)
US GeoSupply
INCORPORATED
WELL SITE GEOLOGICAL SUPPLIES
Very Coarse
1410 – 2000 µ
1000 – 1410 µ
710 – 1000 µ
(b)
The University of Alabama
Department of Geological Sciences
15 CM
www.geo.ua.edu
(c)
(d)
US GeoSupply
INCORPORATED
Very Coarse
1410 – 2000 µ
1000 – 1410 µ

(e)

US GeoSupply
WELL SITE GEOLOGICAL SUPPLIES

(f)

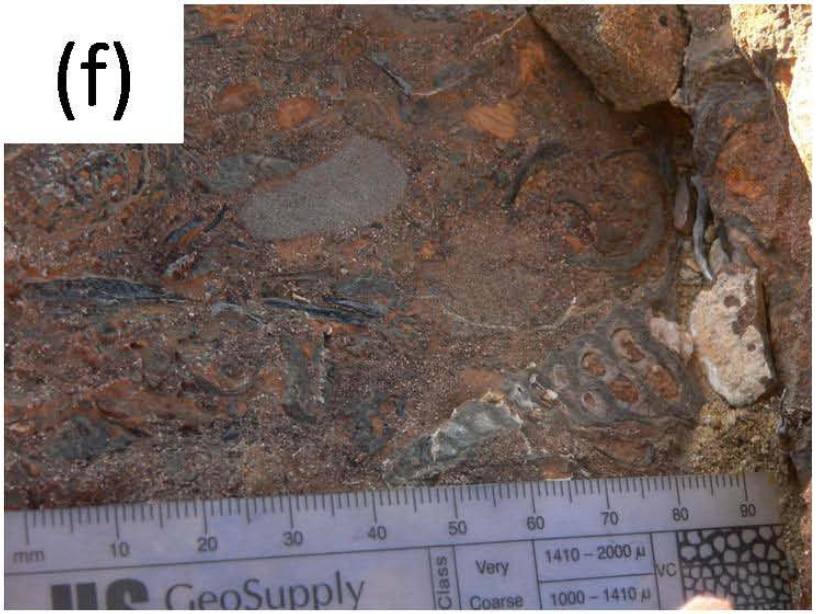
mm
10
20
30
40
50
60
70
80
90
GeoSupply
Class
Very
Coarse
1410 – 2000 µ
1000 – 1410 µ
VC

(g)

mm
10
20
30
40
50
60
70
80
90
1410 – 2000 µ

Figure 12. Field photographs of sandstone with lag facies. (a) Cross-sectional view of a medium-grained sandstone bed weathering brown, which display orderly arranged pisolites, along with rare chert pebbles and shell fragments. Grain-size card is 10 cm long. (b) Cross-sectional view of sandstone with 15 cm thick oyster lag within a medium-grained sandstone matrix. Oyster shells are horizontally bedded and exhibit borings. Card is 15 cm long. (c) Cross-sectional view of 0.5 cm chert clasts imbedded within a well- indurated medium-grained sandstone matrix. The part shown of the rock hammer is ~18 cm long; (d) Cross-sectional view of a lag composed of very coarse-grained sandstone and millimeter-sized shell fragments, encased in a fine-grained sandstone matrix. Grain-card is 10 cm long. (e) Cross-sectional view of well-rounded, 2-3 cm diameter black chert pebbles that exhibit crude imbrications, encased in a 5 cm thick medium-grained sandstone lag deposit. Grain-size card is 10 cm long. (f) Detailed view of amalgamated pebbles of metaigneous clasts and chert pebbles, along with gastropod and oyster shells, contained by a coarse-grained sandstone matrix. Grain-size card is 10 cm long. (g) Imbedded in a coarse-grained sandstone are a well-preserved gastropod next to a subrounded, intermediate, 3 cm in diameter metaigneous clast. Grain-size card is 10 cm long.

4.1.5. Sandstone with mud chips and mud intraclast facies

4.1.5.1. Description

Sandstone beds with mud chips and mud intraclasts are a common facies in the study area. It contains abundant, thin and flat, well rounded and sorted, 1-5 cm mud chips and elongated, 3-12 cm mud intraclasts. The medium-grained sandstone sometimes contains abundant silt and/or exhibits bioturbation, and is usually well-cemented and weathered orange-brown to tan. In addition, it may contain abundant shell and small wood fragments or more rarely mud intraclasts size-equivalent chert and metaigneous clasts. Sometimes, less bioturbated deposits preserve bedform current ripples and fine laminations. Beds exhibit gradational lower and upper contacts, are 2-5 m tick and laterally continuous for tens of meters (Fig. 13).

4.1.5.2. Interpretation

Sandstone with mud chips and mud intraclasts facies represents a near shore to terrestrial depositional setting such as a low-energy beach on the edge of the tidal flats and intertidal terminal distributary channel (Dalrymple and Choi, 2007). Flat mud chips and mud intraclast pebbles are produced by storms ripping up semilithified mud in supratidal settings. Intertidal terminal distributary channel is where the sediment is deposited between normal high tide and normal low tide and is generally exposed twice a day to subaerial conditions at low tide. In addition to storm events, mud chips and mud intraclast could be produced by relatively high-energy floods that eroded upstream delta plain and fluvio-deltaic channel cutbanks, and became rounded during bedload transport. High-energy events were capable of metaigneous and chert pebble bedload transport.

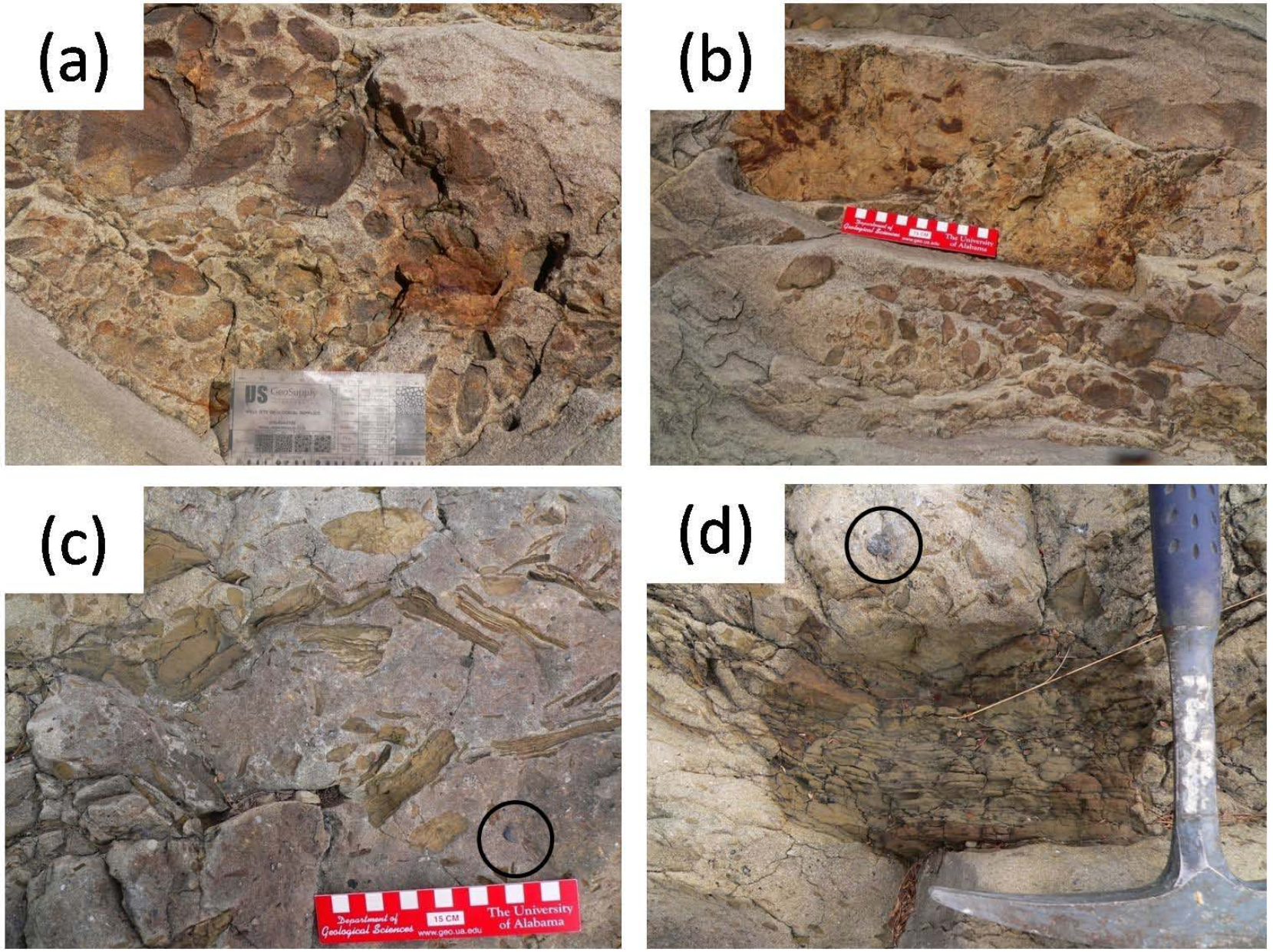
(a)
(b)
(c)
(d)
Department of Geological Sciences
15 CM
www.geo.ua.edu
The University of Alabama

Figure 13. Field photographs of sandstone with mud chips and mud intraclasts facies. (a) Sandstone bed exhibiting abundant, rounded, mud chips. Grain-size card for scale is 10 cm long. (b) Close-up of abundant mud chips in foreground and abundant wood fragments in background. Card for scale is 15 cm long. (c) Common subrounded- to elongated mud intraclasts. The circle encloses a subrounded chert pebble 1.5 cm in diameter. Card for scale is 15 cm long. (d) Rare, cobble-sized angular, mud intraclast, and a 1.5 cm in diameter metaigneous clast is shown in the circle. Pick of the rock hammer is 12 cm long.

4.1.6. Sandstone with wood fragments facies

4.1.6.1. Description

Sandstone with wood fragments facies is common within the Viento Formation It is composed of medium- to coarse-grained sandstone and contains abundant, 2-20 cm long and 2-5 cm wide wood fragments and branches. Rarely, wood fragments measure 20-60 cm long and 10-20 cm wide. Flat, 2-3 cm around mud chips and mud intraclast are common. Chert and metaigneous clasts are rare. Bioturbation is mostly absent. Sedimentary structures are difficult to recognize but this facies preserves occasionally linguloid and asymmetrical wavy ripple bedforms on the upper bedding planes. Basal bedding contacts are concave, non-erosional, gradational and top contacts are transitional to finer-grained sandstone facies. Beds are commonly 5-10 m thick and extend laterally for tens of meters (Fig. 14).

4.1.6.2. Interpretation

Sandstone with wood fragments facies represents deposits accumulated in fluvial delta plain intertidal terminal distributary channels proximal to the terrestrial realm settings, similar to where the sandstone with mud chips and mud intraclasts facies were deposited (Miall, 1985; Dalrymple and Choi, 2007). Wood fragments and medium- to coarse-grained sand were carried downstream by relative high-energy flows. Large wood fragments were likely floating in deltaic fluvial channels while smaller debris accumulated on stabilized point bars and on riverbanks in intertidal channels. Flat mud chips and mud intraclast were sourced from supratidal/intertidal zones and cutbanks deposits during storms and floods.

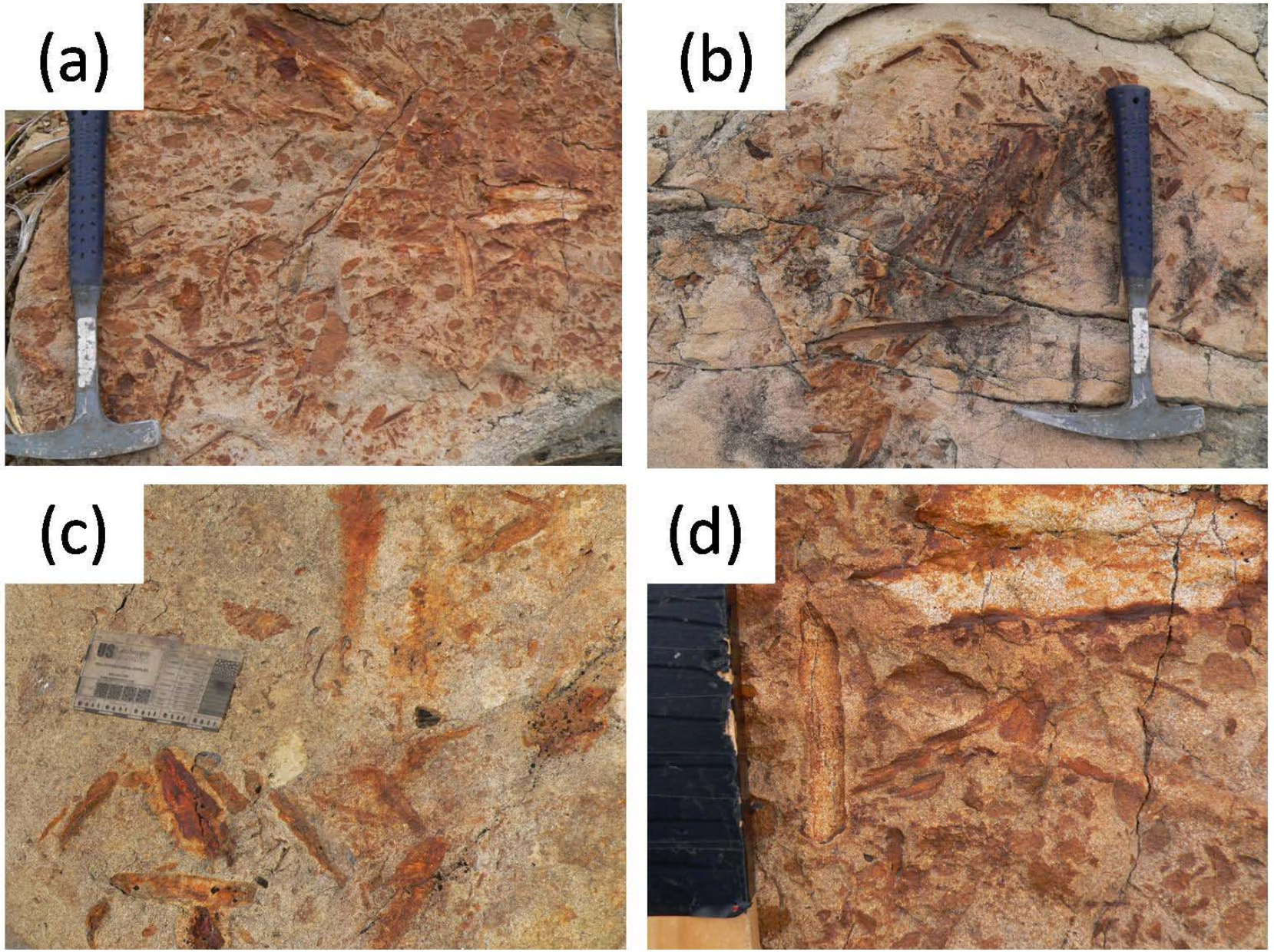
(a)
(b)
(c)
(d)

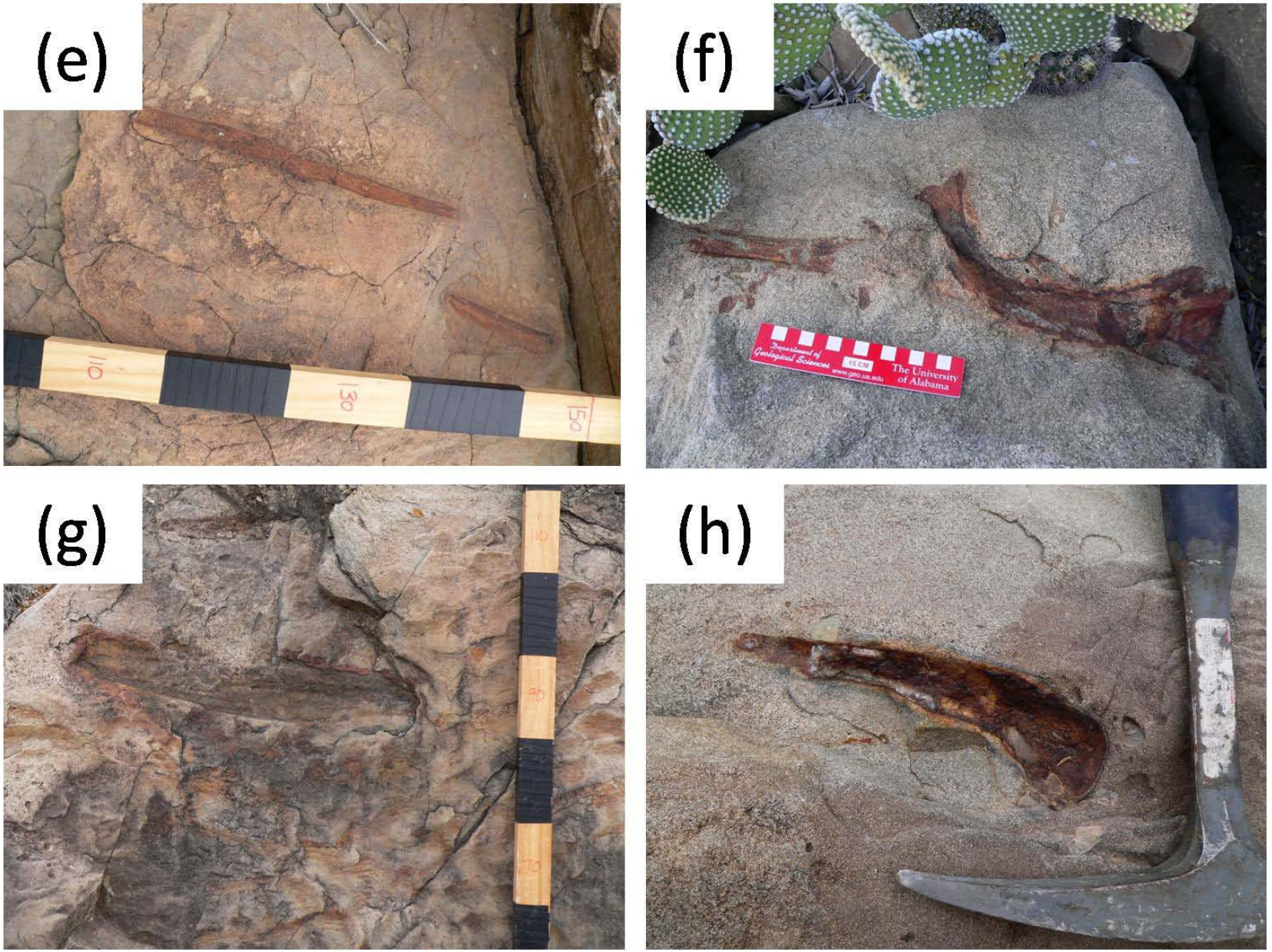
(e)
(f)
(g)
(h)
Department of Geological Sciences
www.geo.ua.edu
The University of Alabama

Figure 14. Field photographs of the sandstone with wood fragment facies. (a) Cluster of wood fragments and abundant mud chips and intraclasts. Rock hammer is 33 cm long. (b) Abundant, elongated twigs/wood fragments. Rock hammer is 33 cm long. (c) Wood fragments 10 cm long, shell debris, and 1.5 cm subrounded chert pebbles. Grain-size card is 10 cm long. (d) Close-up of 10 cm long wood fragments and centimeter- to millimeter mud chips. Division on the Jacob staff is 10 cm long. (e) Wood fragments 50x3 cm (length, wide). Divisions on Jacob staff are 10 cm long. (f) Detail of 40 cm long wood branch with branch ramification. Card for scale is 15 cm long. (g) View of bed surface displaying linguloid and asymmetrical wavy ripple bedforms along with a 50 cm long and 15 cm wide wood fragment. Divisions on Jacob staff are 10 cm long. (h) Detail of wedge-shaped wood fragment replaced by. Pick of the rock hammer is 12 cm long.

4.1.7. Limestone clast-bearing conglomeratic sandstone facies

4.1.7.1. Description

The limestone clast-bearing conglomeratic sandstone facies occur as only one bed located at the top of the Viento Formation deposits and near the contact with the overlying Carroza Formation. Distinguishable from all other sandstone conglomeratic facies, it contains abundant, very well sorted, well-rounded, pebbles- to cobbles (3-8 cm diameter) of blue wackestone within a silt-rich, fine- to medium-grained sandstone matrix that weathers brown- to dark-tan. Clast distribution is homogenous throughout this interval, which lacks sedimentary structures. The limestone clast-bearing conglomeratic sandstone facies lacks metaigneous and chert clasts, mud chips and mud intraclast, oyster shells, lag, log and wood fragments. The limestone clast-bearing conglomeratic sandstone facies overlays and is overlain by horizontally laminated heterolithic sandstone-siltstone facies. The basal contact is slightly erosional and the top contact is sharp. This bed maintains a constant thickness of 3 m and continues laterally for over 2 km. (Fig. 15). Because of its lithologic consistency, lateral extent, and distinctive clast composition, limestone clasts-bearing conglomeratic sandstone facies is used as a datum for correlations across logged sections (Appendix 1, colored dark grey).

4.1.7.2. Interpretation

The limestone clasts-bearing conglomeratic sandstone facies recorded a unique event when extraformational limestone clasts were introduced into the Viento Formation siliciclastic system. These clasts were sourced from the slumping flanks of a unit previously deposited and uplifted in top of adjacent La Popa salt wall crest. Because the age of the limestone clasts is unknown, it is also unknown the formation from which these clast originated. However, the bed length, thickness and internal composition consistency suggests that the limestone clasts were

sourced from the same unit, perhaps a cliff such as La Popa and/or San Jose carbonate lentils that formed parallel with the crest and surface trace of the salt wall. A viable source unit of these clasts is the youngest carbonate lentil of the Potrerillos Formation that were exposed topographically higher on the other side adjacent to La Popa salt diapir or the basal carbonate lentil present in section 1SE of the Viento Formation. La Popa salt diapir could not source the limestone clasts as this facies lacks metaigneous clasts, and it also lacks chert pebbles indicating that Coahuila Platform was not a viable source for the limestone clasts. The limestone clasts-bearing conglomeratic sandstone facies were deposited on the delta plain adjacent to the shore of terminal intertidal distributary channels.

(a)

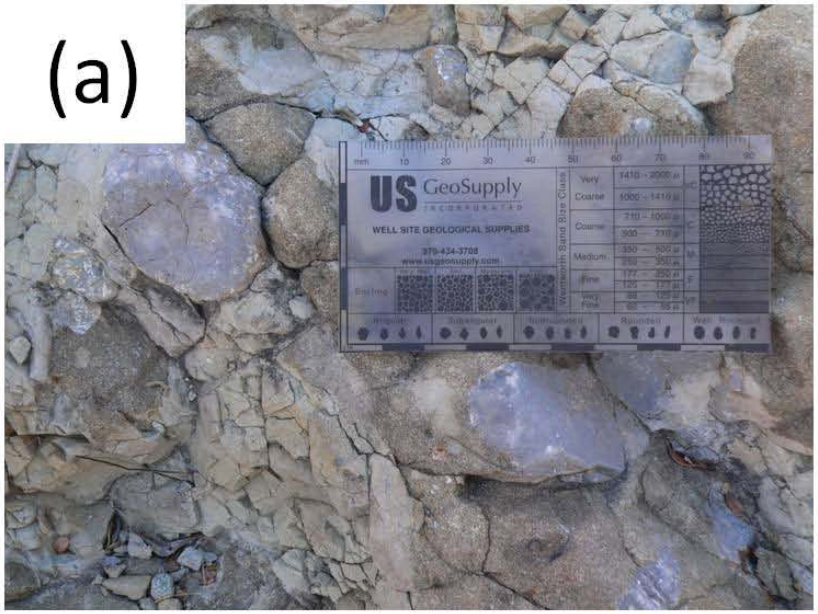
US GeoSupply
INCORPORATED
WELL SITE GEOLOGICAL SUPPLIES
970-424-3708
www.usgeosupply.com

(b)

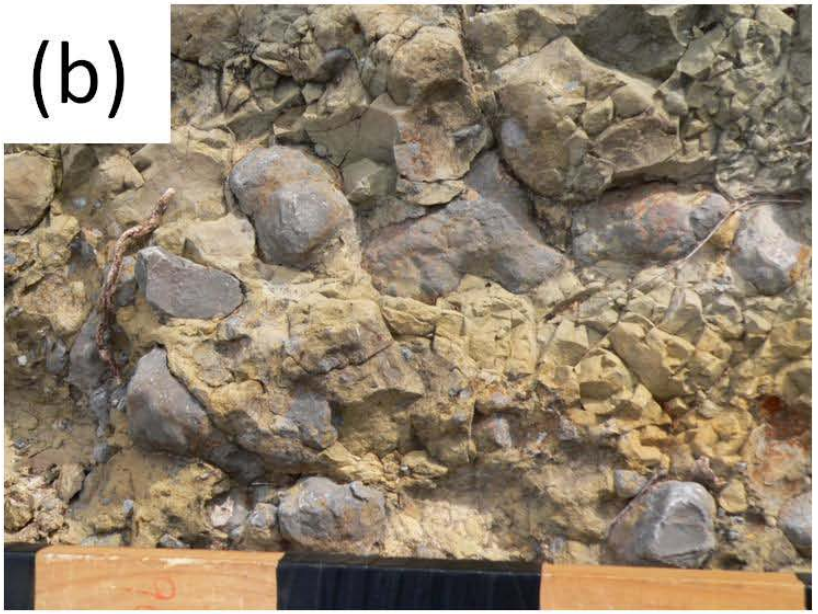

(c)

The University of Alabama

Figure 15. Field photographs of the limestone clast-bearing conglomeratic sandstone facies in basal part of section 2W, 3W and 4W. Note consistent size and roundness of limestone clasts imbedded in silt-rich sandstone matrix, and the lack of sedimentary structures. The scale used in (a) is 10 cm long, in (b) divisions on Jacob staff are 10 cm long, and in (c) card scale is 15 cm long.

4.2. Sandstone facies

4.2.1. Trough cross-bedded sandstone facies

4.2.1.1. Description

Trough cross-bedded sandstone facies are quite abundant within the study area and consist of medium- to coarse-grained, well-sorted sandstone that exhibit decimeter-scale, low-angle trough cross-stratification and rare internal thin mud-drapes. Chert and metaigneous gravel clasts, mud chips, mud intraclast, and wood debris are absent. Occasionally, this facies may be slightly bioturbated with scoured tops that are overlain by pebbly sandstone group facies. Beds weather green, tan, and brown, are extremely indurated, 1-5 m thick and extend laterally over tens of meters forming sandstone ridges across drainages (Fig. 16). In Appendix 1, this facies is colored “Forest green” (dark green).

4.2.1.2. Interpretation

This facies reflects deposition in moderate- to high-energy terminal distributary tidal channels, capable of bedload transport of medium and coarse-grained sand. Facies displaying slight bioturbation may represent periods of low tide or reduced rates of sediment discharge. The low angle, thin, mud-drapes coating the trough cross-strata are interpreted to represent mud settled out of suspension during slack-water periods at tide. Low-angle cross-stratification resulted from the lateral migration of dune bedforms within the distributary tidal channel (Shanley et al., 1992; Willis et al., 1999; Choi et al., 2004; Olariu and Bhattacharya, 2006; Coughenour et al., 2009).

(a)

(b)

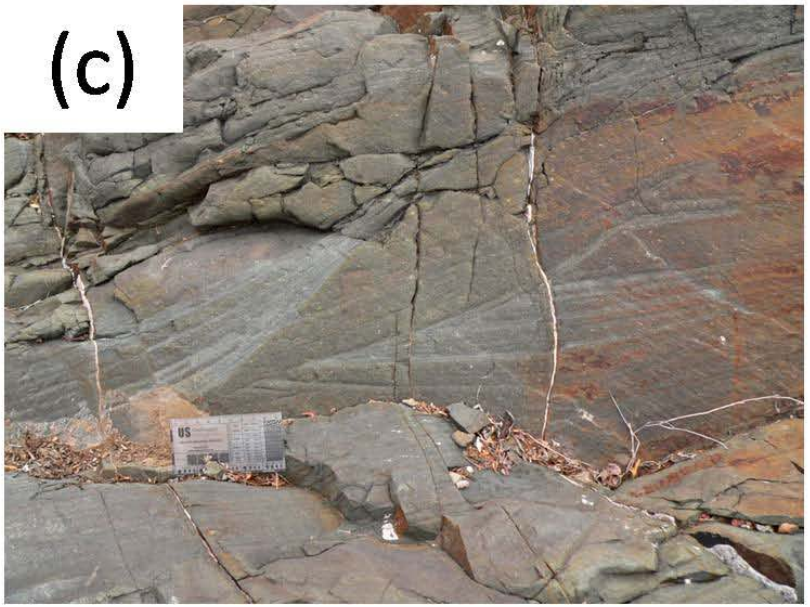
(c)

Figure 16. Field photographs of the trough cross-bedded sandstone facies. (a) Indurated, coarse-grained sandstone bed exhibiting low-angle trough cross-stratification. Rock hammer is 33 cm long. (b) Cross-sectional view of tan weathering sandstone exhibiting low-angle trough cross-bedding and internal mud drapes. Rock hammer is 33 cm long. (c) Cross-sectional view of well-preserved, green weathering, low-angle trough cross-bedding. Card is 10 cm long.

4.2.2. Ripple-laminated sandstone facies

4.2.2.1. Description

Ripple-laminated sandstone facies consists of very fine- to medium-grained sandstone that exhibits well-preserved interference current ripples (asymmetric in cross-section view), and straight-crested wave ripples, locally with persistent mud drapes. Beds are well cemented, tend to fine-upward, and weather light orange and tan- to yellow. Deposits are locally bioturbated and may contain *Ophiomorpha* burrows, 1-10 cm long wood fragments, and 1-2 cm rounded mud chips, and fine particulate shell debris. Typically, beds exhibit abrupt upper and lower contacts and occur adjacent to bioturbated, low-angle trough cross-stratification beds. Ripple-laminated sandstone facies compose ridge-forming beds up to 10 m thick that continue laterally for ≥100 m (Fig. 18). In Appendix 1, this facies is colored “custard yellow”.

4.2.2.2. Interpretation

The formation of interference current ripples and symmetrical straight-crested wave ripples involve a combination of channel (tide) and wave currents and indicates a potentially broad range of transitional deposystems near the shoreline, where river, tide, and wave processes interact (floodplain, tidal flat and stradplain) (Shanley et al., 1992; Bhattacharya and Giosan, 2003; Fielding et al., 2005a; Ponten and Plink-Bjorklund, 2007). The mud-draped ripples indicate a shallow, lower flow regime conditions, such as is found in tidally influenced distributary channels. The symmetrical straight crested ripples indicate wave flows. The wood fragments and mud chips represent terrestrial input and suggest that the depositional environment was near coastal marine environments.

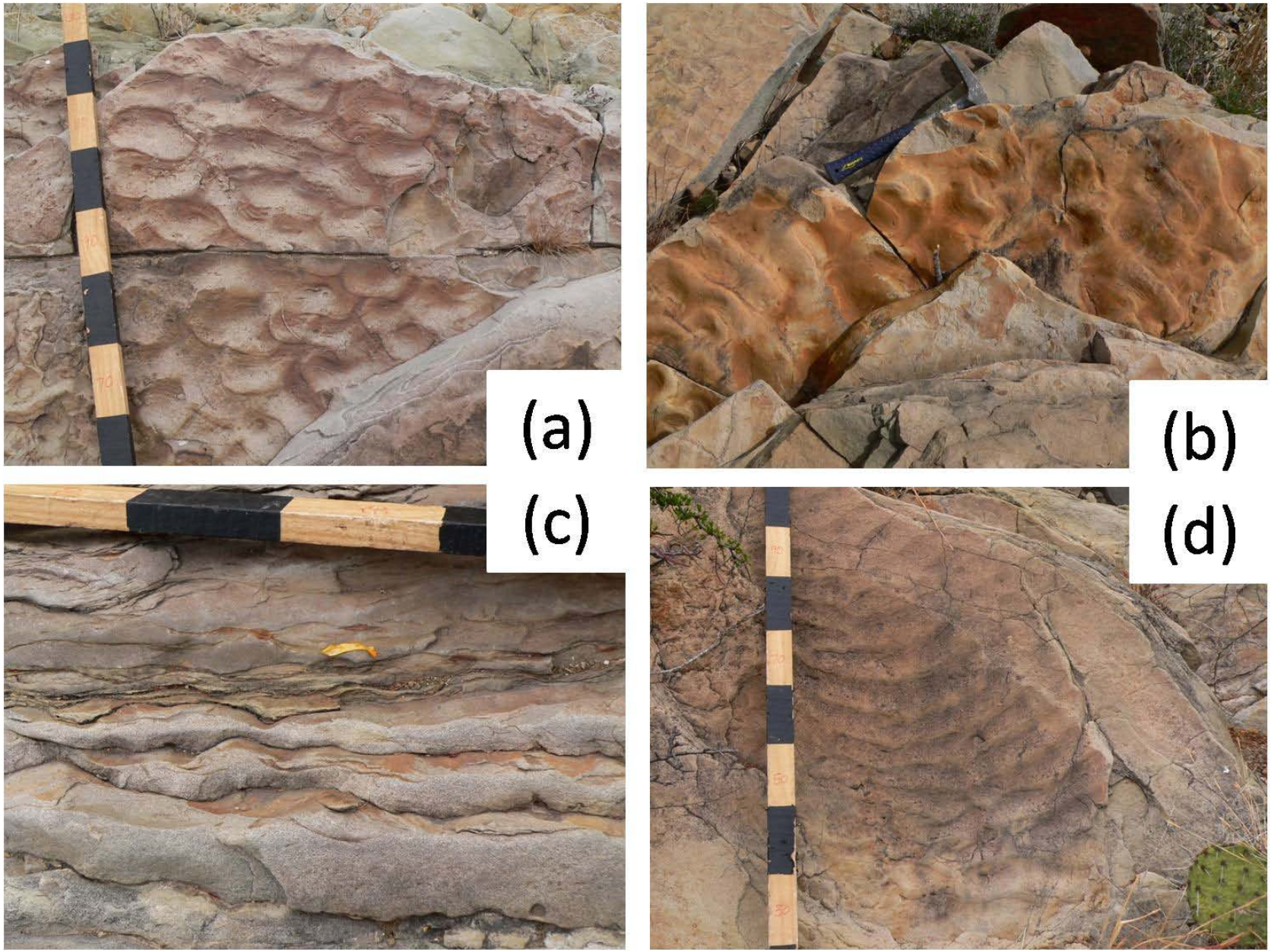
(a)
(b)
(c)
(d)

(e)

(f)

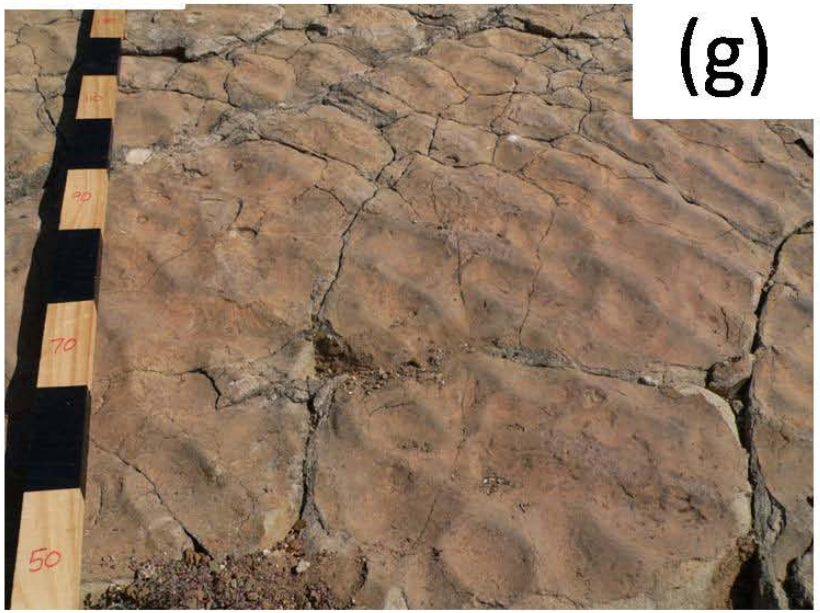

(g)

Figure 17. Field photographs of the ripple laminated sandstone facies. (a) Plan-view of bed surface displaying interference ripples. Divisions on the Jacob staff are 10 cm long. (b) Plan-view of bed surface exhibiting linguloid current ripple bedforms. Approximate paleoflow direction was from left to the right. Rock hammer is 33 cm long. (c) Detailed cross-sectional view of symmetrical current ripples (unidirectional flow) with mud drapes. Divisions on the Jacob staff are 10 cm long. (d) Bed plan-view of current ripples exhibiting slightly sinuous crests. Divisions on the Jacob staff are 10 cm long. (e) Plan-view of bed surface exhibiting straight crested wave-current ripples. Card is 8 cm long. (f) Plan-view of bed surface exhibiting straight crested wave-current ripples. Rock hammer is 33 cm long. (g) Plan-view of bed surface displaying interference ripples. Divisions on the Jacob staff are 10 cm long.

4.2.3. Inclined heterolithic stratified facies

4.2.3.1. Description

Inclined heterolithic stratification facies consist of well sorted and rounded, fine- to medium-grained sandstone exhibiting low-angle herringbone cross-stratification interbedded with ubiquitous millimeter-thick mud drapes. Herringbone cross-sets beds range from centimeters to decimeters thick and are capped by ripple bedforms draped with mud. Locally, inclined heterolithic bedding facies may display flaser bedding and bioturbation with *Ophiomorpha* burrows and may contain shell debris. Set beds weather dark-tan- to light-purple, are well cemented, exhibit abrupt bedding contact and lenticular geometry, and are up to 10 m thick (Fig. 19). This facies is colored “Bright blue” in Appendix 1.

4.2.3.2. Interpretation

Inclined heterolithic stratified facies are characterized by herringbone sedimentary structures, which are key indicator of deposition in moderate- to high-energy tidal flow conditions. The lenticular geometry and low angle cross-stratifications of inclined heterolithic sandstone-siltstone facies suggests lateral accretion deposition on point bar or channel bar surfaces within a tidal distributary channel (Shanley et al., 1992). The mudstone drapes reflect deposition from suspended load during periods of slack water. The meter-scale heterolithic herringbone bedding contain mud drapes represent slack-water intervals between tidal flows (Bhattacharya and Willis, 2001; Choi et al., 2004; Coughenour et al., 2009).

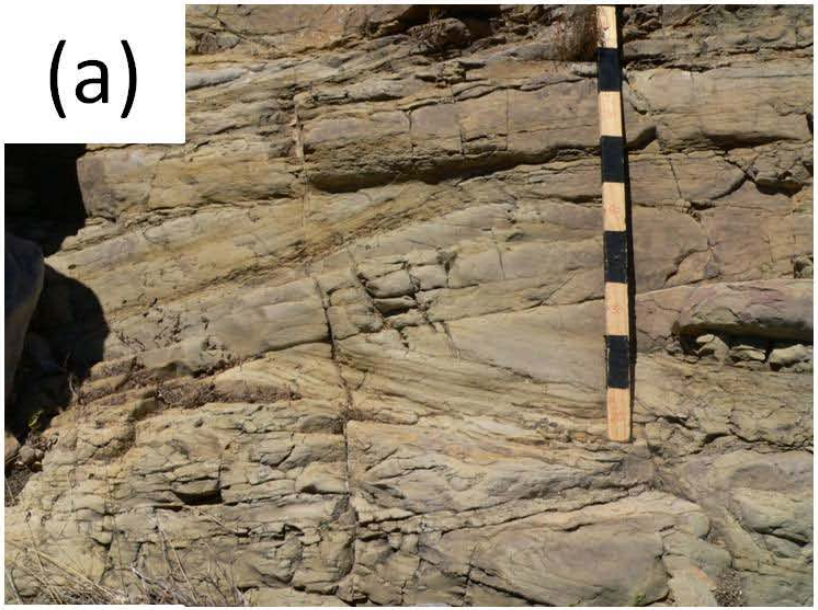
(a)

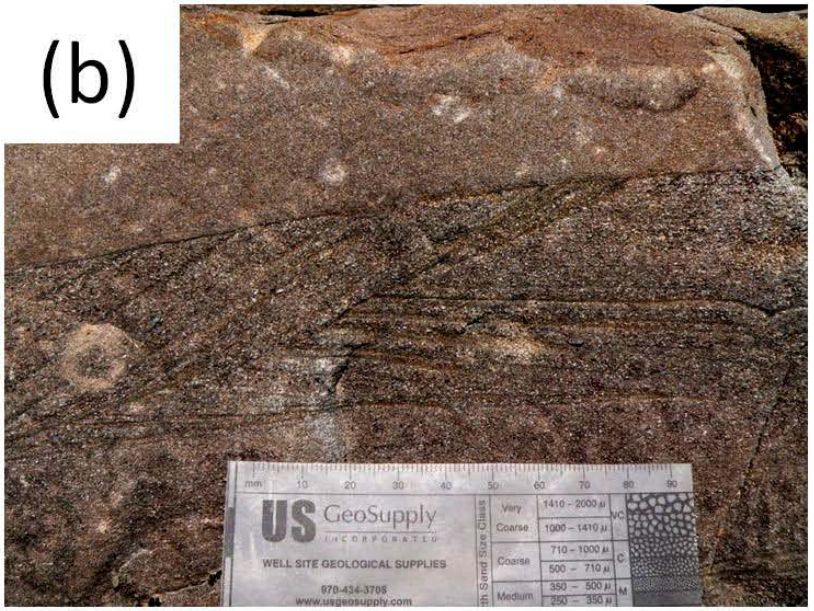
(b)
US GeoSupply
INCORPORATED
WELL SITE GEOLOGICAL SUPPLIES
970-434-3708
www.usgeosupply.com
Very Coarse
Coarse
Medium
1410 – 2000 µ
1000 – 1410 µ
710 – 1000 µ
500 – 710 µ
350 – 500 µ
250 – 350 µ
VC
C
M

(c)
15 CM
The University of Alabama

Figure 18. Field photographs of the inclined heterolithic stratified facies in cross-sectional view. (a) Medium-grained weathering tan sandstone, with internal mud laminae that highlight meters tick herringbone structure. Divisions of Jacob staff are 10 cm long. (b) Fine- to medium-grained sandstone bed exhibiting 5 cm thick herringbone structure. The bed display sharp basal and top contacts and continue laterally. Grain-card is 10 cm long. (c) Sharply capped sandstone bed laterally continuous exhibiting 8 cm thick herringbone stratification. Card is 15 cm long.

4.2.4. Spheroidal weathering sandstone facies

4.2.4.1. Description

Spheroidal weathering sandstone facies consist of well-indurated sandstones that display spheroidal/ concentric-like weathering resembling peeling-onion layers with rounded edges and weathers from brown- to green- to dark-blue. This facies consist of very fine- to fine-grained, very well sorted, and rounded sandstone. Locally, these structures may contain small-scale climbing ripples. Ichnofauna is absent. Contacts with other facies are usually abrupt. Typically, spheroidal weathering sandstones occur in association with inclined heterolithic stratified facies and together form ridges that are 5-10 m thick and laterally continuous for ~50 m (Fig. 17).

4.2.4.2. Interpretation

Spheroidal weathering sandstone facies are interpreted to represent proximal- to distal delta platform and terminal distributary channel as suggested by the association with the inclined heterolithic sandstone facies. Absence of ichnofauna may suggest low preservation potential in conjunction with low-diversity fauna, typical of stressed and possibly brackish water conditions specific to delta platform (MacEachern et al., 2005; MacEachern and Gingras, 2008). Spheroidal weathering is the result of chemically decay processes. Onion-like layers form as the joints of the rock encounter ground water that seeps into the cracks. Joints of sandstone wear away first and allows water to penetrate the rock from all angles and along the edges meters beneath the surface, where chemical decay weathers the minerals forming onion-like erosion. The process of spheroidal weathering is slow at progressively lower temperatures, which slow down the chemical process. In addition to chemical processes, onion-like erosion is facilitated by mechanical weathering processes (expansion, contraction, and exfoliation) and diagenesis.

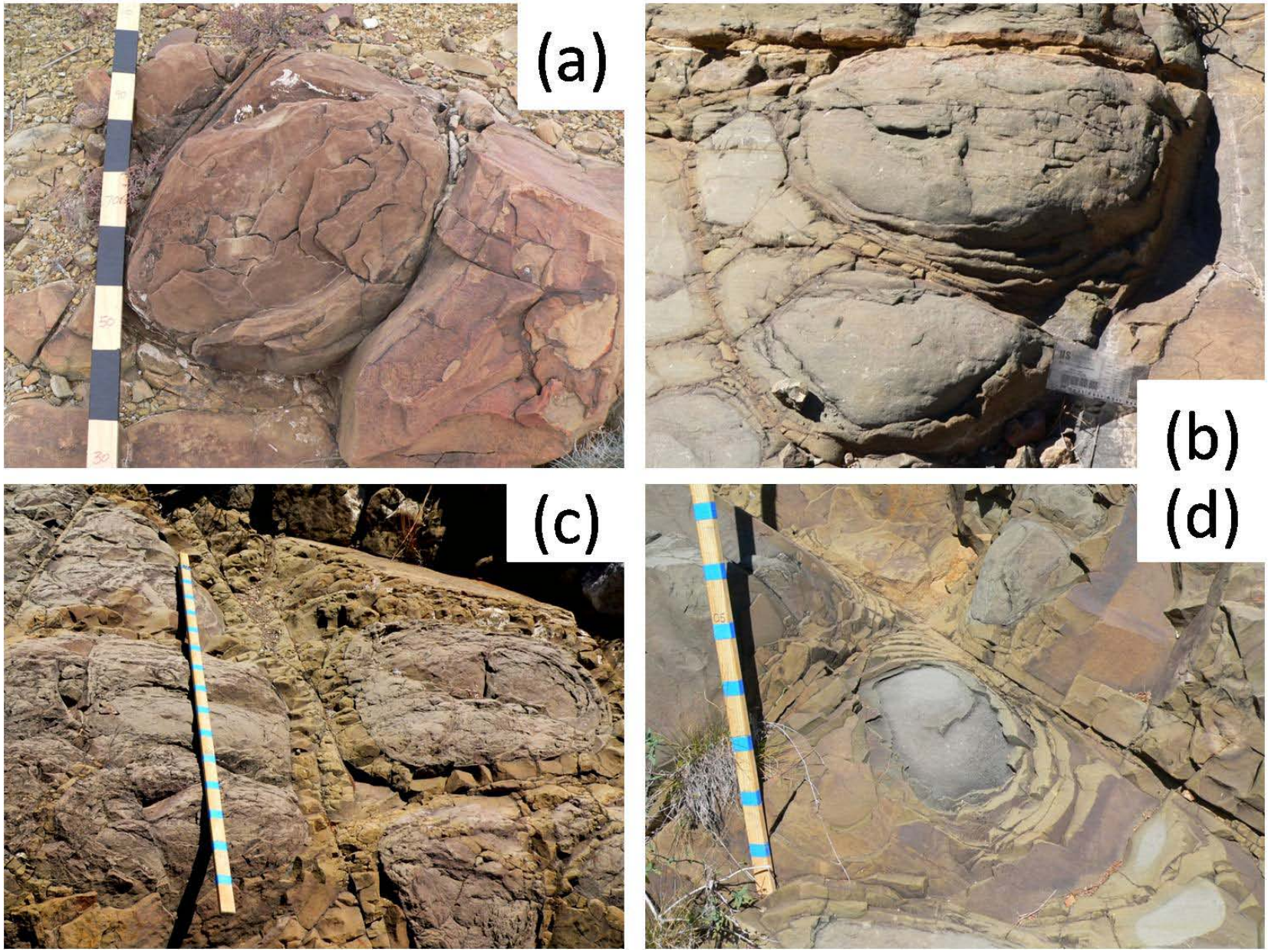
(a)
(b)
(c)
(d)

Figure 19. Field photographs of the spheroidal weathering sandstone facies. (a) Brown- to purple weathering sandstone structures that exhibit peeling-onion layers. Divisions on Jacob staff are 10 cm long. (b) Green- to tan weathering sandstone structures of various shape and size that display spheroidal erosion. Grain-card is 10 cm long. (c) Outcrop of 2 m tick multiple spheroidal weathering sandstone facies. Note arrangement with one another and the material filling in delimitating fractures. Jacob staff is 1.5 m long. (d) Detail of tan-green pillow with spheroidal weathering resembling peeling onion layers. Divisions on Jacob staff are 10 cm long.

4.2.5. Bioturbated sandstone facies

4.2.5.1. Description

Bioturbated sandstone facies are composed of pervasively bioturbated moderately sorted, silt to medium-grained sandstone. This facies contains abundant, robust, vertical and horizontal burrow structures of *Ophiomorpha* that are up to 20 cm long. In addition, locally bioturbated sandstone facies may exhibit scattered, mixed oyster and gastropod shell fragments and/or bivalve molds. Bioturbation intensity varies and ranges 10-70% such that deposits are essentially structureless. Bioturbated sandstone facies weathers red-brown- to light green. Beds have gradational bases and tops and form well-exposed and preserved 2-10 m thick deposits that continue laterally for tens of meters, usually in association with ripple laminated sandstone facies and inclined heterolithic sandstone-siltstone facies (Fig. 20). Bioturbated sandstone facies are colored “Dried sage” (light green) in Appendix 1.

4.2.5.2. Interpretation

The *Ophiomorpha* fauna observed with Viento Formation bioturbated sandstone facies indicate a stressed brackish setting. Oxygenated, brackish, water environments commonly display a low diversity high abundance of species due to the unstable environment and a lack of competition for food and space. Only a few species are equipped to live in stressed environments. Vertical *Ophiomorpha* burrows are interpreted as dwelling structures constructed following rapid sedimentation (Anderson and Droser, 1998; Buatois et al., 2008). The variability in bioturbation intensity may reflect changes in salinity, oxygen, and abundance of organisms (Carmona et al., 2009). Viento Formation bioturbated sandstone facies were highly modified by organisms, obscuring any primary sedimentary structures (extend periods of quiescence after deposition allowed sufficient time for bioturbation to disrupt previously formed sedimentary

structures but no current strong enough to create new structures). Bioturbated sandstone facies represent mouth bar, tidal flat, proximal delta front, and lower shoreface deposits (Anderson and Droser, 1998; MacEachern et al., 2005; MacEachern and Gingras, 2008; Buatois et al., 2008; Carmona et al., 2009).

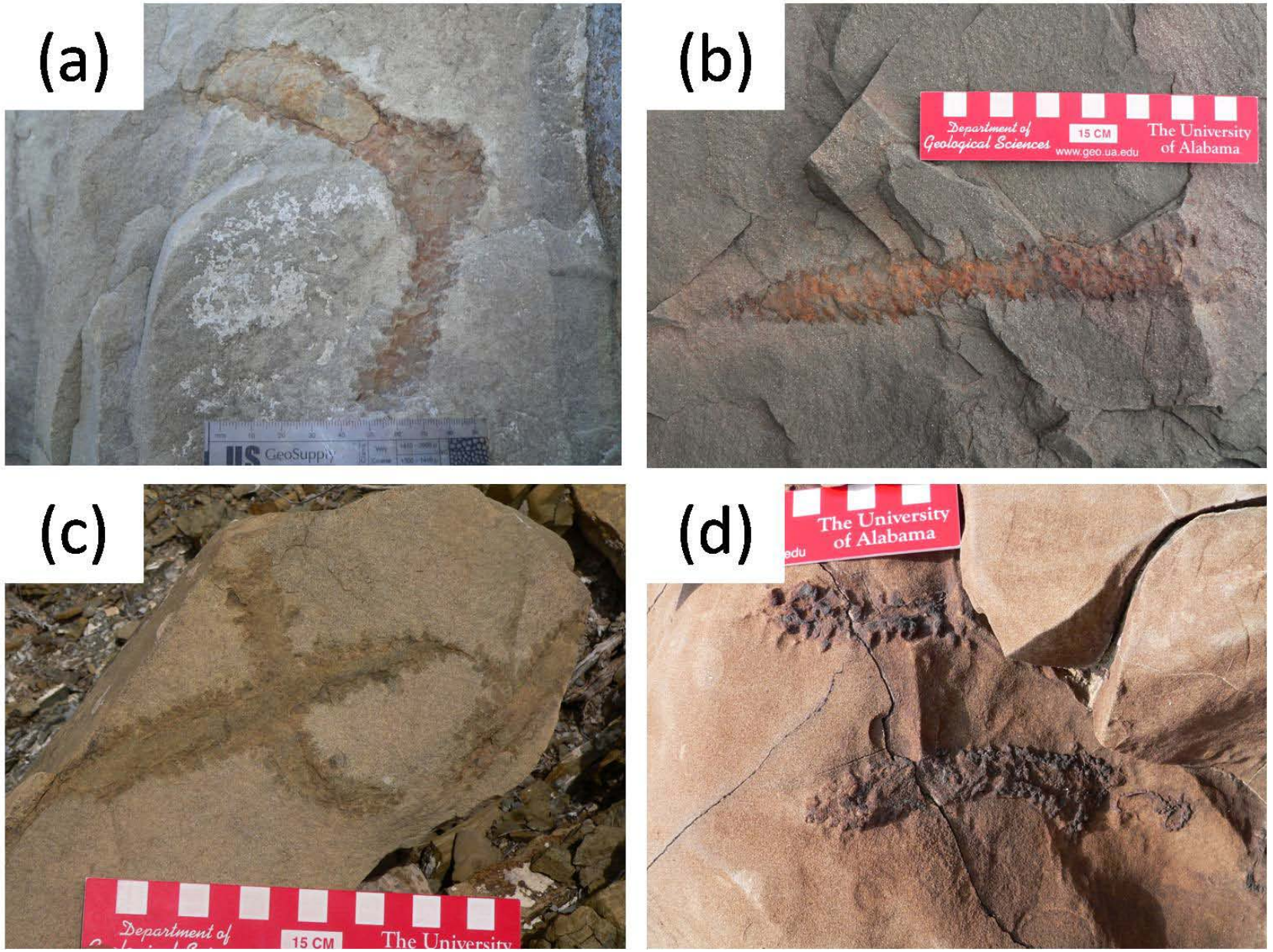
(a)
(b)
Department of Geological Sciences
15 CM
www.geo.ua.edu
The University of Alabama
(c)
(d)
The University of Alabama

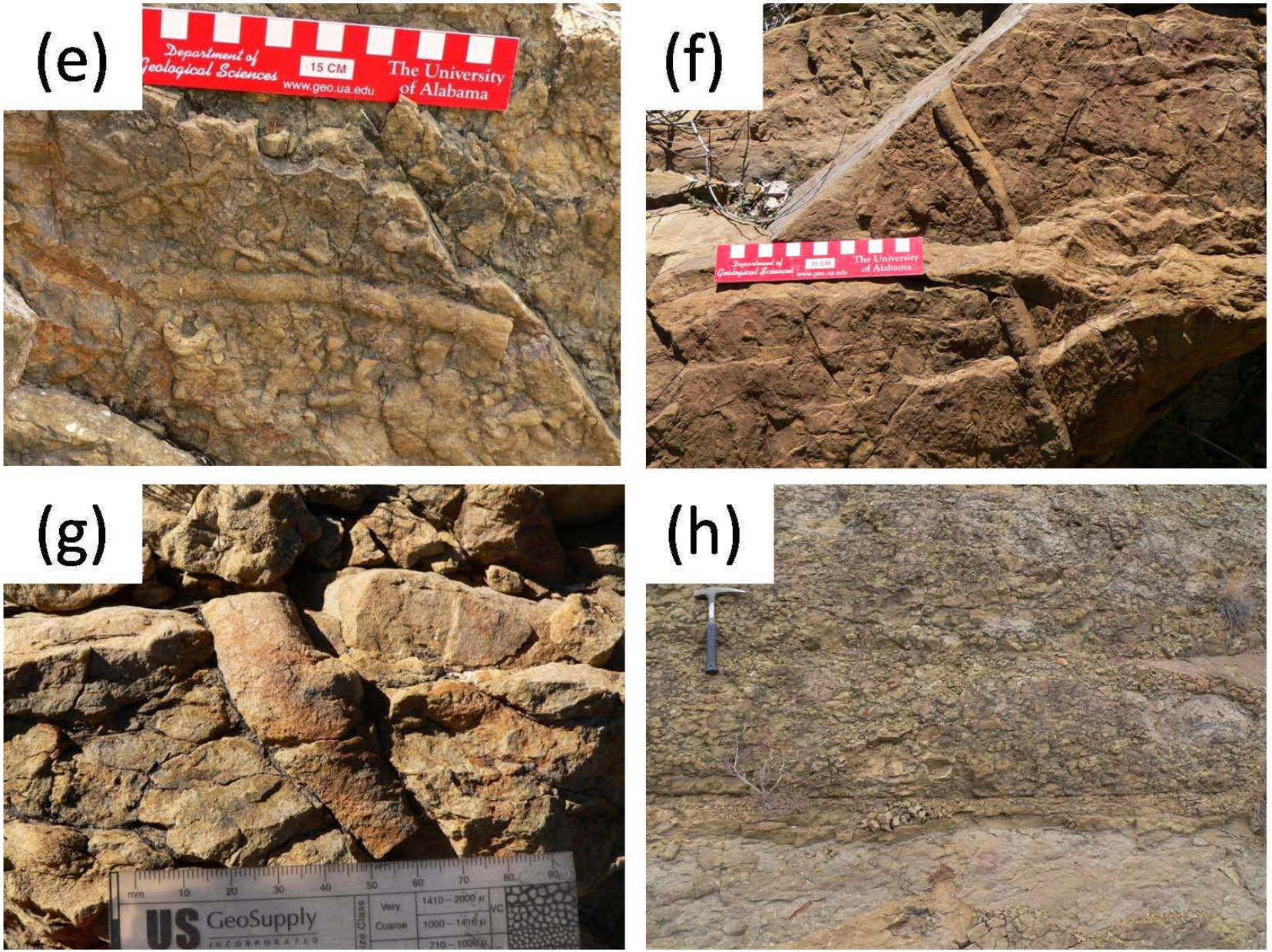
(e)
Department of Geological Sciences
15 CM
www.geo.ua.edu
The University of Alabama
(f)
(g)
US GeoSupply
INCORPORATED
(h)

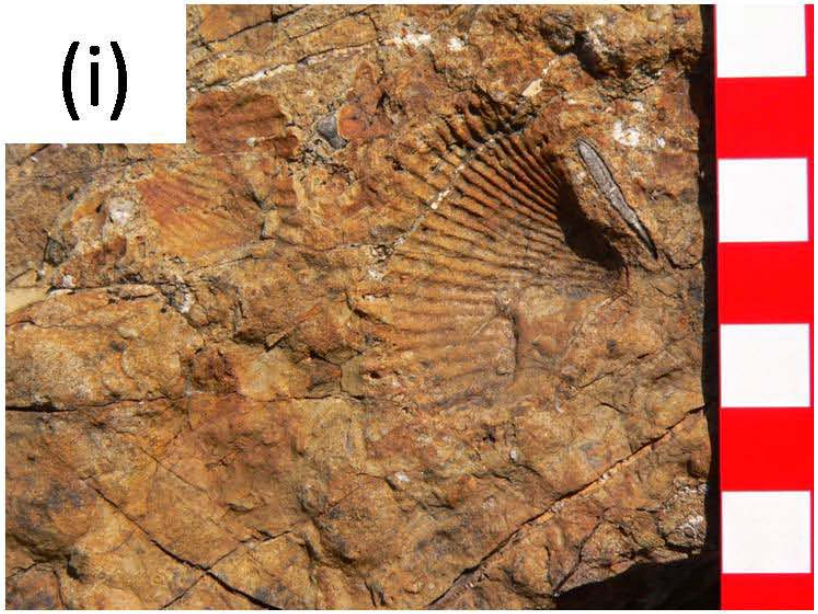
(i)

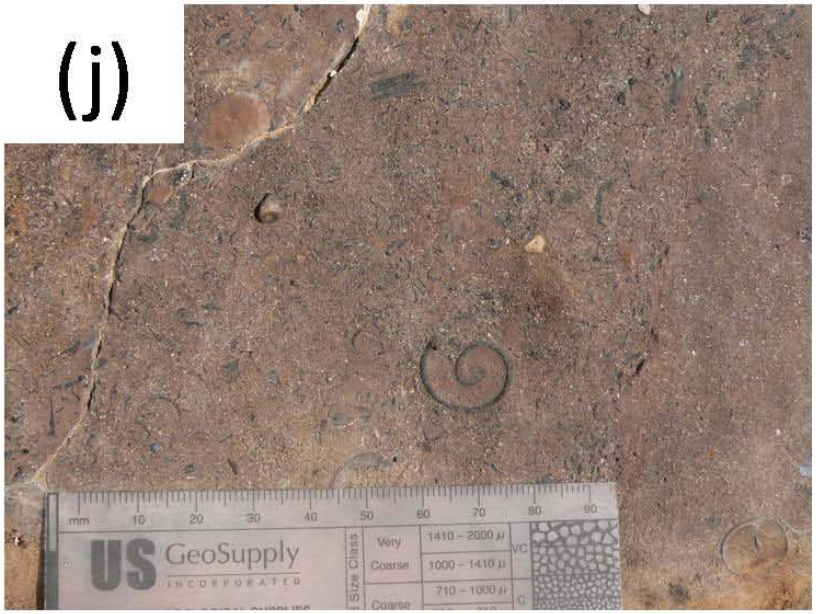
(j)
US GeoSupply
INCORPORATED

(k)
15 CM
The University

(l)
The University of Alabama

Figure 20. Field photographs of the bioturbated sandstone facies. (a) Detail of curved *Ophiomorpha* in plan-view. Note pellets used to consolidate the burrow. Grain-card is 10 cm long. (b) Detail view of robust, 20 cm long, *Ophiomorpha*. Card is 15 cm long. (c) Plan-view of crossing *Ophiomorpha* burrows. Card is 15 cm long. (d) Two nearby *Ophiomorpha* burrows. Card is 6 cm long. (e) Abundant burrows that have destroyed any primary sedimentary structures. Card is 15 cm long. (f) Trace fossils clusters and intense bioturbation that obscured primary sedimentary structures. Card is 15 cm long. (g) Well-preserved *Ophiomorpha* burrow 5 cm long. Stratigraphic up is up. Card is 10 cm long. (h) Outcrop-scale of bioturbated sandstone facies in plan-view. Stratigraphic up is toward the bottom of the picture. Rock hammer is 33 cm long. (i) Bivalve imprints in plan-view. Divisions to the right are in centimeters. (j) Gastropod 1.5 cm in diameter and shell debris in plan-view. Card is 10 cm long. (k) and (l) Plan view of *Ophiomorpha* grazing traces and bioturbation. Card is 15 cm long.

4.2.6. Oyster facies

4.2.6.1. Description

The oyster facies is limited to a single bed in the lowermost part of Viento Formation next to the carbonate facies (in sections 1W and 2W, Appendix 1). Oyster facies contains primarily abundantly, well sorted and sized 2-4 cm large, disarticulated oyster shell fragments, within a fine- to medium-grained sandstone and micrite matrix. The matrix weathers dark tan to light blue, reacts with 10% diluted hydrochloric acid and is extremely well indurated and resistant to erosion. Rare well-rounded, black chert pebbles are also present in this facies. Both lower and upper contacts are sharp. Bedding geometry is tabular and thickness is consistent 3-5 m thick and extends laterally for >100 m (Fig. 21). Oyster facies are colored “Night blue” (navy) in Appendix 1.

4.2.6.2. Interpretation

Oyster facies were deposited in a warm, shallow, and marginal marine- to lagoonal setting. The oyster shell abundance and narrow size range (almost all are 2-4 cm long) indicate high mortality rates and relatively a short period of environment stability that ended abruptly. In addition, oyster shells are aligned horizontally and are disarticulated, suggesting short distance transport from the growing habitat. High concentration of carbonate-mud production indicates degradation of skeletons and nutrient rich waters favorable to organism growth. The exclusive presence of the oyster reef facies near La Popa salt diapir suggest that the oyster deposit may have grown in top of the submerged diapir. Along with seawater carried inland by tide, dissolution of salt may have created a hyposaline (brackish) environment, providing a habitat conducive to fast oyster growth.

(a)
mm
10
20
30
40
50
60
70
80
90

(b)

(c)
Department of Geological Sciences
15 CM
www.geo.ua.edu
The University of Alabama

Figure 21. Field photographs of the oyster facies. Note the abundance of oyster shells and narrow size range from 2-4 cm long. (a) Weathering color of oyster facies bed located in the basal section 1W. Grain-card is 10 cm long. (b) Weathering color of oyster facies bed located in the basal section 2W. Rock hammer is 33 cm long. (c) Weathering color of oyster facies bed located between section 1W and 2W. Card is 15 cm long.

4.2.7. Horizontal heterolithic stratified facies

4.2.7.1. Description

Horizontal heterolithic stratified facies consists of 5 cm to 20 m thick sets of alternation sandstone and siltstone beds. Sandstone beds are 2-12 cm thick, tabular, fine upward, and exhibit massive, plane, or fine ripple laminations. The sandstone beds are composed of very fine-grained, very well sorted, very well rounded sand, and rarely contain0.5-1 cm long scattered shell debris and/or poorly developed trace fossils. Siltstone beds exhibit wavy contacts, internal symmetrical current-ripple laminae and are millimeters to decimeters thick. Individual alternation of sandstone and siltstone layers may display lateral thickness variation, but bedsets show tabular geometries. Siltstone beds weather green-olive- to dark-grey, whereas sandstone beds weather dark-tan to brown-orange. Horizontal heterolithic stratified facies continue laterally for >2 km and are associated with tan fissile shale facies. When rock exposures are not available, lateral continuity within the slope is demarcated by modern lower topography covered by vegetation (Fig. 22). This facies is colored maroon “Mocha” on Appendix 1.

4.2.7.2. Interpretation

Horizontal heterolithic stratified facies were deposited by the combined mechanisms of high energy and strength bottom currents capable of bedload transport, and suspension gravitational-fallout during low-energy conditions. Alternating thin beds of siltstone with fine-grained sandstone and tan fissile shale facies are consistent with deposition in a distal delta front and/or delta mouthbar setting (Bhattacharya and Walker, 1992; Willis et al., 1999; MacEachern et al., 2005; Olariu and Bhattacharya, 2006; Coughenour et al., 2009; Bhattacharya and MacEachern, 2009). Repeatedly interbedded sandstone-siltstone bedsets suggest frequent and abrupt alternations in current strength and fluctuation rates of sediment discharge during

intertidal periods. The finest fraction is composed of siltstone, which indicates deposition in low-energy conditions when mud settled gravitationally out of suspension, perhaps during slack periods. Symmetric, oscillation ripples indicate back-and-forth current movement (tidal inlets). Scattered shell debris and poorly developed trace fossils and structures indicate low-energy conditions and potentially a brackish depositional environment (mouth bar setting). The more bioturbated intervals may reveal periods of slower sedimentation rates that allowed time to bottom feeder organism to develop.

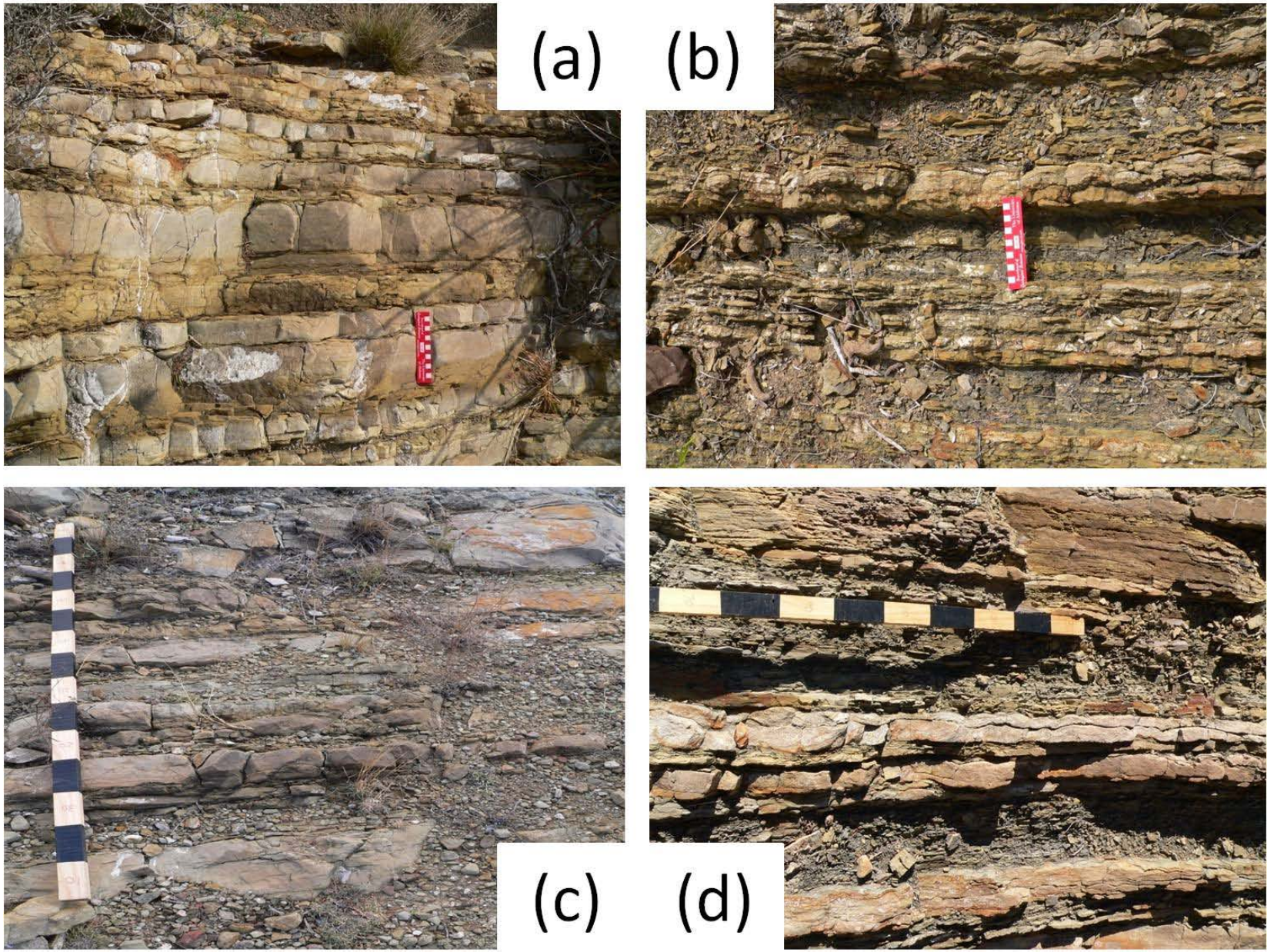
(a)
(b)
(c)
(d)

(e)

(f)

Figure 22. Field photographs of horizontal heterolithic stratified facies. (a) Interbedded sandstone and siltstone couplets exhibiting internal abrupt contacts. Note parallel bedding and distinct weathering color between lithologies. Card is 15 cm long. (b) Sandstone couplets display wavy top and abrupt contact interbedded with siltstone/mudstone layers in cross-sectional view. Card is 15 cm long. (c) Outcrop scale of sand-prone horizontal heterolithic stratified facies. Jacob staff is 1.5 m long. (d) Sandstone-siltstone interbedded unit show wavy top and sharp contact. Divisions on Jacob staff are 10 cm long. (e) View along beds strike of large-scale outcrops. Note bed continuity and local low modern topography demarked by vegetation. Jacob staff is 1.5 m long. (f) Close-up of siltstone prone interbedded sandstone-siltstone units. Divisions on Jacob staff are 10 cm long.

4.2.8. Tan fissile shale facies

4.2.8.1. Description

Tan fissile shale facies exhibits tabular beds 0.5-3 m thick that weather tan-grey and olive-green. Internally, this facies may display planar lamination and contains carbonate mud along with terrigenous clay. Ichnofauna is absent. Although in places exposures are covered, beds tend to continue laterally for hundred of meters and are abruptly capped by trough cross-bedded sandstone and/or conglomerate and conglomeratic sandstone facies deposits. In places, tan fissile shale facies crop in association with horizontal heterolithic stratified facies (Fig. 23). In Appendix 1 this facies is colored “Crimson” (dark purple).

4.2.8.2. Interpretation

Lithology and limited bed thickness development indicate that the tan fissile shale facies was deposited out of suspension in calm waters of abandoned distributary channels/oxbow lakes, and/or intermittently flooded interdistributary bay and prodelta/offshore marine environments (Dalrymple et al., 1992). Tan-gray and olive-green weathering colors indicate an increased concentration of clay minerals (chlorite, illite, and biotite). The outcropping of tan fissile shale in association with horizontal heterolithic stratified indicates decrease in water flux energy and sediment discharge rates.

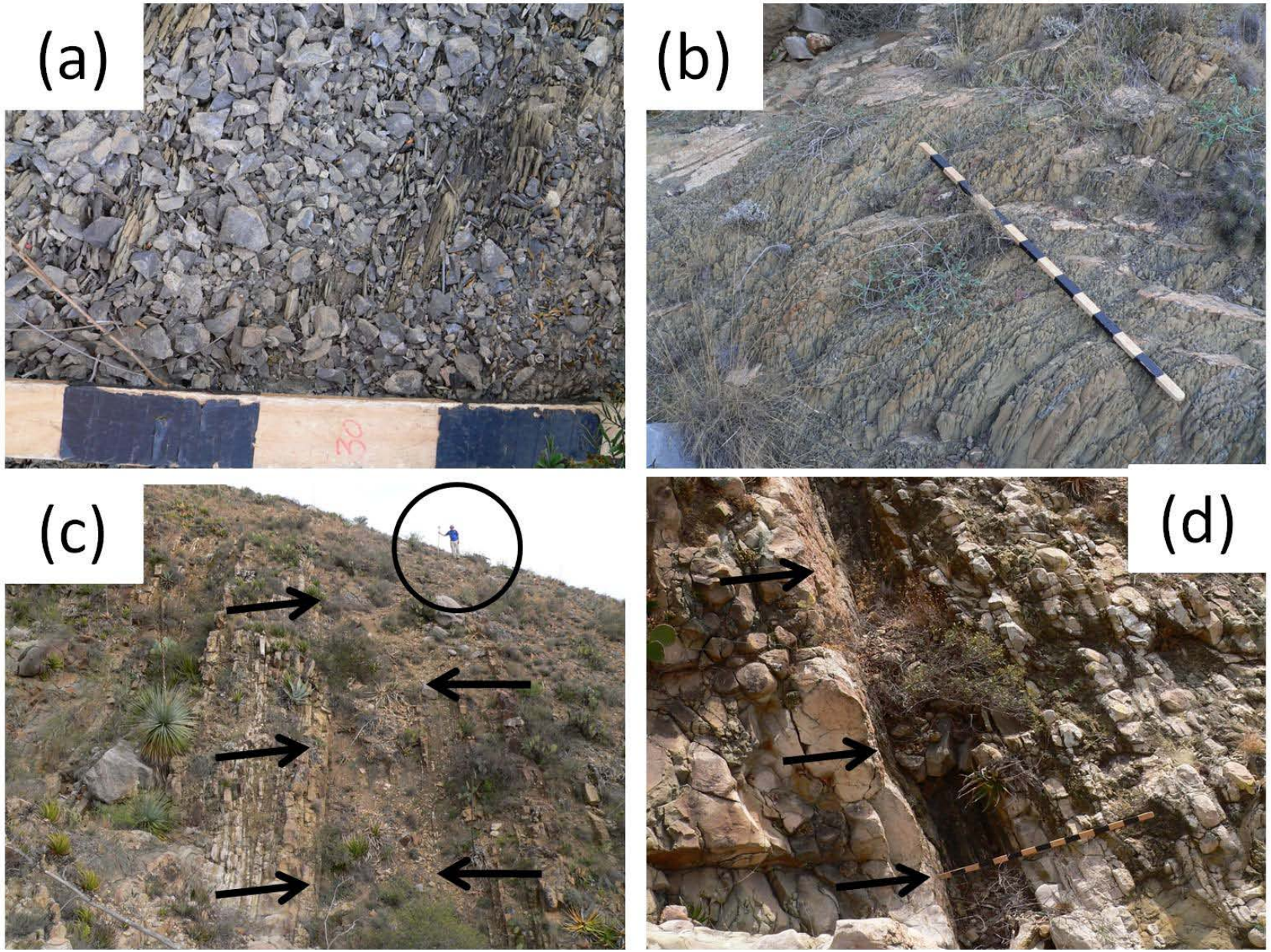
(a)
(b)
(c)
(d)

Figure 23. Field photographs of the tan fissile shale facies. (a) Close-up of tan- to grey weathering fissile shale facies. Divisions on Jacob staff are 10 cm long. (b) Outcrop with tan fissile shale facies weathering olive-green. Jacob staff is 1.5 m for scale. (c) Strike view of tan fissile shale facies bound by sandstone facies. Arrows point at the contact of tan fissile shale facies. Stratigraphic up is to the right. Person circled for scale. (d) Sharp lithology break between ripple laminated sandstone and horizontal heterolithic stratified with 60 cm thick interbedded tan fissile shale facies in section 3W at meter 150. Arrow points at the sharp contact. Stratigraphic up is to the right. Jacob staff is 1.5 m.

4.2.9. Purple mudstone with paleosols facies

4.2.9.1. Description

The purple mudstone with paleosols facies occurs only adjacent to La Popa weld in sections 1SE and 3W, and consists of an up to 3 m thick mudstone bed that weathers purple and contains paleosols. Paleosols exhibit well-developed blocky- to subrounded calcareous nodules 5-20 cm in diameter (Fig. 24). In section 3W, the purple mudstone with paleosols facies exhibits a gradational basal contact with tan fissile shale facies and is capped by the oyster facies. Purple mudstone with paleosols facies crops out discontinuously only near evaporite exposures in the basal part of measured sections. Outside the study area and toward southeast, the purple mudstone with paleosols facies continues along the strike of the surface trace of La Popa weld. This facies is colored “Red” on Appendix1.

4.2.9.2. Interpretation

Well-developed nodular calcareous paleosols indicate subaerial/arid climate and potentially sabkha conditions associated with La Popa salt wall (Lawton and Buck, 2006; Aschoff and Schmitt, 2008; Buck et al., 2009). Purple weathering color is obtained thru post-depositional subaerial oxidation of iron-bearing minerals. Given the stratigraphic and structural vicinity of La Popa salt diapir, the calcareous paleosols nodules may have formed in top of the subaerially exposed crest of the diapir that exhibit topographic relief surrounded by brackish and/or non-marine waters.

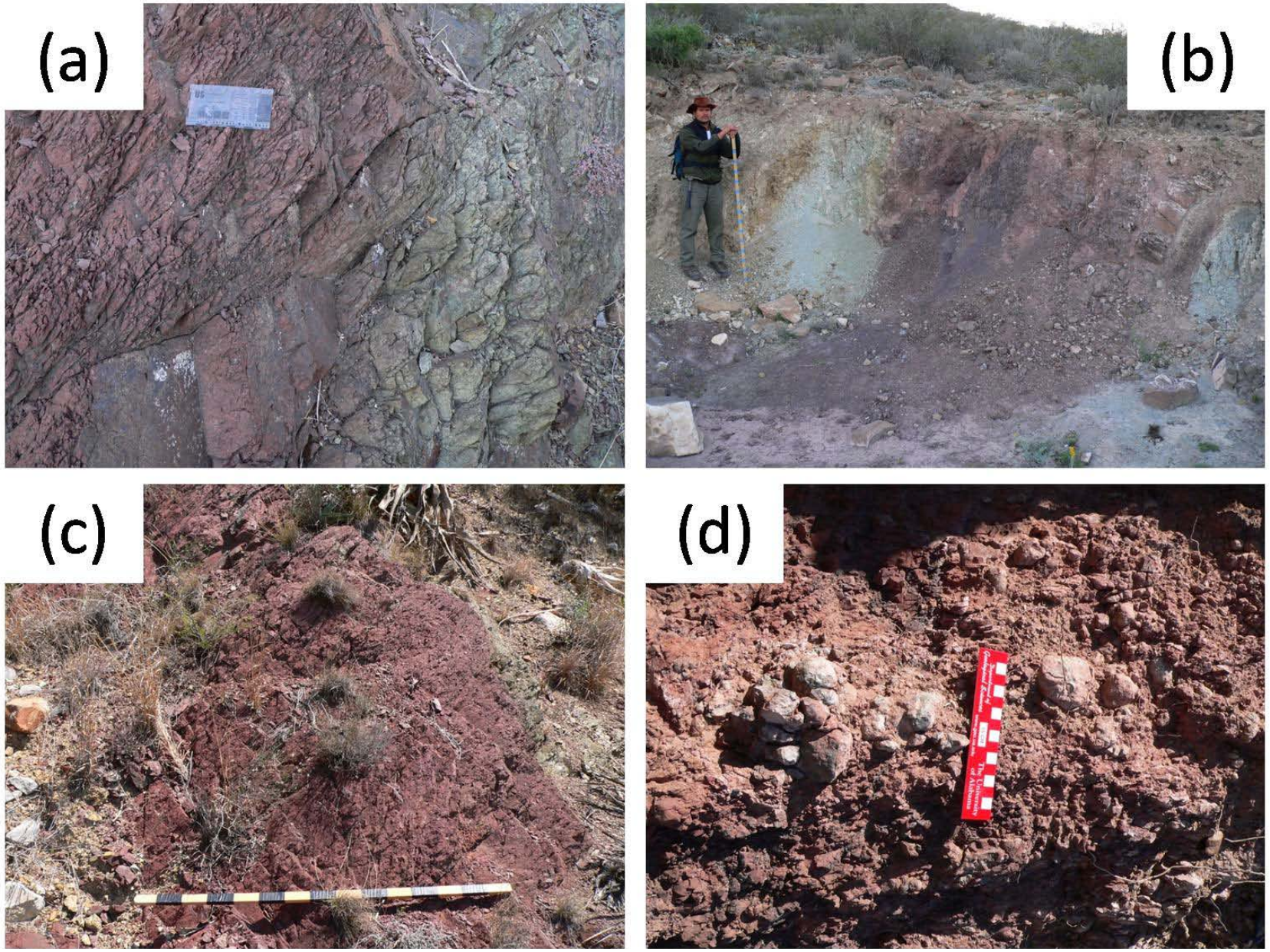
(a)
(b)
(c)
(d)

Figure 24. Field photographs of the purple mudstone with paleosols facies. (a) Close-up of gradational transition from tan fissile shale facies into the purple mudstone with paleosols facies located in basal section 3W. Card is 10 cm long. (b) Purple mudstone with paleosols facies outcrop near the basal section 1SE. Note bed dip is 90° consistent with local beds dip. Stratigraphic up is to the left. Purple mudstone with paleosols facies is flanked by tan fissile shale facies. Person for scale. (c) The purple mudstone with paleosols bed is 1.5 m thick in section 3W. Jacob staff is 1.5 m long perpendicular to the bed strike. (d) Detailed image of subrounded, well-defined calcareous paleosols nodules in section 1SE. Card is 15 cm long.

4.3. Limestone facies

4.3.1. Massive limestone facies

4.3.1.1. Description

The massive limestone facies is exposed in two locations near La Popa, salt weld and consist of discontinuous packestone to wackestone beds 3-15 m thick that exhibit micro-karst weathering cavities. Weathering color is light- to dark-grey and internal bedding is not distinguishable. It lacks macrofossils but biserial foram/echinoid spine and coral fragments were observed in thin-section. At the location in section 1SE, the massive limestone facies crops out as a massive, well-defined topographic structure, referred as a lentil, with concave basal and convex upper contacts, and continues laterally for approximately 100 m in either direction. In contrast, at the second location near the bend of the weld, massive limestone facies exhibit subrounded, poorly sorted, blocky, limestone boulders (Fig. 25). This facies is colored “Pigeon” (light gray) on Appendix 1.

4.3.1.2. Interpretation

Carbonate mud (micrite) forms commonly in low-energy, clear, warm, and shallow-marine settings. Micrite may be precipitated chemically or biochemically from seawater, derived from the abrasion of pre-existing calcium grains, or form during disintegration of calcareous green algae in still water of protected/sheltered lagoons and/or tidal flats. The massive limestone facies formed on the crest of La Popa diapir. The second outcrop, which consists of blocky limestone boulders, resembles debris flow and avalanche deposits of carbonate slumps that may have fallen from the top of the diapir and its flanks at the time when the diapir was inflated.

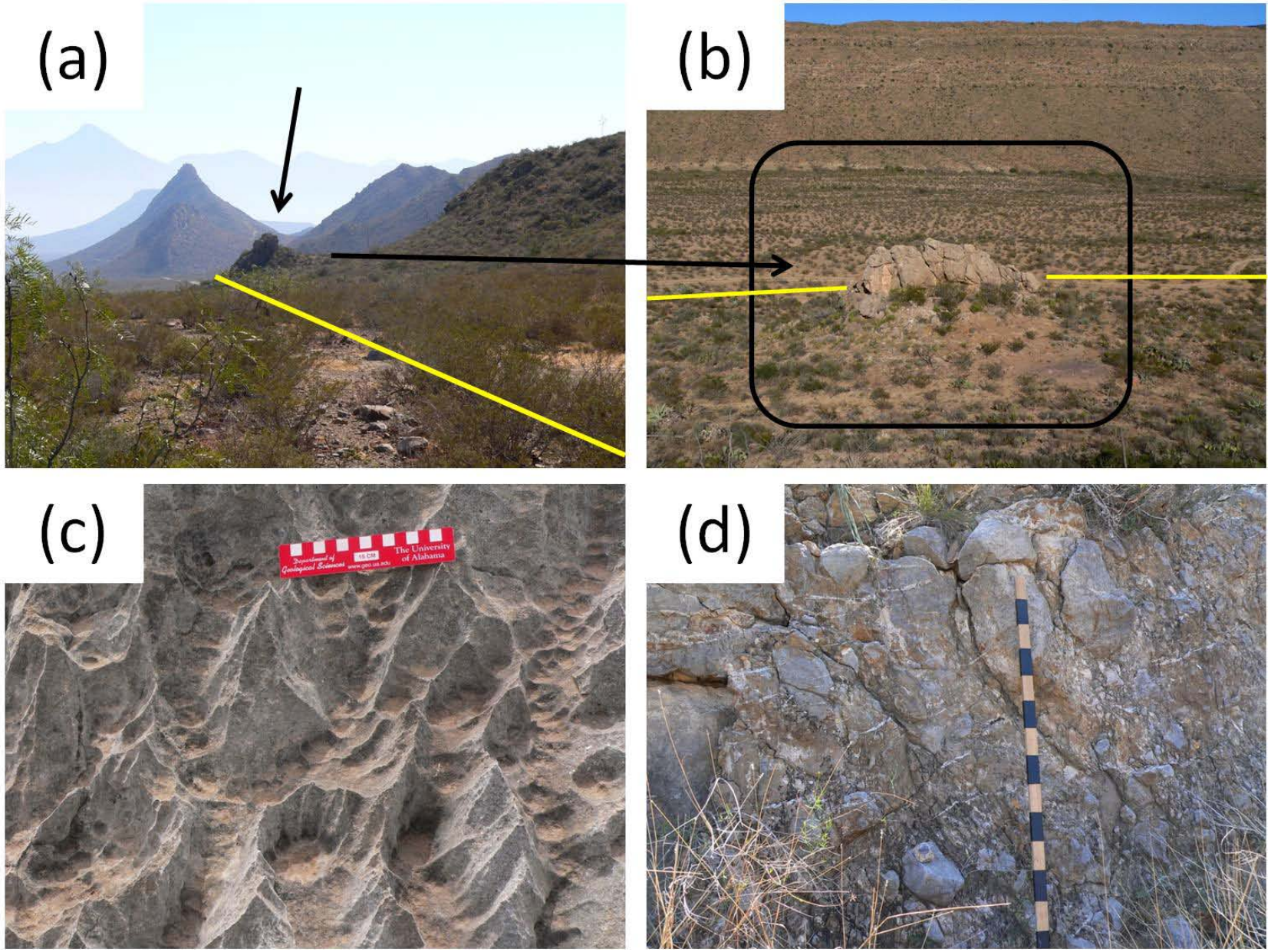
(a)
(b)
(c)
(d)
Department of Geological Sciences
www.geo.ua.edu
15 CM
The University of Alabama

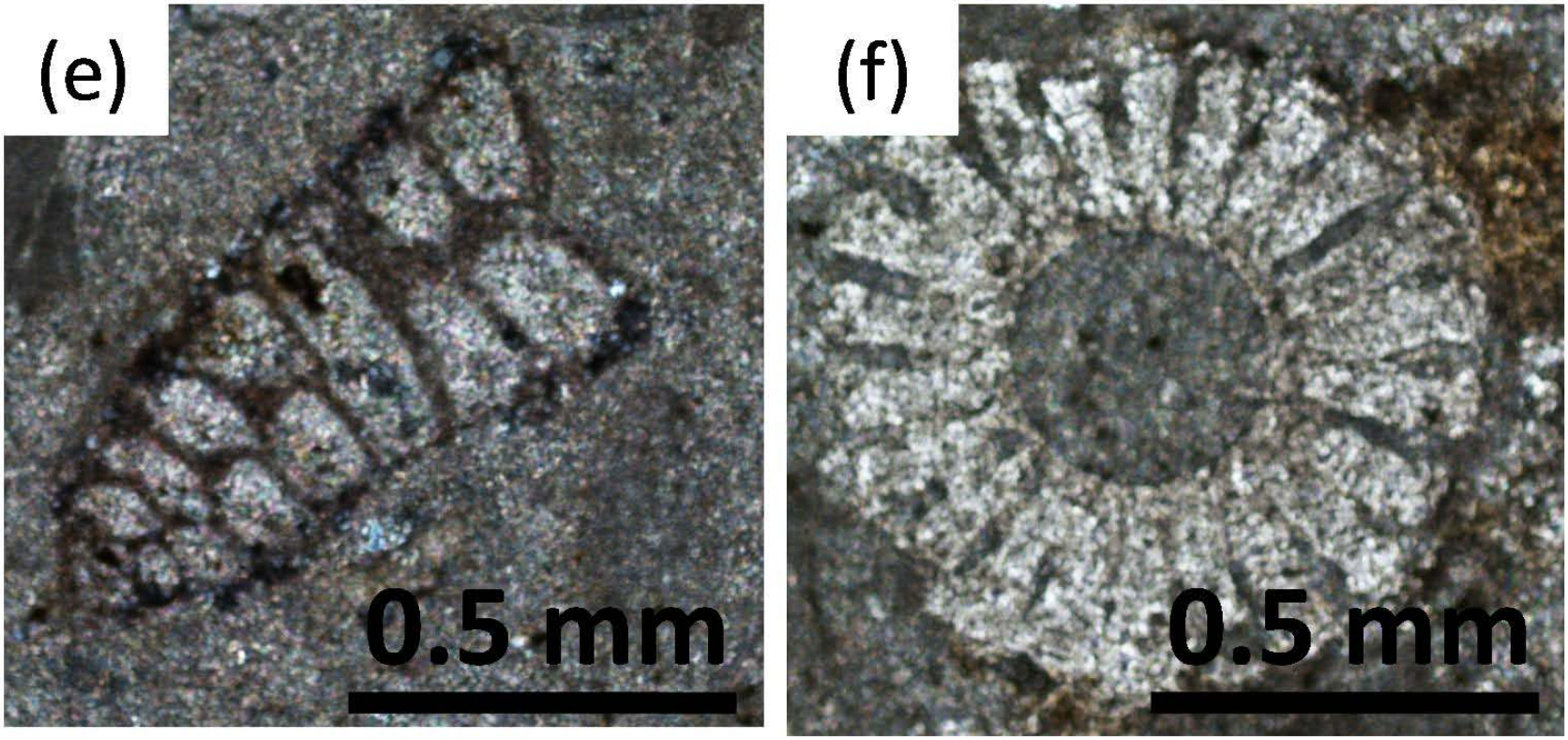
(e)
0.5 mm
(f)
0.5 mm

Figure 25. Field photographs of the massive limestone facies. (a) Cross-sectional view along the strike of La Popa weld surface trace (yellow line) in the basal section 1SE. The arrows point to the limestone lentil in basal section 1SE. The slope to the right of the limestone lentil is part of the Viento deposits and the surface trace of La Popa weld is to the left. (b) Viewer located on the Viento deposits is looking eastward and facing the limestone lentil in the box (frontal view, basal section 1SE). The yellow line represents the surface trace of La Popa weld. (c) Close-up of micro karst structures resulted from subaerial weathering. Card is 15 cm long. (d) Plan view exposure of steeply dipping, isolated debris flow carbonate bed adjacent to the weld surface at the bend of the wall, interpreted to form as avalanche deposits falling from the flanks of the diapir during inflation. Deposit is abundantly crosscut by calcite veins indicating salt evacuation. Jacob staff 1.5 m long for scale. (e) and (f) Photographs of agglutinated foram and coral fragments under the microscope. Bar scale is 0.5 mm long.

CHAPTER 5 – VIENTO FORMATION STRUCTURE AND COMPOSITE HALOKINETIC SEQUENCE STRATIGRAPHY CLASSIFICATION

5.1. Framework

Strata of the Viento Formation were correlated using halokinetic sequence stratigraphy, which is based on the models developed from outcrop investigations in La Popa basin, Mexico (Giles and Lawton, 2002; Giles et al., 2004; Giles and Rowan, *in press*), and eustatic sequence stratigraphy using the relative T-R curve of Embry (1993; 2002). The model of Embry (1993; 2002) is the most suitable approach for this outcrop data set because of the lateral variation in depositional facies from one measured section to another, and practical ease in subdividing the sequence into two systems tracts, transgressive (T) below and regressive (R) above, with the maximum flooding surface (MFS) being the mutual boundary. Other sequence stratigraphic models use system tracts such as lowstand, highstand, shelf margin, falling sea level, and forced regressive systems tract, which depend on the base level as a reference surface. However, base-level in La Popa basin was influenced by tectonics and halokinesis in addition to eustasy, such that associating the above mentioned surfaces solely to eustasy is highly subjective and inadequate for Viento Formation halokinesis correlation. Adapted from Embry's model and used for this outcrop data set, the surfaces having the greatest utility include unconformities, maximum regressive surfaces, and maximum flooding surfaces (Appendix 1).

Halokinetic sequences differ from traditional eustatic sequences. Halokinetic sequences packages develop in response to the rate of net vertical evaporite rise relative to the rate of local sediment accumulation, typically extend only locally within 1-2 km from the salt structure and may be bound by angular unconformities (Giles and Lawton, 2002; Giles and Rowan, *in press*). In contrast, eustatic sequences develop in response to the rate of sea-level changes that influence accommodation space availability relative to the rate of sediment accumulation, correlate basin-

wide and usually maintain relatively constant thickness (Vail et al., 1977, Posamentier et al., 1992; Posamentier and Allen, 1999; Catuneanu, 2002; Catuneanu et al., 2010).

A transgression (T) is defined as the landward migration of the shoreline and facies due to relative sea level rise. Transgressive packages are bounded by maximum regressive surfaces (MRS) at the base and maximum flooding surfaces (MFS) at the top. In contrast, a regression (R) is the seaward migration of the shoreline and facies due to relative sea level fall. Regression occurs during a net decrease in accommodation space due to a relative sea level fall or when the rate of creation of accommodation space is less than the rate at which it is filled, and results in a progradational stacking pattern. Idealized composite regressive packages within the Viento Formation stack in the following overall coarsening upward succession of facies: shale facies at bottom, overlain by thick-beds of bioturbated sandstone facies and inclined heterolithic stratification facies, which in turn are overlain by ripple-laminated sandstone facies, with trough-cross bedded sandstone and conglomeratic sandstone facies at the top. Regressive packages are delimited by a MFS at the base and a MRS at top.

5.2. Subdivisions within the study area

As with other sand-rich siliciclastic units deposited adjacent to La Popa weld, such as the Muerto Formation (Weislogel and Lawton, 2000; Hon, 2001), the Potrerillos Formation (Shelly and Lawton, 2005), the Delgado Sandstone (Aschoff and Giles, 2005) and the Carroza Formation (Andrie and Giles, 2010), the Viento Formation deposits thin and beds are steeply dipping adjacent to the weld (Fig. 26) (Giles and Lawton, 1999; Giles and Rowan, *in press*). The thickness and overall stratal geometry of the Viento Formation varies considerably across the field study area, and for practical purposes the study area is divided into a southeastern diapir-distal area, and a northwestern diapir-proximal area (Fig. 8). The southeastern diapir-distal area

is characterized by measured sections 1SE and 1W. Section 1W is located within the bend of the La Popa weld (Fig. 1 and Fig. 8). The bend in La Popa weld may reveal different orientations of underlying basement faults (Rowan et al., *in press*). The southeastern diapir-distal area exposes strata from structurally deeper levels, which were deposited distal to the crest and flanks of the diapir relative to Viento Formation exposures to the northwest, and thus are composed of more basinward facies. The northwestern diapir-proximal area is delimited by measured sections1W located within the bend of the La Popa weld, through section 13W where Viento thins to zero (Fig. 8; Appendix 1). The northwestern diapir-proximal area exposes strata from structurally shallower levels that contain more proximal facies that accumulated next to the crest and flanks of the diapir.

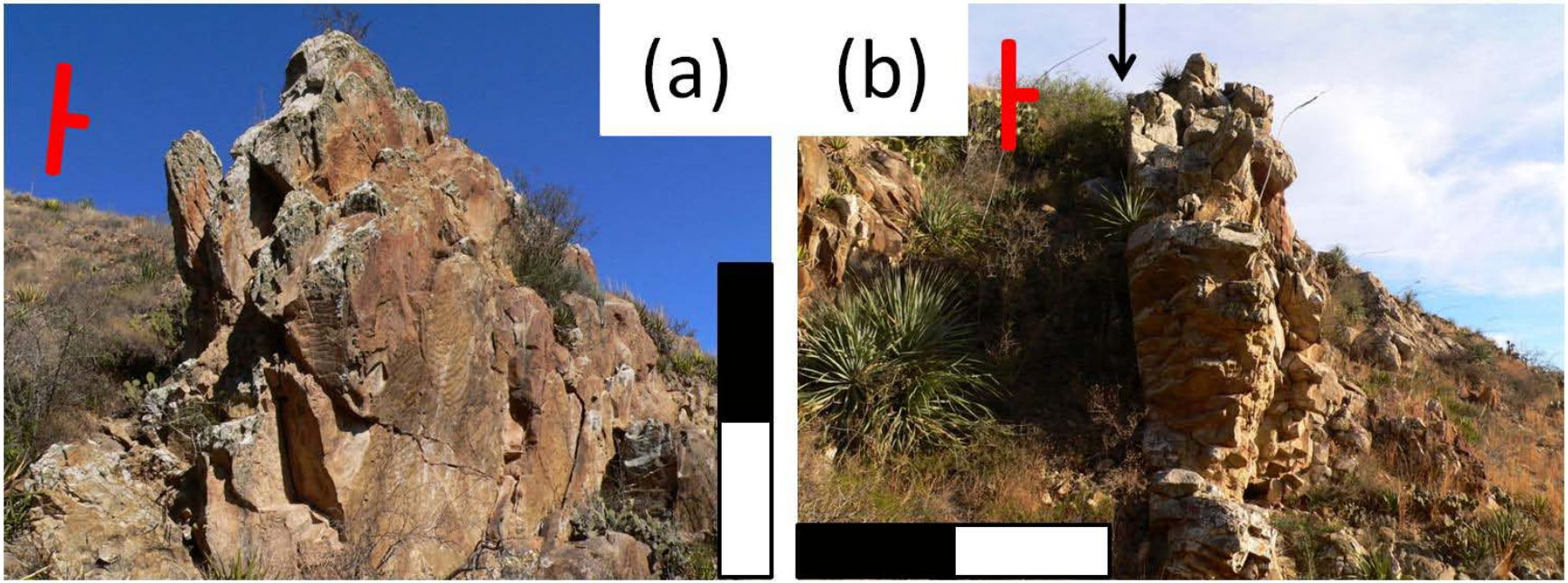

Figure 26. Field photograph of steeply dipping beds in the lowermost Viento Formation adjacent to La Popa salt wall. Occasionally, such beds form ridges that can be traced across drainages from one section to another. In both photographs, the stratigraphic up is to the right. Red symbol represents beds strike and dip. (a) Thick bed of ripple-laminated sandstone facies in section 4W at meter 30 dipping vertically. View toward northeast. Scale bar to the right is approximately 5 m high. (b) Cross-sectional view of vertically dipping, ridge-forming sandstone bed in section 2W meter 210. Vertical arrow is pointing to the sharp, erosional basal contact of vertically dipping bed with adjacent, older horizontal heterolithic sandstone facies. Scale bar in the lower left is approximately 5 m long.

5.3. Viento Formation stratigraphic contacts

The Viento Formation overlies the Adjuntas Formation and is in turn overlain by the Carroza Formation The Adjuntas Formation red beds (Lawton et al., 2001; Lawton et al., 2009) are not exposed in the study area. Instead, lower Viento Formation strata are in contact with La Popa weld surface. Because the Adjuntas Formation contact is not exposed, the lowermost beds of Viento Formation in the measured sections may not actually be the oldest Viento Formation strata preserved next to La Popa weld. It is possible that the older Viento Formation strata are buried underneath the lowermost beds in structural contact with La Popa salt wall and weld, such that the Viento Formation may be much thicker than in the sections exposed at the surface. The contact between the Viento Formation and the Carroza Formation is a covered interval in all sections except for section 2W (Fig. 27; Appendix 1). Field observations reveal that the contact between the Viento Formation and the Carroza Formation is transitional, dominated by tan and purple shale, siltstone and mudstone intercalated with rare, 5 cm thick, tan, fine-grained sandstone beds (Fig. 27). Viento beds dip steeply adjacent to the weld (Fig. 26), but dip decreases upsection to ~30°.

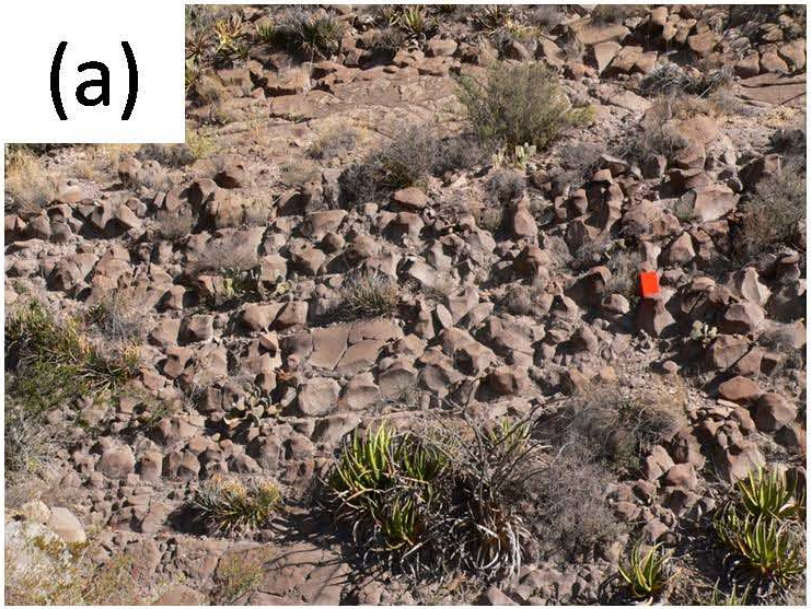
(a)

(b)

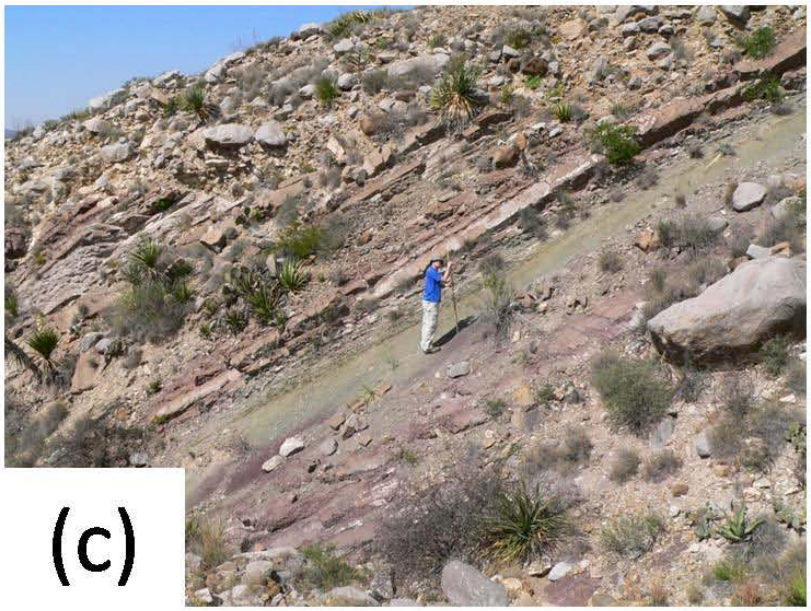
(c)

Figure 27. Field photographs of the contact between Viento Formation with the overlying Carroza Formation (a) Typical exposure of the purple fluvial Carroza Formation sandstone adjacent to Viento deposits. Note sandstone beds have distinct weathering pattern and purple color. Orange notebook is 19 cm long. (b) Exposed contact between the Carroza Formation and the Viento Formation in section 2W. Stratigraphic up is to the left. The massive purple sandstone bed is part of the lower Carroza Formation, while the siltstone deposits to the right are part of the upper Viento Formation Jacob staff is 1.5 m long. (c) Transitional contact between the Carroza Formation and the Viento Formation in section 3W. Stratigraphic up is to the left. Person for scale. Note intercalated tan and purple mudstone deposits that comprise a ~20 m thick transitional rock package at the contact.

5.4. Datum

A distinctive limestone clast-bearing conglomeratic sandstone bed that appears only once in the Viento succession is used as the datum for stratigraphic correlation (Fig. 15). This bed is found near the contact of Viento Formation with the overlying Carroza Formation in sections 2W, 3W, and 4W, and was walked out laterally across drainages for over one kilometer (Appendix 1). Although it does not crop out everywhere, it is inferred that this clast-bearing conglomeratic sandstone bed should be present in covered intervals found near the top of other sections that lie along strike with exposures of the conglomerate elsewhere (Appendix 1). Conveniently, this bed is present in the northwestern diapir-proximal area where most of the data used in this study were generated.

5.5. The southeastern diapir-distal area

The basal Viento contact in the southeastern diapir-distal area rests against the weld surface, which contains no remnant gypsum. The rock is damaged (fractured) and displays iron-oxidation at the contact between the two units exposed on each side of the weld because these rocks accommodated the strain after evaporite was evacuated (Fig. 28; Rowan and Giles, *in press*).Deposits in the southeast diapir-distal area thin from ~1000 m thick in section 1SE to ~800 m thick in section 1W. For most of the distance, the Viento Formation strata strike approximately parallel with the surface trace of the salt weld. Based on strike trend, field, and aerial observations, it appears that the ~200 m thickness decrease from section 1SE toward section 1W was primarily accompanied within the lowermost part of the Viento Formation (Appendix 1; Fig. 8). Strike trend of Viento Formation strata changes abruptly near section 1W where the weld trace also changes orientation, causing an apparent bend of the weld trace (Fig. 8).

In section 1SE, dip decreases from 85° to 65° within the first 50 m walking upsection and away from the salt weld contact. In the overlying 600 m, dip gradually decreases to ~45°, and at the Carroza Formation contact, Viento Formation strata dip ~30° to SW. In the basal section 1W, strata dip 75° to the NE and dip increases upsection to 85° at meter 150. Furthermore, around meter 280 dip changes from NE toward SW and dip starts to decrease from 75° at meter 300, to 45° at meter 500 near the contact with the overlaying Carroza Formation

The southeastern diapir-distal area records one 13° angular unconformity present in the upper part of section 1W at meter 485, at the contact between a 12 m thick trough cross-bedded sandstone bed dipping 65°, sharply overlain by 1.5 m thick conglomeratic sandstone with chert pebbles bed dipping 52° (Fig. 29; Appendix 1). Shallow angular unconformity formed in conjunction with passive upward salt movement (halokinesis) triggered by differential loading on the evaporite source-layer. Additional to halokinesis, overlapping in time and space, operated the regional Hidalgoan orogeny. Upward salt movement caused by differential loading tilted (rotated) the initially flat trough cross-bedded sandstone bed. Erosion and deltaic autocyclic sedimentary processes thinned and removed the top of the trough cross-bedded sandstone bed along with any other overlying facies that had been deposited, such that the rotated trough cross-bedded sandstone bed was erosionally thinned and capped by the conglomeratic sandstone bed. The low-angle unconformity becomes conformable with a distance of over hundred of meters away from the diapir.

In general, in order to assess erosion rate, a series of environmental parameters need to be evaluated, including latitude, elevation, relief, mean annual precipitation, temperature, seismicity, basin slope and area, and percent of surface covered by vegetation. Modern mean erosion rates vary greatly around the world from ~12 m Ma^{-1} at outcrop scale to ~218 m Ma^{-1} at

basin scale (Portenga and Bierman, 2011). In La Popa basin in particular, it is difficult to quantify the rock thickness that is missing due of thinning caused by erosion because of the overlapping processes and subsequent effects of halokinesis, Hidalgoan orogeny and deltaic autocyclicity that intermittently destroyed older deposits as the delta continuously builds out. Comparing facies successions and stratal thickness consistency from section 1W meter 485 across 2W and toward 1SE, is estimated that as much as 20 m of rock representing deeper water facies may have been removed from this one location.

Figure 28. Field photographs of the La Popa weld deformed zone exposed in the southeastern diapir distal area (a) Field photograph of ~0.5 m thick, tan – orange weathering, laminated mudstone that represents the weld zone. This is the appearance of La Popa weld zone where the salt wall has been fully welded such that no gypsum or other diapiric material has been trapped between the two sides of the former evaporate wall. This outcrop is located in basal of section 1W (Appendix 1). Oxidation and deformation is because these rocks accommodated the strain after the salt has been evacuated. Such exposure extends laterally tens of meters. Rock hammer is 33 cm long. The head-hammer points toward the Viento Formation deposits.

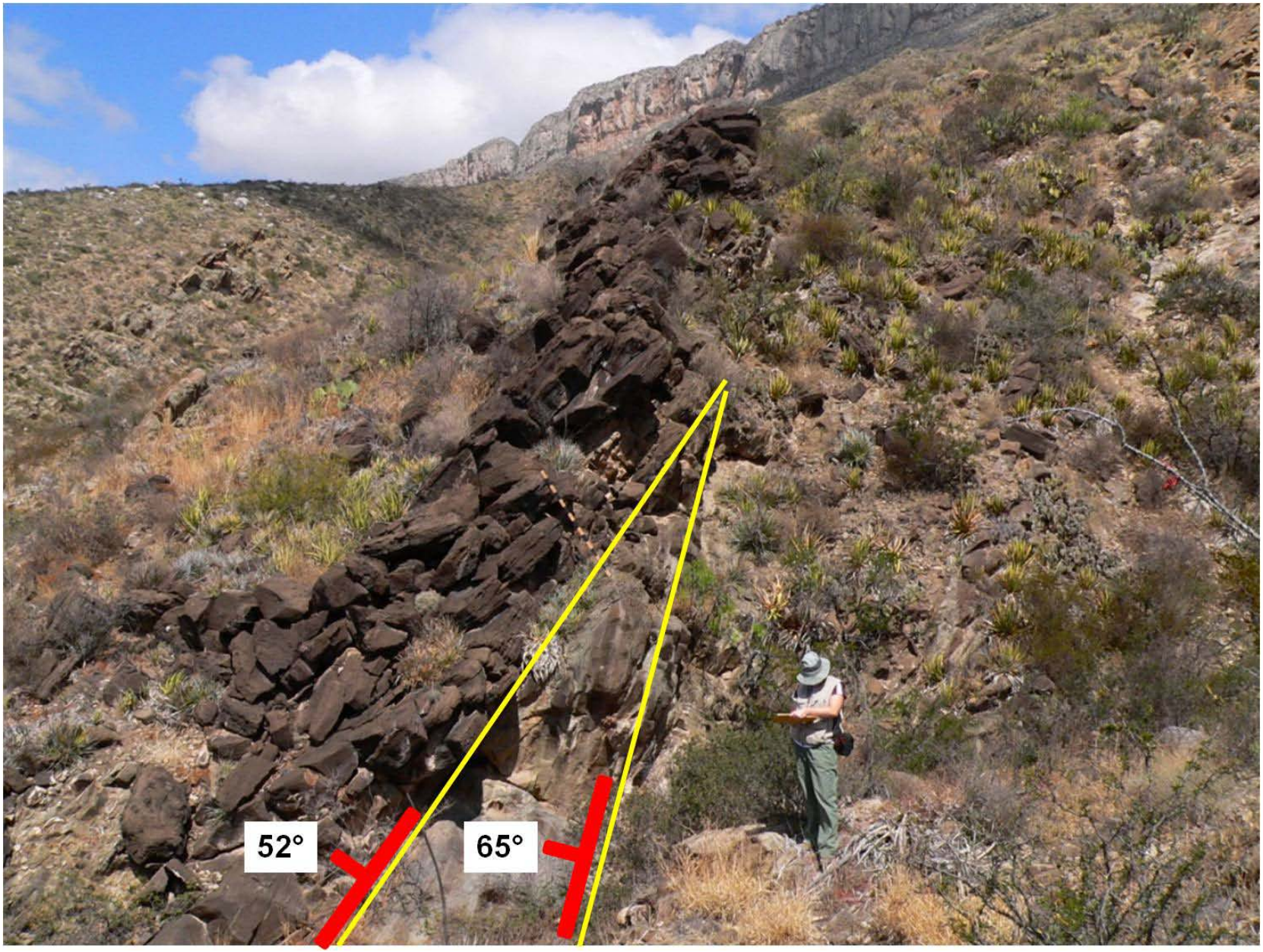
52°
65°

Figure 29. Field photograph of an angular unconformity with 13° of discordance located in the uppermost part of the Viento Formation (section 1W at meter 485). View toward northwest and stratigraphic up is to the left. Yellow lines highlight the trace of the unconformity and red lines show the relative dip orientations of the beds below and above the unconformity surface. Person for scale. The lower bed is composed of trough cross-bedded sandstone facies and was rotated then partially eroded. The upper bed exhibiting conglomeratic sandstone with chert pebbles facies was subsequently deposited on top of the angular unconformity. The conglomeratic sandstone with chert pebbles bed exhibits lenticular geometry indicative of incision, and form black ridges that continue laterally hundred of meters across drainages.

5.5.1. Position of La Popa salt weld in the southeastern diapir-distal area

In the southeastern part of the study area, La Popa salt wall is apparently fully welded (no remnant gypsum), and exposure of its surface trace continuity is scarce (Rowan et al., *in press*). A bed of massive limestone facies, interpreted as a limestone lentil, is present at the base of section 1SE (Fig. 25, Fig. 30, and Fig. 31). To the east of the limestone lentil, appear to be in place numerous carbonate boulders that exhibit orange oxidation (Fig. 31 and Fig. 32), a specific attribute similar to other lithologies (laminated mudstone Fig. 28a) trapped in the weld zone at other locations along the weld trace. The weld zone resembles the salt wall welded, with no remnant gypsum between the sides of the wall. This implies that the massive limestone bed is part of the lower Viento Formation

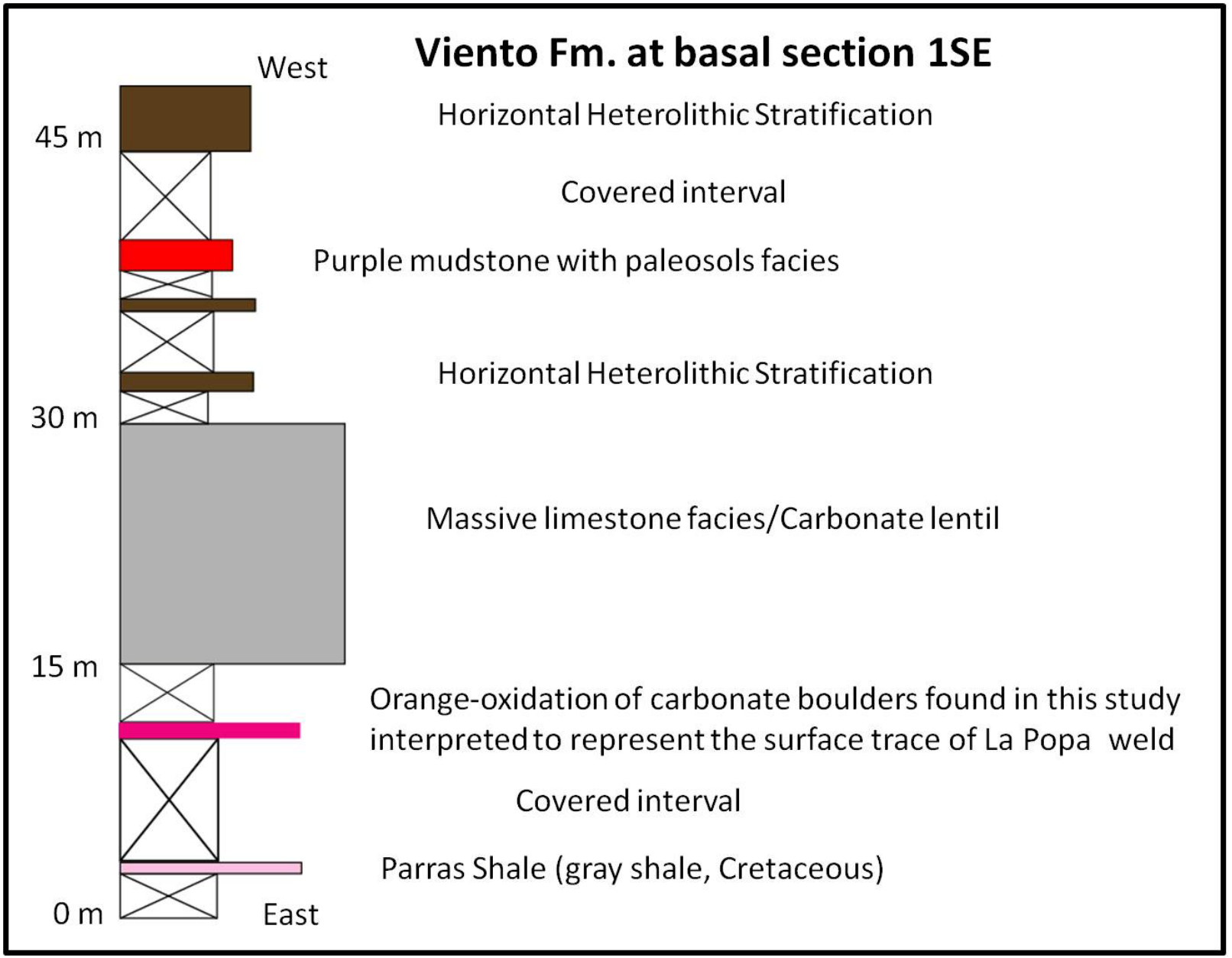
Viento Fm. at basal section 1SE
West
45 m
30 m
15 m
0 m
East
Horizontal Heterolithic Stratification
Covered interval
Purple mudstone with paleosols facies
Horizontal Heterolithic Stratification
Massive limestone facies/Carbonate lentil
Orange-oxidation of carbonate boulders found in this study interpreted to represent the surface trace of La Popa weld
Covered interval
Parras Shale (gray shale, Cretaceous)

Figure 30. Stratigraphy of the basal Viento Formation at section 1SE (Fig. 8 and Appendix 1), showing the relationship between the position of the massive limestone bed and the orange carbonate boulders displaying orange oxidation, interpreted to represent the weld zone and surface trace of La Popa weld in the southeastern diapir-distal area. Upsection is to the west and downsection is to the east.

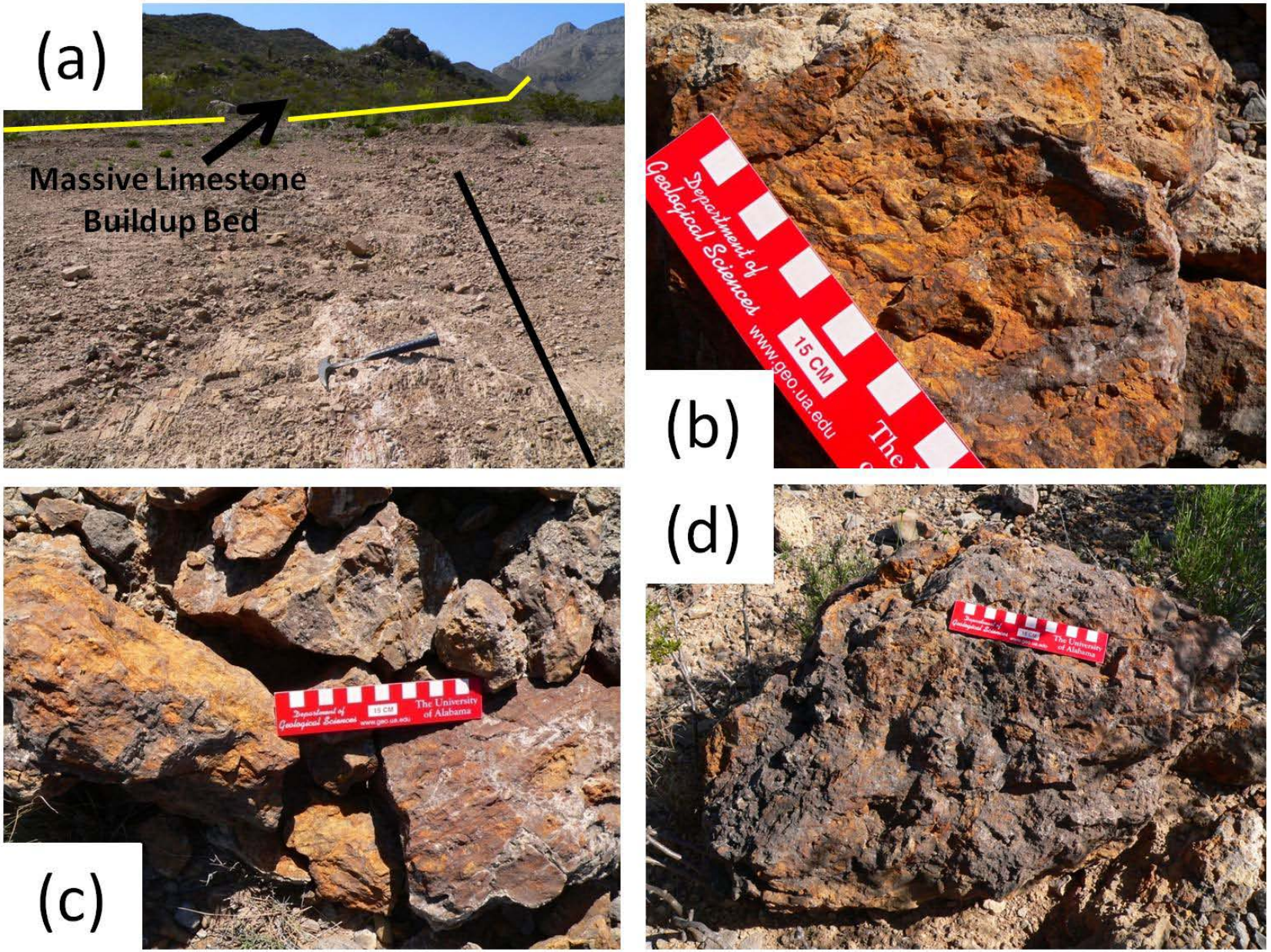
(a)
Massive Limestone
Buildup Bed
(b)
Department of
Geological Sciences
www.geo.ua.edu
15 CM
(c)
(d)

Figure 31. Field photographs illustrating the stratal relationship and lithologies present in the basal part of section 1SE. (a) View is from southeast toward northwest with black arrow pointing to the massive limestone/carbonate lentil. The black line in foreground represents the approximate strike of the Parras Shale. The yellow line represents the approximate surface trace of La Popa salt weld and the location of the orange-oxidized carbonate boulders. Rock hammer is 33 cm long. (b), (c) and (d) Close-up field photographs of the carbonate boulders that appear to be *in situ* to the east of the massive limestone bed. Boulders exhibit orange iron oxidation similar to other deposits within the study area found between the two sides of the weld where the weld zone contains no remnant gypsum or other evaporite material. Bar card is 15 cm long.

5.6. The northwestern diapir-proximal area

Strata in the northwestern diapir-proximal area thin significantly from ~800 m in section 1W, to zero meters in section 13W (Fig. 5, Fig. 8, and Appendix 1). The base of the Viento Formation between sections 1W, 2W, and 3W is demarcated by the exposures La Popa salt weld surface, with no remnant gypsum between the two sides of the weld (Fig. 28). In contrast, the base of the Viento Formation from sections 4W through 13W rests in contact with outcropping pods of gypsum that are ~30 m in diameter or larger (Fig. 33). These pods of gypsum may represent cusps at major halokinetic sequences boundary between the Potrerillos Formation and Parras Shale (Rowan et al., *in press*). The salt wall did not form a perfect parallel geometry but rather irregularities due to variable salt-sediment interaction on each side of the wall, juxtaposing different stratigraphic levels, faults and halokinetic cusps caused an irregular content surface.

Calcite and gypsum, and/or anhydrite veins of multiple orientations decrease in amount and crosscut Viento beds within ~50 m from the salt wall contact (Fig. 34). These veins contained minerals that precipitated from solution at the interface between diapiric evaporite and adjacent siliciclastic deposits. Geochemical analysis of the fluid inclusions contained within the mineral of these veins indicated that the deposition of the Viento Formation was coeval with upward evaporite movement (Fisher et al., 2009).

The Viento Formation strata in contact with remnant gypsum at the salt wall are slightly overturned with 20-30° past vertical, but only 5-10 meters away upsection the strata are upright and steeply dipping (80-90°). The deformation fabric (slicken lines) at the contact between the Viento beds and the remnant gypsum indicates that the sandstone beds moved up. Hundreds of meters upsection from the salt wall, the dip of the Viento Formation strata decreases to ~65° adjacent to the Carroza Formation strata. The trend of La Popa weld in the northwestern diapir-

proximal area is oriented essentially E to W, whereas Viento Formation strata strike ~300° in northwestern direction, and thus intersect the salt wall at~45° and terminate (Fig. 8).

The significant thinning from ~800 m to zero in the northwestern diapir-proximal area is partially accommodated by two minor-displacement normal faults and three low-angle unconformities, ~10° each. The Viento Formation beds thin and onlap the weld, and terminate (Appendix 1). There is a normal fault is located in section 2W at meter 65 and records ~2 m displacement. A second normal fault of ~8 m displacement is located in section 4W at meter These normal faults displacements represent times of diapir inflation that tilted/rotated strata on its flanks and favored slip (Giles et al., 2011). Alternatively, they may have formed post burial.

A ~15 low-angle unconformity is present at meter 40 in section 3W, between underlying tan fissile shale facies overlying ripple-laminated sandstone facies. Section 4W exhibits two low-angle angular unconformities located at meter 125 and at meter 165 respectively. The unconformity at meter 125 occurs between tan fissile shale facies overlying by conglomerate with chert pebbles facies, and the unconformity at meter 165 lies between ripple-laminated sandstone facies overlying by inclined heterolithic stratification facies (Fig. 35; Appendix 1).

The Viento Formation strata in proximity of La Popa diapir are truncated by erosion, onlap and subsequently overlap one another and produce angular unconformities. Overall, angular unconformities within the Viento deposits occur between deep-water facies and shallow-water facies and become conformable within hundred of meters away from the salt wall. Because these unconformities are located in proximity of the diapir, are interpreted to represent erosional events associated with the passive salt inflation of La Popa diapir (triggered by halokinesis), rather than with diapir inflation due to squeezing compression, and therefore active diapirism.

Angular unconformities define bounding surfaces separating genetically related packages of halokinetic sequences (Giles et al., 2011). The evaporite minerals within La Popa diapir rose up from beneath to shallower levels or to the surface, driven by differential loading on the sourcing salt layer and combined with episodic horizontal Hidalgoan compression. Viento strata overlying the top of the rising diapir were rotated in small increments and fluvio-deltaic erosion processes thinned these strata. In addition, because different angles of dip proximal and distal to the diapir, sediments did not accumulate in even thicknesses. Different strata dip angles determined water column depth, which in turned controlled the sediment accommodation space. While the accommodation space was depleted, more sediment accumulated and continuously loaded the underlying salt layer and drove diapir inflation and passive salt rise.

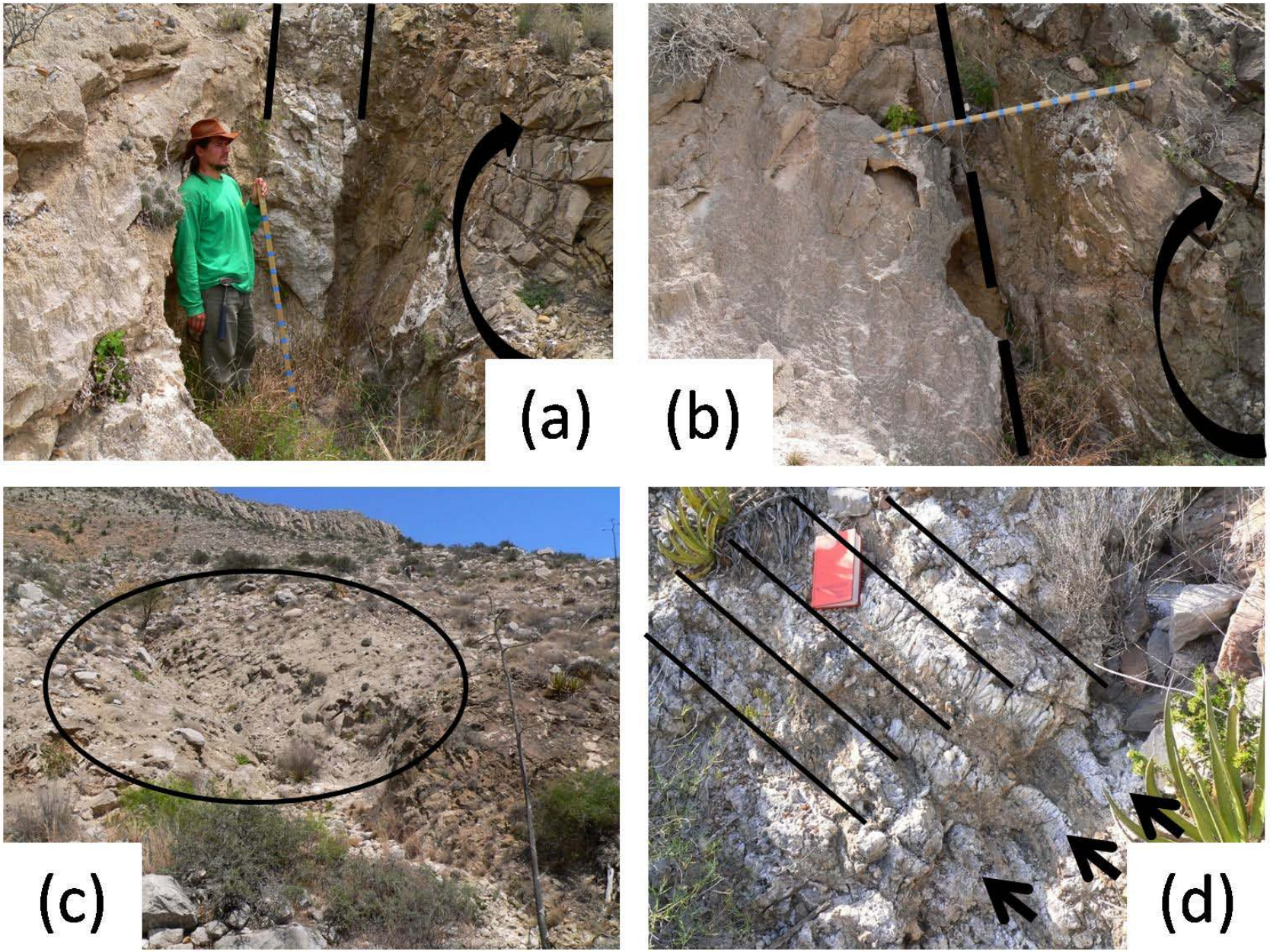
(a)
(b)
(c)
(d)

Figure 32. Field photographs of the contact between the lowermost strata of Viento Formation and pods of remnant gypsum of La Popa salt wall in the northwestern diapir-proximal area. (a) Slightly overturned Viento Formation sandstone bed juxtaposed against a 50 cm thick vertical barite wall, next to a pod of gypsum. This site is located at the base of the Viento Formation in section 4W. The deformation fabric (slickenlines) at the contact between the Viento beds and the remnant gypsum indicates that the sandstone beds moved up. The vertical 50 cm thick barite wall is white and highlighted by two black lines. The curved arrow indicates the direction of rotation (overturn) of the sandstone bed. Stratigraphic up is to the right. Person for scale. (b) Slightly overturned Viento Formation sandstone bed next to pod of remnant gypsum. This site is located at the base of section 6W.The curved arrow indicates the direction of rotation (overturn) of the sandstone bed. Stratigraphic up is to the right. Jacob staff is 1.5 m long. (c) Pods of evaporite >30x30 m that crop out below the Viento Formation in section 5W. Sandstone beds are located in the lower left side of the picture. View towards northeast. (d) Detail of interbedded gypsum and sandstone beds at the contact between the Viento Formation strata and La Popa salt wall. Black lines highlight the orientation of sandstone and gypsum beds. Arrows point to the white gypsum beds. Orange notebook is 19 cm long.

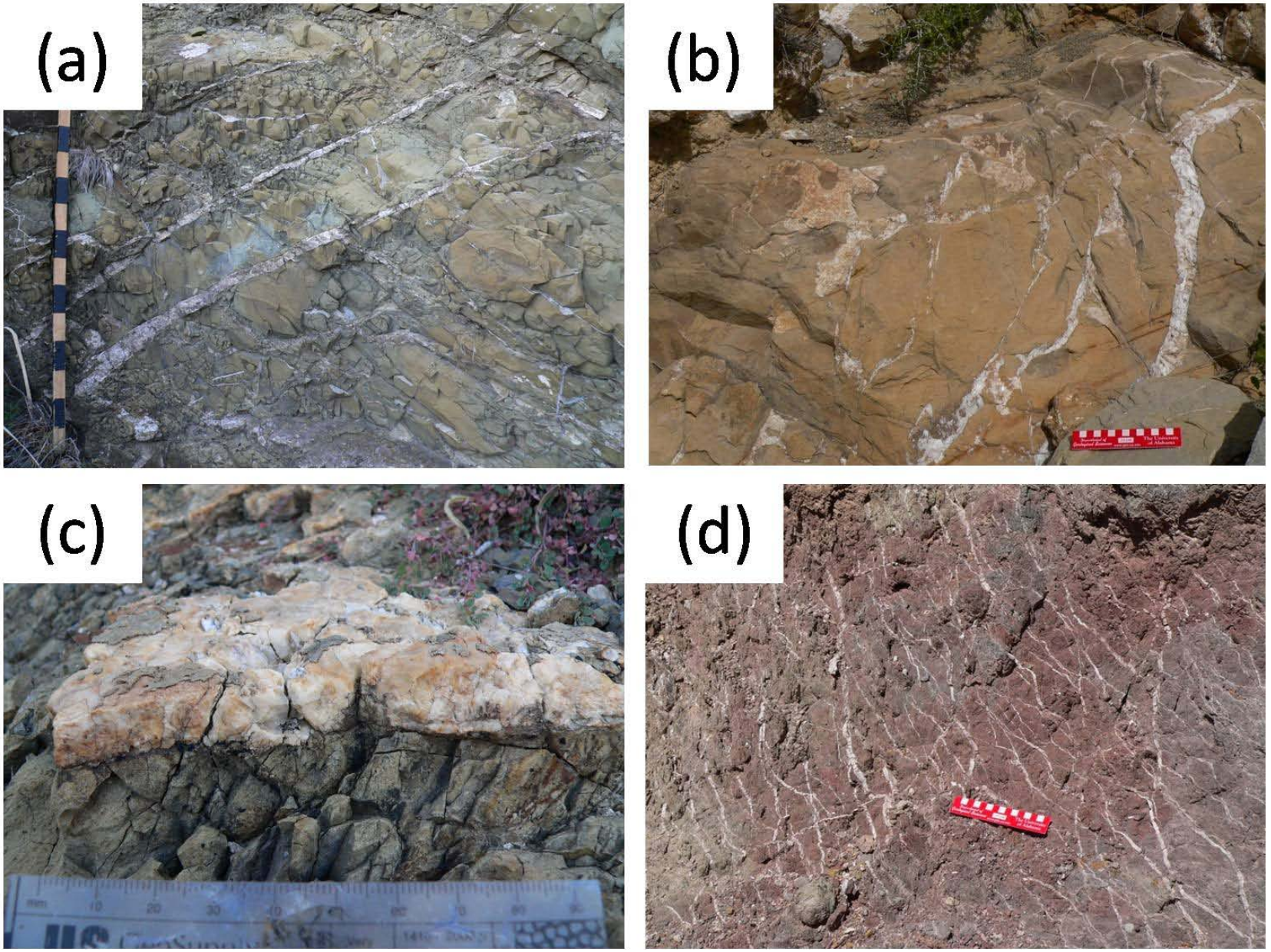
(a)
(b)
(c)
(d)

Figure 33. Field photographs of Viento Formation beds crosscut by veins within ~50 m from La Popa salt wall. (a) Bioturbated sandstone facies crosscut by ~10 cm thick, parallel, gypsum veins in section 2W. Jacob staff is 1.5 m long. (b) Ripple-laminated sandstone facies crosscut by ~5 cm irregular thickness and multiple orientations calcite veins. Card is 15 cm long. (c) Close-up of 2 cm thick, impure, calcite mineralization that used to be part of a vein in section 2W. Grain-card is 10 cm long. (d) Purple mudstone with paleosols facies in the lower Viento Formation of section 3W, cross-cut by millimeter to centimeter thick veins of calcite. Card is 15 cm long.

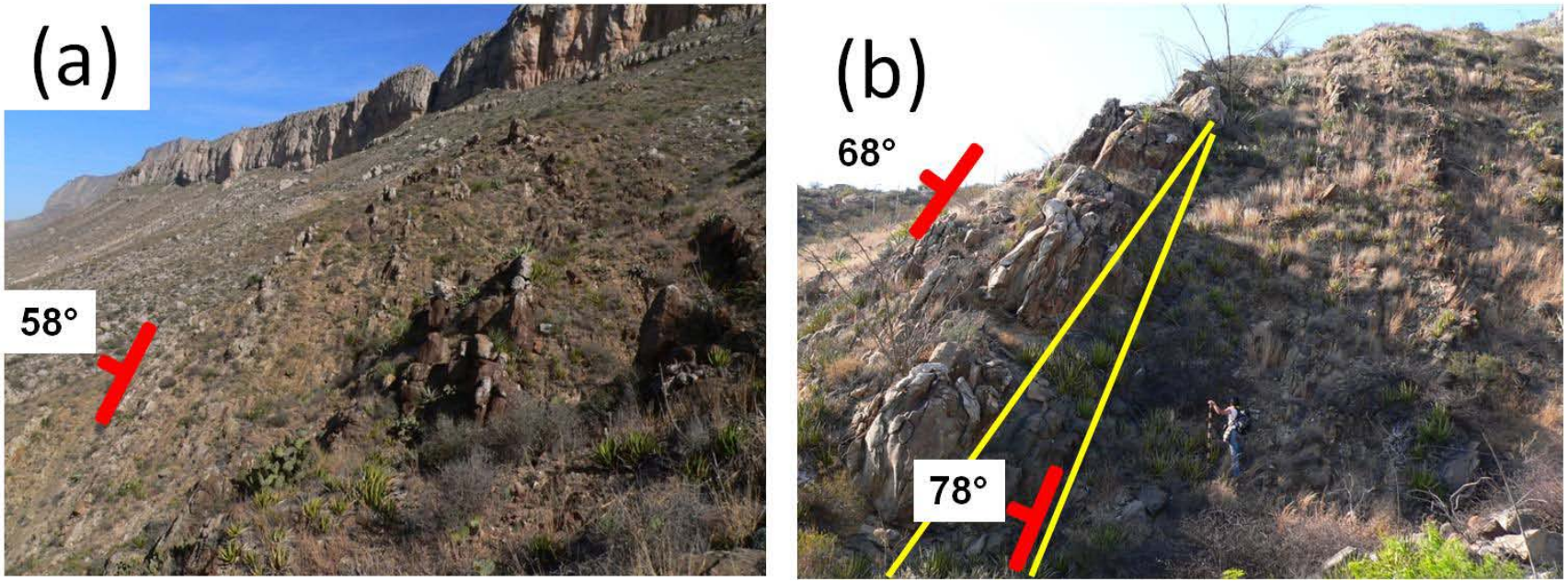

Figure 34. Field photographs of the Viento Formation strata exposed in the northwestern diapir-proximal area. Stratigraphic up is to the left and view is westward in both photographs. (a) Ridge-forming sandstone beds exhibiting steep dip angle (~65°) strike run into La Popa salt wall that is located approximately at the base of San Jose cliff in background. The relative strike and dip of sandstone beds is shown in picture. This view is westward from section 5W. For reference, the San Jose cliff is ~30 m high. (b) Low-angle stratal discordance in section 4W at meter 165.

5.7. Metaigneous-bearing conglomeratic sandstone beds prevalence and distribution

The prevalence and distribution of the metaigneous-bearing conglomeratic sandstone beds is significant and provides clues into the history and evolution of La Popa evaporite wall and weld. The metaigneous clasts composition are typical of continental rift magmas (thermally metamorphosed to chlorite-epidote and preserve remnant igneous texture but without metamorphic foliation fabrics), were produced during continental rifting, interbedded with the evaporite minerals of the Minas Viejas Formation, which was mobilized to form the La Popa evaporite wall. Exposed diapiric evaporate of the Minas Viejas is the only source of the metaigneous clasts, as no other exposures of the Minas Viejas occurs in La Popa basin or nearby that could provide the metaigneous clasts (Garrison et al., 1999; Lawton et al, 2001; Lawton et al., 2009). The abundance of metaigneous-bearing conglomeratic sandstone beds indicates that the La Popa diapir crest and/or its flanks were continuously exposed, either subaerially or subaqueously, and/or present near the surface and subject to erosion. In addition, metaigneous clasts and natric soils are present in the overlaying Carroza Formation (Buck et al., 2009; Andrie and Giles, 2010), indicating that diapirism and evaporite extrusion continued after the Viento Formation depositional system ceased and that La Popa evaporite wall had not completely welded during Viento Formation deposition.

In the study area, the metaigneous clasts size and angularity decreases with increasing distance of La Popa salt diapir, as gravel-sized and well rounded metaigneous clasts were transported from the crest and flanks of the diapir-source area toward the withdrawal basin by fluvio-deltaic distributary channels. Prevalence of metaigneous-bearing conglomeratic sandstone beds is directly proportional to the thickness of each section and their prevalence varies across the study area. Although section 1SE records the highest number of metaigneous-bearing

conglomeratic sandstone beds, metaigneous clasts in these beds are less abundant, smaller size, and so well rounded as to be perfectly spherical. In contrast, metaigneous-bearing conglomeratic sandstone beds in the northwest diapir-proximal area contain more abundant, larger, and more angular metaigneous clasts.

Metaigneous-bearing conglomeratic sandstone beds represent pulses associated with the vertical stresses of localized differential loading and the horizontal stresses of regional Hidalgoan compression, which caused La Popa evaporite extrusion of Minas Viejas Formation evaporite from La Popa basin salt diapirs. Viento Formation recorded the effects of the vertical and horizontal stresses, however, distinguishing between the two is challenging as these pulses overlapped in time and space. Metaigneous-bearing conglomeratic sandstone beds that correlate across the study area are interpreted to represent halokinetic sequence boundaries and are equivalent with pulses associated with regional shortening events that squeezed the diapir and drove evaporite and metaigneous clast extrusion from the diapir. Salt diapirs modeled in the lab and known from other geologic settings show that tectonic shortening overprints differential loading and has the strength to evacuate evaporite from diapirs to produce a vertical secondary weld (Vendeville and Jackson, 1992; Vendeville and Nilsen, 1995; Rowan et al., 2003; Rowan et al., 2004; Vendeville, 2005; Rowan and Vendeville, 2006; Rowan et al., *in press*). Thus, metaigneous-bearing conglomeratic sandstone beds that appear in the section and correlate only across short distances are interpreted to record local differential loading and downbuilding such that metaigneous clasts were extruded from the diapir. Metaigneous-bearing conglomeratic sandstone beds that result from downbuilding are very common in the northwest diapir-proximal study area (Appendix 1). The metaigneous-bearing conglomeratic sandstone beds compose the

coarser fraction of the Viento Formation deposits and commonly cap erosionally truncated parasequences.

5.8. Comparison of the SE diapir-distal and the NW diapir-proximal areas

Viento Formation stratigraphy exhibits variable characteristics across the study area. In southeastern diapir-distal area the beds strike parallel to the surface trace of La Popa salt weld, which is welded with no evaporite minerals between the two sides of the weld, while in the northwestern diapir-proximal area the beds strike northwest and intersects the east-west striking La Popa weld at ~45° . Moreover, the strata terminate and abut >50x50 m large pods of evaporite minerals that crop out within the weld. The southeastern diapir-distal area records 200 m thinning, whereas the northwestern diapir-proximal area thin significantly from 800 m to pinch out. Detailed measured sections reveal that the Viento Formation strata thicken into the Carroza syncline (Appendix 1).

5.9. Parasequence development

Parasequence is defined as “relative conformable successions of genetically related beds or bedsets bounded by flooding surfaces” (Van Wagoner and Bertram, 1995). Parasequences of the Viento Formation strata consist of a progradational succession of non-marine, marginal marine and marine facies, range 3-40 m thick (commonly average ~20 m thick) (Dalrymple and Choi, 2007). Parasequences prograde from offshore shale or horizontal heterolithic facies, through bioturbated sandstone, inclined heterolithic sandstone-siltstone and ripple-laminated sandstone facies, and are capped by the prevalent conglomeratic sandstone and trough cross-bedded sandstone facies.

5.10. T-R cycles and Sequence Boundaries

The Viento Formation strata record repetitive cycles of sedimentation formed in response to a combination of factors including salt withdrawal/diapiric rise, regional contractile tectonism (Hidalgoan orogeny), and eustatic fluctuations. Thick deposits previously accumulated in La Popa minibasin, along with massive sediment input from the fluvio-deltaic Viento system, created differential loading, and drove evaporite rise. Coeval with deposition of the Viento Formation, episodic compressional events associated with the Hidalgoan orogeny and rise of the Sierra Madre Oriental, in turn, squeezed and enhanced the rise of La Popa salt wall. These factors and their subsequent processes interfered to produce the stratal architecture and internal facies arrangement of the Viento Formation Eustatic sea level was relatively high during the Paleocene- Eocene but on the verge of falling (Haq et al., 1988). The sea-level curves of Haq et al. (1988) suggest that the cycle represented by the Viento Formation sequence might be a 3rd order cycle. From the southeastern diapir-distal area toward the northwestern diapir-proximal area were identified five sequences (Appendix 1). Regressive packages range 40-175 m thick and transgressive packages range 25-90 m thick. Sequences become thinner through time, suggesting progressive short-lasting cycles and quicker turnaround from regression to transgression. It appears that during transgressive cycles the number of metaigneous-bearing conglomeratic beds is larger than during regression indicating slower sediment accumulation rates and more diapir inflation.

5.11. Composite halokinetic sequence stratigraphy

Changes in net salt rise rate versus net local sediment accumulation rate form and determine the style of halokinetic sequences (e.g. wedge versus hook) (Giles and Lawton, 2002; Rowan et al., 2003; Giles et al., *in press*). Viento wedge-type halokinetic sequences thin in

direction of La Popa diapir, stack stratigraphically and form a tapered composite halokinetic sequence (Tapered-CHS). Tapered-CHS are defined by convergent basal and top boundaries, form when the relative diapir-rise rate versus the sediment accumulation rate is high, and represent time scale-equivalent 3rd order cycles (Giles and Rowan, *in press*). Topographic relief over the diapir during deposition of Tapered-CHS is minimal because overall sediment accumulation keeps pace or exceeds the accommodation space created by salt withdrawal and diapir rise. An exception to this is during the formation of the carbonate lentil located at the base of section 1SE. Inflation of La Popa diapir into the shallow and clear water during deposition of the carbonate lentil found in basal section 1SE of the Viento Formation created an ideal environment for locally high rates of carbonate production and accumulation. Alternatively, this carbonate lentil may represent preserved caprock produced in relationship with La Popa diapir.

The Viento Formation strata flanking La Popa weld thin significantly, overturn near the salt wall, and locally display low-angle angular unconformities that separate packages of halokinetic sequences. The significant thinning of the Viento Formation creates a large wedge-shaped geometry, which suggests that the amount of roof sediments overlying the diapir was relative thin and most of the sediments accumulated in the minibasin. The accommodation space is a function of both, sea level rise and basin floor subsidence, and in La Popa basin, this was due to both flexural subsidence and salt withdrawal subsidence. Shallow angle unconformities are produced when salt rise rates exceeded sediment accumulation rates; increased salt rise rates were due to episodic compression associated with tectonic shortening.

5.12. Processes of halokinetic sequence development

It is unknown the exact time and process that initially triggered salt mobilization in La Popa wall, but is hypothesized to be related to thick-skinned extension due of opening of the

Gulf of Mexico, and/or differential and thermal subsidence, and/or initial progradational differential loading during late Jurassic (Rowan et al., *in press*). The interfering process of salt withdrawal, diapiric rise, Hidalgoan compression, and relative sea level change are the major controls that produced the stratigraphic architecture of the Viento Formation deposits (Fig. 35). Hidalgoan compression squeezed the diapir while sedimentary deposits were loading the mother salt layer, causing diapiric rise, diapir inflation, and exposure of diapir evaporite. The ancient Viento fluvio-deltaic system reworked the crest and flanks of the inflated diapir and metaigneous material from within the diapir was extruded and subsequently incorporated within the Viento Formation deposits. Locally, in shallow waters, carbonate and/or oyster reefs deposits formed on top of the diapir, which later were reworked into the minibasin during regressions.

5.12.1. Hidalgoan shortening vs. local downbuilding

Measured sections correlated across the study area provide insight in distinguishing between the processes of regional compression versus passive diapir salt rise due to differential loading that caused the extrusion of diapiric evaporite and metaigneous clasts. Most of the metaigneous-clast bearing beds are located with packages deposited during transgressive periods (Appendix 1). Transgressive periods triggered extensive erosion resulting in increased amounts of metaigneous material that was extruded from the salt wall during these times. The metaigneous-clast bearing beds associated with MFS of transgressive times tend to correlate across measured sections in the study area. In contrast, the metaigneous-clast bearing beds associated with regression tend to have localized development and usually correlate only across two or three sections, and are as such interpreted to represent only local passive salt rise due of halokinesis rather than regional contractile events and periods of eustatic sea level rise.

5.12.2. Contrast between Giles et al. wedge halokinetic sequence model vs. Viento Formation model

The Viento Formation. strata deposited adjacent to La Popa salt wall display a large-scale wedge geometry that fits with the general model for wedge halokinetic sequences described by Giles and Lawton (2002), and Giles and Rowan (2012), although with some differences. First, in the wedge halokinetic sequences model of Giles and Lawton (2002) and Rowan (*in press*), strata do not terminate at the diapir as in the case of Viento Formation. strata, but are spatially separated from the diapir by a thick/wide package of older, tightly folded strata. Secondly, wedge halokinetic sequences are associated with periods of regionally higher sediment accumulation rates present during marine regression in Giles and Lawton (2002) and Rowan (*in press*) model, while the wedge displayed by the Viento strata formed during both transgression and regression times. Third, in contrast with the model of Giles and Lawton (2002) and Rowan (*in press*), the Viento Formation strata shows that higher and deeper in the wedge sequences reach the salt-sediment interface, are highly deformed adjacent to the salt body and strata preserve continuous beds away from the salt.

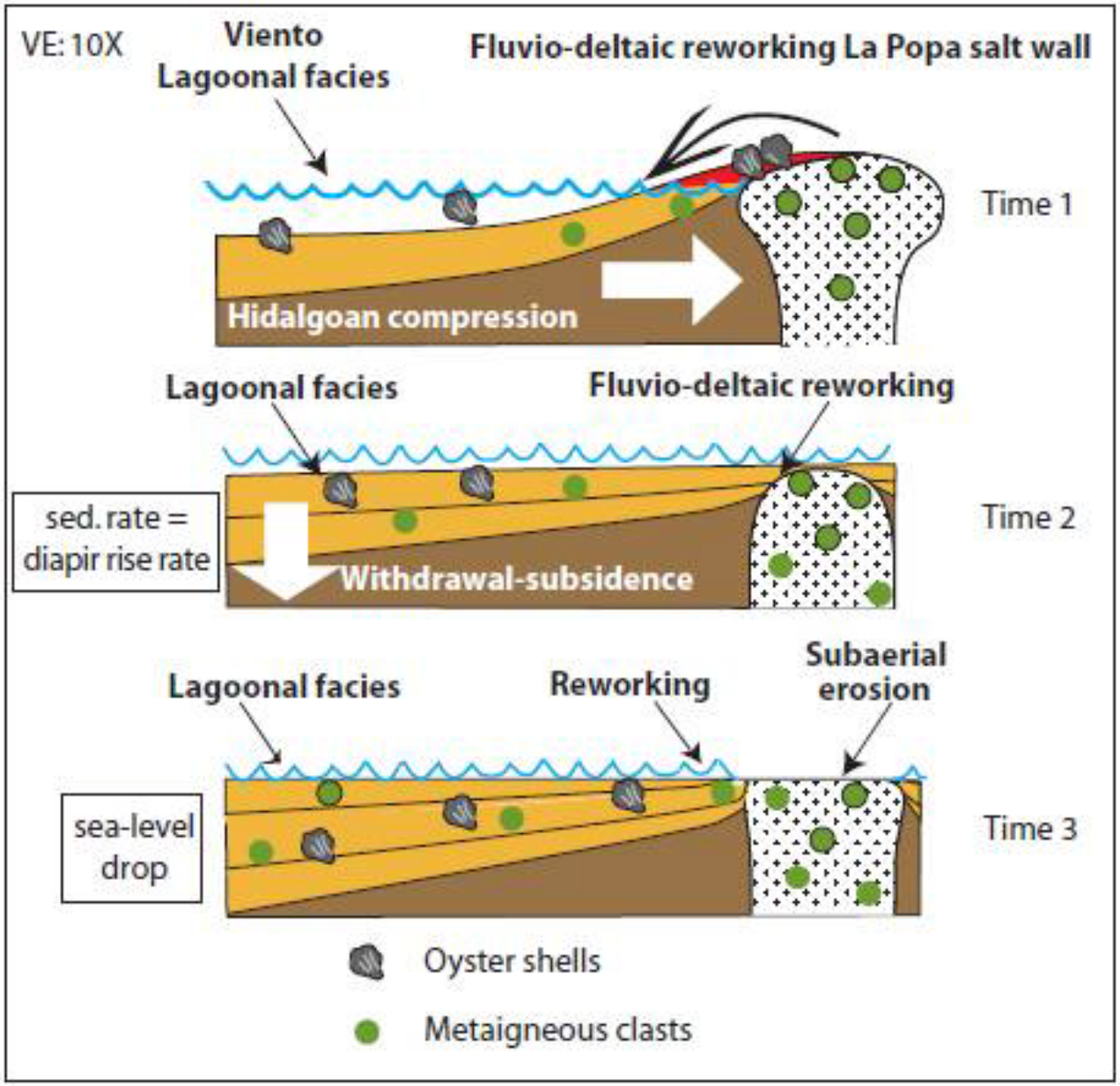
VE: 10X
Viento
Lagoonal facies
Fluvio-deltaic reworking La Popa salt wall
Time 1
Hidalgoan compression
Lagoonal facies
Fluvio-deltaic reworking
sed. rate =
diapir rise rate
Time 2
Withdrawal-subsidence
Lagoonal facies
Reworking
Subaerial
erosion
sea-level
drop
Time 3
Oyster shells
Metaigneous clasts

Figure 35. Drawing depicting schematically the processes that accompanied and modeled the stratigraphic architecture of the Viento Formation deposits. Discussion in text and on figure.

CHAPTER 6 – DISCUSSIONS

6.1. La Popa minibasin paleogeography and the Viento Formation deposition system

Regional tectonic and sedimentologic investigations (e.g. Dickinson and Lawton, 2001; Lawton et al., 2001; Soegaard et al., 2003; Lawton et al., 2009;) show that during the Late Cretaceous to mid-Paleogene paleocurrent flow direction in La Popa basin was from NW toward SE, and thus parallel with La Popa salt wall crest and weld surface trace trend. In addition, extensive minibasin field-based studies of units older and younger than the Viento Formation and exposed adjacent to La Popa salt wall, also indicate that dispersal systems prograded into a southeasterly direction (*e. g*: Hon, 2001; Shelley and Lawton, 2005; Aschoff and Giles, 2005; Buck et al., 2009; Andrie and Giles 2010). During the Late Cretaceous to mid-Paleogene, La Popa salt wall had the effect of a local topographic barrier 1-2 km wide (Rowan et al., *in press*), with the flanks of the salt wall restricting waters to flow toward the north. This setting created a confined depositional system, in which the Viento fluvio-deltaic system followed previously established minibasin topography causing channels to align parallel with La Popa salt wall crest and flanks. The trough cross-bedded sandstone and conglomeratic sandstone beds are much thinner in the southeastern diapir-distal area as the fluvial system transitioned in basinward direction into predominantly bioturbated sandstone facies, inclined heterolithic sandstone facies and ripple-laminated sandstone facies.

Facies characteristics and stacking pattern suggests that the Viento strata deposited in a shallow delta characterized by multiple terminal distributary channels, with compound channel bodies ranging 100-400 m wide and locally extending to over 1 km width. Deltas formed in shallow-waters typically exhibit a lobate delta front with complex morphology that contains multi-scale coeval terminal distributary channels and mouthbar deposits (Olariu and

Bhattacharya, 2006). The number of terminal distributary channel increases in deltas with high sediment discharge ratios (Bhattacharya and Giosan, 2003; Dalrymple and Choi, 2007). When terminal channels become filled with sediment, they avulse laterally and start building another delta lobe (Bhattacharya and Walker, 1992; Bhattacharya and Giosan, 2003; Olariu and Bhattacharya, 2006; Dalrymple and Choi, 2007). The delta front is the most dynamic deltaic setting, dominated by fluvial and marine processes that create complex facies interfingering, which sometimes are difficult to correlate across hundreds of meter distance (Appendix 1). The high variability in the number of channels between measured sections is due to erosion associated diapirism and autogenic processes of periodic fluvio-deltaic channel meandering.

Inflation of the diapir created a bump/barrier which was intermittently subaqueous and subaerial, where oyster bank deposits formed in restricted waters confined to topographic lows. The Carroza syncline area provided space for sediment accumulation and maintained the deepest bathymetry in the minibasin (Lawton et al., 2009; Rowan et al., *in press*). The sediments accumulated in La Popa minibasin from Cretaceous to Paleogene total are ~10 km thick in total, of which Viento Formation deposits compose ~1 km. The first ~9 km of strata gravitationally loaded the Jurassic Minas Viejas Fm. salt underneath the Carroza syncline area, initiated passive salt rise, and fed evaporite minerals to La Popa diapir. Thus, downbuilding/differential loading was the main process operating in La Popa basin prior to the Cenozoic, causing constant salt rise rates during that time. Viento Fm deposits accumulated during a time when regional contractile Hidalgoan tectonics and downbuilding both applied additional stresses to the salt diapirs, caused the salt to rise more quickly than before. The Hidalgoan orogeny squeezed the region in roughly a northeast direction, thus perpendicular to the roughly east-west axis of the Carroza syncline and La Popa salt wall crest (Rowan et al., 2003; Rowan et al., *in press*).

6.2. Active diapirism during the Viento Formation deposition time

Salt-withdrawal controlled the local distribution of accommodation space adjacent to the salt structures present in La Popa basin (Lawton et al., 2001; Giles and Lawton, 2002; Shelley and Lawton, 2005; Lawton et al., 2009; Giles et al., 2004; Giles and Rowan, *in press*), and this study reveals that the Viento Formation deposition was significantly complicated by salt diapirism. The Viento fluvio-deltaic system discharged large volumes of sediment and the thickest part accumulated within the axis of the Carroza syncline, a salt-derived depocenter adjacent to La Popa salt wall. The conglomeratic sandstone beds exhibiting diapir-derived metaigneous clasts are prevalent in the northwestern diapir-proximal area and indicates that during the time of the Viento Formation deposition, the evaporite within La Popa diapir was rising due to differential loading and contractile Hidalgoan orogenic events. In addition, the conglomeratic sandstone beds exhibiting diapir-derived metaigneous clasts indicate that the evaporite minerals including the metaigneous clasts reached the surface, thus La Popa salt wall was inflated, and expressed significant relief relative to the adjacent topography, and its crest was subaerially exposed nearly constantly. Significant relief of the crest was facilitated likely by inflation related to an increased diapir rise rate, overstepping, and failure of its flanks occasionally shedding exotic detritus material into the adjacent Viento Formation fluvio-deltaic system and La Popa minibasin. In addition to gravitational failure, fluvio-deltaic processes eroded the flanks of the salt wall during regression. Extruded exotic detritus material was reworked, transported short distances and then reincorporated within the Viento fluvio-deltaic conglomeratic sandstone beds. The Viento deposits in touch with pods of remnant gypsum in the northwestern diapir-proximal area indicate that thin siliciclastic beds onlapped and occasionally overlapped the diapir.

The external wedge architecture and internal facies distribution pattern of the Viento Formation strata reflect that the rates of sediment accumulation were high and triggered increased rates of evaporite upward mobilization. While the Viento system discharged large volumes of sand, the crest and flanks of La Popa salt wall maintained pace and were constantly subaerially and/or subaqueous exposed or near the land surface (the diapir was inflated) (Giles and Lawton, 2002; Giles et al., 2004; Giles and Rowan, *in press*). Variation in La Popa weld character along its length may reflect local variation in downbuilding rates. La Popa salt wall became welded with no remnant gypsum between the two sides of the wall in the southeastern diapir-distal area after the cessation of Viento Fm. deposition (Rowan et al., *in press*), as evidence of active diapirism (i.e., exotic diapir-derived detritus) is found within the younger Carroza Formation sandstone beds (Andrie and Giles, 2010; Andrie, 2010).

6.3. Distinguishing delta from estuary deposits

The Viento Formation formed in the shallow-waters of La Popa minibasin during the Paleocene-Eocene (Lawton et al., 2001; Lawton et al., 2009). Both deltas and estuaries form at the shoreline/coastline where freshwaters and seawaters meet and mix. In general, deltas form sand-prone deposits, exhibit a progradational stacking pattern, and are associated with regression periods (Shanley et al., 1992; Willis et al., 1999; Choi et al., 2004; Willis, 2005; Gani and Bhattacharya, 2007). In contrast, estuarine deposits are muddier and dominated by sediments of marine origin, exhibit a retrogradational stacking pattern, and are associated with transgression times when sea level rise drown river valleys (Dalrymple et al., 1992).

Because of the interfingering and overlapping actions of fluvial, tide and waves, deposits attributed to deltaic environments are easy to misinterpret and careful documentation of the physical sedimentary structures of each facies and of the facies association vertical stacking

arrangement is required in distinguishing the dominant processes. The Viento Formation facies exhibit sedimentary structure, external shape, internal composition, and vertical stacking arrangement consistent with deposition in a marginal marine setting. The Viento Formation strata was influenced significantly by the modeling action of fluvial and tide energy, but did not record significant influence by wave currents.

The Viento Formation strata represent an ancient tidally influenced fluvio-deltaic regressive system, characterized by large volumes of sand-rich sediments that stacked progradationally in a setting structurally controlled and influenced by active diapirism. Tides are the main energy source responsible for mixing freshwater and seawaters and for controlling sediment distribution patterns in tidally influenced deltas (Fielding et al., 2005; Olariu and Bhattacharya, 2006). Sedimentary process triggered by tidal influences, especially during periods of reduced discharge, can occur over tens of kilometers distance inland and can significantly affect strata otherwise interpreted as fluvial or shallow marine deposits (Shanley et al., 1992). The prevalent conglomeratic sandstone facies and trough cross-bedded sandstone facies, consisting of medium- to coarse-grained sand, various clasts size composition amalgamated with organic material of terrestrial origin are consistent with a fluvial deltaic system. Ripple-laminated sandstone facies, the inclined heterolithic stratified facies, and the horizontal heterolithic stratified facies, preserve abundant mud laminae mantling ripples or separating beds, which is consistent with deposits of tidally influenced deltas. In addition, abundant mud laminae reflect fluctuations in current velocity and mud fallout during periods of slack water and are regarded as key indicators of tidal settings (Dalrymple and Choi, 2007)

6.4. Comparison between wedge-forming units outcropping in La Popa basin

Due to the combined processes of sediment gravitational subsidence into the mother salt layer and the horizontal compressional forces of the Hidalgoan orogeny, the Viento Fm. exhibits progradational internal lithofacies arrangement, contains metaigneous clasts derived from the diapir, and forms a series of broad wedges locally bound by shallow angular unconformities that stack together and form a Tapered-CHS. Older formations of La Popa basin such as the Muerto Fm., the Delgado Sandstone Member, and the Upper Sandstone Member of the Potrerillos Fm. were deposited in marginal marine settings, exhibit similar siliciclastic lithofacies content and external wedge geometries. Below, in stratigraphic succession, each of these units is compared with the younger fluvio-deltaic wedge forming Viento Fm. deposits.

6.5. Comparison of the Viento Formation with the Muerto Formation

The Muerto Formation of Upper Cretaceous Maastrichtian is exposed in the distal part of the Sierra Madre Oriental foreland, and was studied adjacent to El Gordo diapir and La Popa salt weld in La Popa basin (Hon, 2001; Weislogel and Lawton, 2000). It is separated from the underlying Campanian Parras Shale by a lowstand delta complex interpreted as a forced regression (Weislogel and Lawton, 2000) and is in turn conformably overlying by the Maastrichtian Lower Mudstone Member of the Potrerillos Formation. The Muerto Formation strata represent the first significant, coarse sediment influx, and comprise shelfal/shoreface, tidal, and back-barrier/estuarine lithofacies, accumulated in a prograding lobate to elongate deltaic system of mixed wave and tide energy (Weislogel and Lawton, 2000; Lawton et al., 2001; Lawton et al., 2009). Regionally, the Muerto Formation strata exhibit asymmetric thickness trends: 410 m thick in Sabina basin, 570 m thick at type locality in La Popa basin (McBride et al., 1974), and 1325 m thick in the Parras basin (Weislogel and Lawton, 2000). The Muerto

Formation strata wedges toward both the El Gordo diapir and La Popa salt weld (Weislogel and Lawton, 2000).

Distinctive from the Paleocene/Eocene Viento Formation, the Muerto Formation strata was deposited prior to the initiation of the contractile Hidalgoan orogeny. Thin-skinned folds resulting from Hidalgoan contraction deformed strata that post-date the Muerto Formation. Thickness trends do not vary with respect to the Hidalgoan structures, in contrast, thickness increases proportional with distance from the El Gordo diapir, indicating prolonged vertical gravitational subsidence into the underneath salt layer, subsidence estimated at a rate of 1 m per 1000 years (Weislogel and Lawton, 2000). The Muerto Formation internal lithofacies arrangement and stratal geometries were primarily controlled by the topographic expression of diapirs, by the relationship between sedimentation rates and halokinetic processes and by eustacy (Weislogel and Lawton, 2000; Giles et al., 2004; Giles and Rowan, *in press*). Muerto Fm. strata do not contain metaigneous clasts derived from surface exposure of the evaporite Minas Viejas Fm. in diapiric structures, indicating that salt structures were not exposed at the surface during the deposition of the Muerto Formation. Further, the Muerto Formation strata exposed in the diapir-proximal area do not exhibit dramatic upturning or visible intraformational angular discordances such as those beds present within the Viento Formation adjacent to La Popa salt weld. The lack of metaigneous clasts, internal lithofacies arrangement, thickness trends, and overall geometry of the Muerto Formation indicates that the El Gordo diapir was covered and the net rates of salt rise were relatively low comparative with the net rates of sediment accumulation (Hon, 2001; Weislogel and Lawton, 2000).

6.6. Comparison of the Viento Formation with the Delgado Sandstone Member

The Upper Cretaceous Delgado Sandstone Member of the Potrerillos Fm. forms a ~100 m thick ridge that exhibits lithofacies somewhat similar with those of the Viento Fm. in that sediment was transported by fluvio-deltaic systems from the highlands of the Sierra Madre Oriental and Coahuila Platform. Aschoff and Giles (2005) investigated outcrop exposures of the Delgado Sandstone Member adjacent to El Papalote and El Gordo diapirs. Their results demonstrate that relatively uniform regional sediment dispersal is locally disrupted by diapirism. Stratal thinning initiates at ~1-3 km away from the El Gordo and El Papalote salt stocks, suggesting that the balance between the net rates of salt rise relative to the net rates of sediment accumulation differs from location to location. Similar to the Viento Fm., the Delgado accumulated in depocenters related to diapirism that contain primarily shallow water facies (Aschoff and Giles, 2005). Distinct from the Viento Fm. lithofacies, metaigneous clast extruded from the diapir are not reported to appear within the Delgado Sandstone Member of the Potrerillos Fm., even though Delgado strata were deposited during regional contractile Hidalgoan orogenesis in La Popa basin.

6.7. Comparison between the Viento Formation and the Upper Sandstone Member

The Paleocene Upper Sandstone Member is part of the uppermost unit within the Potrerillos Formation, which is exposed in La Popa basin only within the Carroza, Delgado, and Chaparral synclines. The Upper Sandstone Member overlies the Upper Mudstone Member of the Potrerillos Formation and is turn overlain by the fluvial Adjuntas Formation. Shelley and Lawton (2005) investigated the Upper Sandstone Member adjacent to El Papalote diapir and concluded that diapirism, regional Hidalgoan shortening, and deposition were simultaneous and complexly interrelated.

Similar to the younger Viento Formation, the Uppers Sandstone Member exhibits high sand to mud ratio content. Primary sedimentary structures include trough cross bedding, wave ripple laminations, current ripples cross laminations, and planar laminations, along with *Ophiomorpha* burrows and oyster shells, consistent with deposition in a delta setting dominated by wave and tide processes. The coarser fraction of the Upper Sandstone Member deposits consists of extrabasinal chert pebbly conglomerates sourced from the Sierra Madre Oriental and Coahuila Platform to southwest, which also supplied sediment to the Viento deltaic system (Shelley and Lawton, 2005). The Uppers Sandstone Member represents a regressive siliciclastic succession of marginal marine/deltaic deposits (McBride et al., 1974) consisting of six system tracts that record three successive fourth-order eustatic cycles (Shelley and Lawton, 2005). The Uppers Sandstone Member like the Viento Formation represents a prograding deltaic system confined within the Carroza syncline.

Distinctive from the Viento Formation, metaigneous clast were not reported being present within the Upper Sandstone Member, indicating that the El Papalote diapir was covered by sediment. Additionally, the Upper Sandstone Member of the Potrerillos Formation formed a thin siliciclastic deposit comparative to the Viento Formation deposit. Overall, during the deposition of the Upper Sandstone Member the net rate of sediment accumulation was higher relative to the net rate of evaporite rise. The lack of metaigneous clast also suggests that the regional contractile events of the Hidalgoan orogeny were relatively insignificant during the time of the Upper Sandstone Member deposition comparative with the times of the Viento Formation deposition. However, unconformity-bounded strata of the Upper Sandstone Member onlap the El Gordo anticline and suggest syndepositional folding.

6.8. Lateral compression influence on generating wedge-geometries halokinesis

Comparing the Viento Formation strata geometries that formed under both halokinesis and compression processes, with older strata of La Popa basin that exhibit wedge-geometries but formed under halokinesis alone, resulted few similarities and discrepancies. In general, strata affected by pure passive diapirism is deformed only locally with 1-2 km in the proximity of the diapir, strata wedge broadly toward the salt stock, internal beds bounded by shallow angle unconformities onlap one another and the diapir, and the coarser-grained lithofacies tend to accumulate toward the center of the basin. Strata that is deposited adjacent to salt stocks in settings undergoing active shortening pulses (such as the Viento Formation deposited in La Popa basin during the Hidalgoan orogeny), record in the lithofacies composition and geometries the influence of compressional pulses in addition to downbuilding. For example, the Viento Formation beds onlap one another at shallow angles unconformities, but at the contact with the salt stock beds dip vertically or are slightly upturned and locally may preserve faults. Also, deposits accumulated under both halokinesis and compression tend to form thicker deposits. The timing of deposition, halokinesis and shortening play a tremendous role in shaping the external-geometries and internal composition of stratal accumulation at both regional and local scale and determine to form, specific with the conditions on each case, wedge-shaped strata or J-hook shaped strata or a combination of the two.

CHAPTER 7 – CONCLUSIONS

This work is the first detailed lithologic investigation and interpretation of the Viento Formation as deposited alongside La Popa salt wall and weld in La Popa minibasin, Mexico. The results of this research aid in understanding the geologic history of the La Popa minibasin. In addition, this work has significant implication for hydrocarbon exploration by defining bed geometries and facies relationship. The Viento Formation outcrops serve as excellent analogues for other salt basins where the resolution of subsurface data cannot define the complex internal stratigraphic arrangement of the salt-related sequences.

Seventeen facies were identified and interpreted to represent environments associated within a prograding fluvio-deltaic tide-influenced delta system, and include non-marine, marginal marine and marine deposits. Deposits shallow upward and form a regressive system characterized by prevailing non-marine and marginal marine deposits. Overall, Viento Formation records a lateral significant decrease in thickness from ~900 m to pinch out, form a series of five wedges that stack stratigraphycally, are locally bounded by ~15° angular unconformities that become conformable within tens of meters away from the salt wall, and together form a Tapered - CHS. Viento beds flatten out in the basin (~30° dipping) but dip vertically to slightly overturn at the salt wall. Sandstone with metaigneous clast appear abundantly through the sequences indicating that La Popa salt wall was continuously exposed at or near the surface for the entire duration of Viento Formation deposition. Sandstone with metaigneous clast correlate across study area indicate an inflated diapir due to pulses of the regional contractile Hidalgoan orogeny additionally to halokinesis, while the more narrow extent of such beds is interpreted to reflect local effects of downbuilding.

REFERENCES

Anderson Brian G. and Droser Marry L., 1998, Ichnofabrics and geometric configurations of Ophiomorpha within a sequence stratigraphic framework: an example from the Upper Cretaceous US western interior, in Sedimentology, v. 45, pg. 379-396.

Andrie Joseph and Giles Katherine, 2010, Halokinetic sequence stratigraphy and structural geometry of the Eocene Fluvial Carroza Formation along the La Popa salt weld, La Popa basin, Mexico, AAPG ACE, Abstracts with Programs, New Orleans, LA.

Andrie Joseph, 2010, Halokinetic sequence stratigraphy and structural geometry of the Eocene Fluvial Carroza Formation along the La Popa salt weld, La Popa basin, Mexico, [M.S thesis]: New Mexico State University, 110 pg.

Aschoff L. Jennifer and Giles A. Katherine, 2005, Salt diapir-influenced, shallow-marine sediment dispersal patterns: Insights from outcrop analogs, in AAPG Bulletin, v. 89, no. 4, pg. 447-469.

Aschoff L. Jennifer and Schmitt G. James, 2008, Distinguishing syntectonic unconformity types to enhance analysis of growth strata: an example from the Cretaceous, southeastern Nevada, USA, in Journal of Sedimentary Research, v. 78, pg. 608-623.

Bhattacharya, J.P., and Giosan, L., 2003, Wave-influenced deltas: geomorphological implications for facies reconstruction: Sedimentology, v. 50, pg. 187-210.

Bhattacharya, J.P., and MacEachern, J.A., 2009, Hyperpycnal rivers and prodeltaic shelves in the Cretaceous seaway of North America: Journal of Sedimentary Research, v. 79, pg. 184-209.

Bhattacharya, J.P., and Walker, R.G., 1992, Deltas, in Walker, R.G., and James, N.P., eds., Facies Models: Response to Sea Level Change: St. John's, Newfoundland, Geological Association of Canada, pg. 157-177.

Bhattacharya, J.P., and Willis, B.J., 2001, Lowstand deltas in the Frontier Formation, Powder River Basin, Wyoming: implications for sequence stratigraphic models: AAPG Bulletin, v. 85, pg. 261-294.

Buatois A. Luis, Santiago Nubia, Parra Kaolu, and Steel Ron, 2008, Animal-substrate interactions in an Early Miocene Wave-Dominated tropical delta: delineating environmental stresses and depositional dynamics (Tacata field, eastern Venzuela), in Journal of Sedimentary Research, v. 78, pg. 458-479.

Buck J. Brenda, Lawton F. Timothy and Brock L. Amy, 2009, Evaporitic paleosols in continental strata of the Carroza Formation, La Popa basin, Mexico: Record of Paleogene climate and salt tectonics, in GSA Bulletin, 30089, pg. 1-16.

Carmona B. Noelia, Buatois A. Luis, Ponce J. Juan, Mangano G. Maria, 2009, Ichnology and sedimentology of a tide-influenced delta, Lower Miocene Chenque Formation, Patagonia, Argentina: Trace-fossil distribution and response to environmental stresses, in Palaeogeography, Palaeoclimatology, Palaeocology, v. 273, pg. 75-86.

Catuneanu O., Bhattacharya J. P., Blum M. D., Dalrymple R. W., Eriksson P. G., Fielding C. R., Fisher W. L., Galloway W. E., Gianolla P., Gibling M. R., Giles K. A., Holbrook J. M., Jordan R., Kendall C. G. St., Macurda B., Martinsen O. J., Miall A. D., Nummendal D., Posamentier H. W., Pratt B. R., Shanley K. W., Steel R. J., Strasser A., and Tucker M. E., 2010, Sequence stratigraphy: common ground after three decades of development, in First Break, Stratigraphy, v. 28, pg. 21-34.

Catuneanu Octavian, 2002, Sequence stratigraphy of clastic systems: concepts, merits, and pitfalls, in Journal of African Earth Sciences, v. 35, pg. 1-43.

Choi S. Kyung, Dalrymple W. Robert, Chun S. Seung, and Kim P. Seong, 2004, Sedimentology of modern, Inclined Heterolithic Stratification (IHS) in the macrotidal Han River delta, Korea, in Journal of Sedimentary Research, v. 74, no. 5, pg. 677-689.

Coughenour L. Christopher, Archer W. Allen and Lacovara J. Kenneth, 2009, Tides, tidalites, and secular changes in the Earth-Moon system, in Earth-Sciences Reviews, v. 97, pg. 59-79.

Dalrymple, R.W., and Choi, K., 2007, Morphologic and facies trends through the fluvial–marine transition in tide-dominated depositional systems: a schematic framework for environmental and sequence-stratigraphic interpretation: Earth-Science Reviews, v. 81, pg. 135-174.

Dalrymple, R.W., Zaitlin, B.A., and Boyd, R., 1992, Estuarine facies models: conceptual basin and stratigraphic implications: Journal of Sedimentary Petrology, v. 62, pg. 1130-1146.

Dickinson R. William and Lawton F. Timothy, 2001, Carboniferous to Cretaceous assembly and fragmentation of Mexico, in GSA Bulletin, v. 113, no. 9, pg. 1142-1160.

Embry, Ashton F., 1993, Transgressive – Regressive (T – R) sequence analysis of the Jurassic succession of the Sverdrup Basin, Canadian Arctic Archipelago, Canadian Journal of Earth Sciences, v. 30, pg. 301-320.

Embry, Ashton F., 2002, Transgressive-Regressive (T-R) Sequence Stratigraphy, 22nd Annual Gulf Coast Section SEPM Foundation Bob F. Perkins Research Conference, pg. 151–172.

Emery Dominic and Keith Myres, 1996, Sequence stratigraphy, in Blackwell Science Ltd., London, pg. 297.

Fielding C.R., Trueman J.D., and Alexander J., 2005a, Sharp-based, flood dominated mouth bar sands from the Burdekin River Delta of northeastern Australia: extending the spectrum of mouth bar facies, geometry, and stacking patterns: Journal of Sedimentary Research, v. 75, pg. 55–66.

Fielding R. Christopher, 2010, Planform and facies variability in asymmetric deltas: facies analysis and depositional architecture of the Turonian Ferron sandstone in the western Henry Mountains, south-central Utah, USA, in Journal of Sedimentary Research, v. 80, pg. 455-479.

Fischer P. Mark, Higuera-Diaz I. Camilo, Evans A. Mark, Perry C. Eugene and Lefticariu Liliana, 2009, Fracture-controlled paleohydrology in a map-scale detachment fold: Insights from the analysis of fluid inclusions in calcite and quartz veins, in Journal of Structural Geology v. 31, pg. 1490-1510.

Gani, M.R., and Bhattacharya, J.P., 2007, Basic building blocks and process variability of a Cretaceous delta: internal facies architecture reveals a more dynamic interaction of river, wave, and tidal processes than is indicated by external shape: Journal of Sedimentary Research, v. 77, pg. 284-302.

Garrison, J.M., and McMillan, N.J., 1999, Evidence for Jurassic continental rift magmatism in northeast Mexico: Allogenic meta-igneous blocks in El Papalote diapir, La Popa basin, Nuevo Leon, Mexico, in Bartolini, C., Wilson, J.L., and Lawton, T.F., eds., Mesozoic sedimentary and tectonic history of north-central Mexico: Boulder, Colorado, GSA Special Paper 340, pg. 319-332.

Giles A. Katherine and Lawton F. Timothy, 1999, Attributes and evolution of an exhumed salt weld, La Popa basin, northeastern Mexico, in Geology, v. 27, no. 4, pg. 323-326.

Giles A. Katherine and Lawton F. Timothy, 2002, Halokinetic sequence stratigraphy adjacent to the El Papalote diapir, northeastern Mexico, in AAPG Bulletin, v. 86, no. 5, pg. 823-840.

Giles, K., Lawton, T., and Rowan, M., 2008, Institute of Tectonic Studies, Las Cruces, NM, La Popa basin field guide, pg. 129.

Giles, K.A., and Rowan, M.G., *in press*, Concepts in halokinetic-sequence deformation and stratigraphy. Geological Society of London Special Publication – Salt, Sediment, and Prospectivity annual conference proceedings January 20-22, *in press.*

Giles, K.A., Lawton, T.F., & Rowan, M.G. 2004. Summary of halokinetic sequences stratigraphy from outcrop studies of La Popa salt basin, northeastern Mexico; GCS-SEPM 2004 Conference Proceedings.

Goldhammer, R.K., 1999, Mesozoic sequence stratigraphy and paleogeographic evolution of northeast Mexico: Geologic Society of America Special Paper 340, pg. 1-58.

Gray, G. G., R. J. Pottorf, D. A. Yurewicz, K. I. Mahon, D. R. Pevear, and R. J. Chuchla, 2001, Thermal and chronological record of syn- and post-Laramide burial and exhumation, Sierra Madre Oriental, Mexico, in C. Bartolini, R. T. Buffler, and A. Cantu-Chapa, eds., The western Gulf of Mexico Basin: Tectonics, sedimentary basins, and petroleum systems: AAPG Memoir 75, pg. 159–181.

Haq, B.U., Hardenbol, J., and Vail, P.R., 1988, Mesozoic and Cenozoic Chronostratigraphy and Cycles of Sea-Level Change: Sea-Level Changes, An Integral Approach, SEPM Special Publication No. 42, pg. 71-108.

Hon, K.D. 2001. Salt-influenced growth-stratal geometries and structure of the Muerto Formation adjacent to an ancient secondary salt weld, La Popa Basin Nuevo Leon, Mexico. [M.S thesis]: New Mexico State University, 97 pg.

Hudec R. Michael and Jackson P. A. Martin, 2006, Advance of allochthonous salt sheets in passive margins and orogens, in AAPG Bulletin, v. 90, no. 10, pg. 1535-1564.

Hudson M. Samuel and Hanson D. Andrew, 2010, Thermal maturation and hydrocarbon migration within La Popa basin, northeast Mexico, with implications for other salt structures, in AAPG Bulletin, v. 94, no. 3, pg. 273-291.

Instituto nacional de estadistica geografia e informatica Mexico, 1996, Carta Topografica 1:50,000 San Jose de la Popa, Nuevo Leon y Coahuila, G14A84, secunda impresion.

Jackson P. A. Martin and Talbot C. J., 1991, A glossary of salt tectonics, in Geological Circular 91-4, 44 pg.

Jackson P. A. Martin, Vendeville C. Bruno, and Schulz-Ela D.D., 1994, Salt-related structures in the Gulf of Mexico: A field guide for geophysicists, in The Leading Edge, pg. 837-842.

Kroeger F. Karsten and Stinnesbeck Wolfgang, 2003, The Minas Viejas Formation (Oxfordian) in the Area of Galeana, Northeastern Mexico: Significance of Syndepositional Volcanism and Related Barite Genesis in the Sierra Madre Oriental, in C. Bartolini, R. T. Buffler and J. Blickwede, eds., The Circum-Gulf of Mexico and the Caribbean: Hydrocarbon habitats, basin formation, and plate tectonics: AAPG Memoir 79, pg. 515-528.

Latta K. Diana, Anastasio J. David, 2007, Multiple scales of mechanical stratification and decollement fold kinematics, Sierra Madre Oriental foreland, northeast Mexico, in Journal of Structural Geology, v. 29, pg. 1241-1255.

Lawton F. Timothy and Buck J. Brenda, 2006, Implications of diapir-derived detritus and gypsic paleosols in Lower Triasic strata near the Castle Valley salt wall, Paradox Basin, Utah, in GSA Bulletin, v. 34, no. 10, pg. 885-888.

Lawton F. Timothy and Rowan G. Mark, 2008, Style and timing of Laramide deformation in northeastern Mexico, GSA Abstracts with Programs, v. 40, no. 6, pg. 546.

Lawton F. Timothy, Bradford A. Ira, Vega J. Francisco, Gehrels E. George, and Amato M. Jeffrey, 2009, Provenance of the Upper Cretaceous-Paleogene sandstones in the foreland basin system of the Sierra Madre Oriental, northeastern Mexico, and its bearing on fluvial dispersal systems of the Mexican Laramide Province, in GSA Bulletin, v. 121, pg. 820-836.

Lawton F. Timothy, Vega J. Francisco, Giles A. Katherine and Rosales-Dominguez Carmen, 2001, Stratigraphy and origin of the La Popa basin, Nuevo Leon and Coahuila, Mexico, in C. Bartolini, R. T. Buffler and A. Cantu-Chapa, eds., The western Gulf of Mexico

basin: Tectonics, sedimentary basins, and petroleum systems, AAPG Memoir 75, pg. 219-240.

Lawton, T.F., and Giles, K.A., 1997, Field Guide to El Papalote Diapir *in* Soegaard, K., Giles, K.A., Vega, F.J., and Lawton, T.F., (eds.), Structure, stratigraphy, and paleontology of Late-Cretaceous-Early Tertiary Parras-La Popa foreland basin near Monterrey, northeastern Mexico, AAPG Field Trip 10, p. 55-73.

Lee Keumsuk, McMechan A. George, Gani M. Royhan, Bhattacharya P. Janok, Zeng Xiaoxian, and Howell D. Charles Jr., 2007, 3-D architecture and sequence stratigraphic evolution of a forced regression top-truncated mixed-influenced delta, Cretaceous Wall Creek Sandstone, Wyoming, USA, in Journal of Sedimentary Research, v. 77, pg. 303-323.

Leleu Sophie, Hartley J. Adrian, and Williams P. J. Brian, 2009, Large-scale alluvial architecture and correlations in a Triassic pebbly braided river system, Lower Wolfville Formation (Fundy Basin, Nova Scotia, Canada), in Journal of Sedimentary Research, v. 79, pg. 265-286.

MacEachern J.A., and Gingras, M.K., 2008, Recognition of brackish-water trace fossil suites in the Cretaceous Western Interior Seaway of Alberta, Canada, in Bromley, R.G., Buatois, L.A., Ma´ngano, M.G., Genise, J.F., and Melchor, R.N., eds., Sediment-Organism Interactions: A Multifaceted Ichnology: Society for Sedimentary Geology Special Publication, v. 89, pg. 149–194.

MacEachern J.A., Bann K.L., Bhattacharya J.P., and Howell, C.D., JR., 2005, Ichnology of deltas: Organism responses to the dynamic interplay of rivers, waves, storms, and tides, in Giosan, L., and Bhattacharya, J.P., eds., River Deltas— Concepts, Models, and Examples: Society for Sedimentary Geology Special Publication, v. 83, pg. 49–85.

Matthews J. Wendy, Hampson J. Gary, Trudgill D. Bruce, and Underhill R. John, 2007, Controls on the fluviolacustrine reservoir distribution and architecture in passive salt-diapir provinces: Insights from outcrop analogs, in AAPG Bulletin, v. 91, no. 10, pg. 1367-1403.

McBride, E. F., A. E. Weidie, J. A. Wollenben and R. C. Laudon, 1974, Stratigraphy and structures of the Parras and La Popa basins, northeastern Mexico, in GSA Bulletin, v. 84, pg. 1603-1622.

Miall A.D., 1985, Architectural-element analysis: a new method of facies analysis applied to fluvial deposits: Earth Science Reviews, v. 22, pg. 261–308.

Millan-Garrido Hector, 2004, Geometry and kinematics of compressional growth structures and diapirs in the La Popa basin of northeast Mexico: Insights from sequential restoration of a regional cross-section and three-dimensional analysis, in Tectonics, v. 23, TC5011, pg. 1-21.

Olariu C., and Bhattacharya, J.P., 2006, Terminal distributary channels and delta front architecture of river-dominated delta systems: Journal of Sedimentary Research, v. 76, pg. 212–233.

Pattison A. J. Simon, 1995, Sequence Stratigraphic Significance of Sharp-Based Lowstand Shoreface Deposits, Kenilworth Member, Book Cliffs, Utah, AAPG Bulletin, v. 79, No. 3, pg. 444–462.

Perrilliat, M.C., Vega, F.J., Espinosa, B., and Naranfo-Garcia , E., 2008, Late Cretaceous and Paleogene freshwater gastropods from northeastern Mexico: Journal of Paleontology, v. 82, pg. 255–266, doi: 10.1666/06-062.1.

Ponten Anna and Plink-Bjorklund Piret, 2007, Depositional environments in an extensive tide-influenced delta plain, Middle Devonian Gauja Formation, Devonian Baltic basin, in Sedimentology, v. 54, pg. 969-1006.

Portenga W. Eric and Bierman R. Paul, 2011, Understanding Earth's eroding surface with ^{10}Be, in GSA Today, v. 21, no 8, pg. 4-10.

Posamentier, H. W., G. P. Allen, 1999, Siliciclastic sequence stratigraphy: Concepts and applications: SEPM Concepts in Sedimentology and Paleontology 7, 210 pg.

Posamentier, H. W., G. P. Allen, D. P. James, and M. Tesson, 1992, Forced regressions in a sequence-stratigraphic framework: Concepts, examples and exploration significance: AAPG Bulletin, v. 76, pg. 1687–1709.

Rowan G. Mark and Vendeville C. Bruno, 2006, Foldbelts with early salt withdrawal and diapirism: Physical model and examples from the northern Gulf of Mexico and the Flinders Ranges, Australia, in Marine and Petroleum Geology, v. 23, pg. 871-891.

Rowan G. Mark, Lawton F. Timothy, and Giles A. Katherine, *in press*, Anatomy of an exposed vertical salt weld flanking strata, La Popa basin, Mexico, in Geological Society, London, *in press.*

Rowan G. Mark, Lawton F. Timothy, Giles A. Katherine, and Ratliff A. Robert, 2003, Near-salt deformation in La Popa basin, Mexico, and the northern Gulf of Mexico: A general model for passive diapirism, in AAPG Bulletin v. 87, no. 5, pg. 733-756.

Rowan, M. G., Peel, F. J. & Vendeville, B. C. 2004. Gravity-driven foldbelts on passive margins. *In*: McClay, K.R. (ed) *Thrust Tectonics and Hydrocarbon Systems*. AAPG Memoir, 82, 157-182.

Shanley W. Keith, McCabe J. Peter, and Hettinger D. Robert, 1992, Tidal Influence in Cretaceous fluvial strata from Utah, USA: a key to sequence stratigraphic interpretation, Sedimentology, v. 39, pg. 905-930.

Shanmugam G., 2000, 50 years of the turbidite paradigm (1950's-1990's): deep-water processes and facies models – a critical perspective, Marine and Petroleum Geology v. 17, pg. 285–342.

Shelley D. C. and Lawton T. F., 2005, Sequence stratigraphy of tidally influenced deposits in a salt-withdrawal minibasin: Upper sandstone member of the Potrerillos Formation (Paleocene), La Popa basin, Mexico, in AAPG Bulletin, v. 89, no. 9, pg. 1157-1179.

Soegaard K., Ye H., Halik N., Daniels A. T., Arney J. and Garrick S., 2003, Stratigraphic evolution of the Latest Cretaceous to Early Tertiary Difunta foreland basin in northeastern Mexico: Influence of salt withdrawal on tectonically induced subsidence by the Sierra Madre Oriental fold and thrust belt, in C. Bartolini, R. T. Buffler and J. Blickwede, eds., The Circum-Gulf of Mexico and the Caribbean: Hydrocarbon habitats, basin formation, and plate tectonics: AAPG Memoir 79, pg. 364-394 .

Vail, P.R., Mitchum Jr., R.M., Thompson III, S., 1977. Seismic stratigraphy and global changes of sea level. Part 3: relative changes of sea level from coastal onlap. In: Payton, C.E. (Ed.), Seismic Stratigraphy—Applications to Hydrocarbon Exploration, vol. 26. American Association of Petroleum Geologists Memoir, pg. 63–81.

Vakarelov K. Boyan and Bhattacharya P. Janok, 2009, Local tectonic control on parasequence architecture: Second Frontier sandstone, Powder River basin, Wyoming, in AAPG Bulletin, v. 93, no. 3, pg. 295-327.

Van Wagoner, J. C., Bertram, G. T., (Eds.), 1995, Sequence stratigraphy of foreland basin deposits, v. 64, AAPG Memoir, pg. 487.

Vega, F.J., and Perrilliat, M., 1989b, La presencia del Eoceno marino en la cuenca de la Popa (Grupo Difunta),Nuevo León: Orogenia post-Ypresiana: Universidad Nacional Autonóma de México, Instituto de Geología: Revista, v. 8, pg. 67–70.

Vega, F.J., and Perrilliat, M.C., 1989a, On a new species of *Venecardia* from the lower Eocene in northeastern Mexico (Difunta Group): Tulane Studies in Geology and Paleontology, v. 22, pg. 101–106.

Vega, F.J., and Perrilliat, M.C., 1992, Freshwater gastropods from the lower Eocene Difunta Group, northeastern Mexico: Journal of Paleontology, v. 66, pg. 603–609.

Vega, F.J., Perrilliat, M.C., Duarte-Torres, L., Durán-Herrera , G., Rivas-García, R., Aguilar-Piña, M., and Ventura, J.F., 2007, Eocene strata from Sabinas basin and their bearing in sedimentary basin correlation in NE Mexico: Boletín de la Sociedad Geológica Mexicana,v. 59, pg. 115–123.

Vendeville C. Bruno, 2005, Salt tectonics driven by sediment progradation: Part I – Mechanics and kinematics, in AAPG Bulletin, v. 89, no. 8, pg. 1071-1079.

Vendeville, B. C. and Jackson, M. P. A. 1992. The rise of diapirs during thin-skinned extension. *Marine and Petroleum Geology*, 9, 331-353.

Vendeville, B. C. and Nilsen, K. T. 1995. Episodic growth of salt diapirs driven by horizontal shortening. *In*: Travis, C. J., Harrison, H., Hudec, M. R., Vendeville, B. C., Peel, F. J. & Perkins, B. F. (eds) *Salt, Sediment, and Hydrocarbons*. Society of Economic and Paleontologists and Mineralogists, Gulf Coast Section, 16th Annual Research Foundation Conference, 285-295.

Verges J., Marzo M., and Munoz J. A., 2002, Growth strata in foreland settings, in Sedimentary Geology, v. 146, pg. 1-9.

Warren K. John, 2010, Evaporites through time: Tectonic, climatic and eustatic controls in marine and nonmarine deposits, in Earth-Sciences Reviews, v. 98, pg. 217-268.

Weislogel L. Amy and Lawton F. Timothy, 2000, Diapir-flanking facies assemblages and stratal geometries within the tidally influenced deltaic system of the Maastrichtian Muerto Formation, La Popa basin, northeastern Mexico: An analogue for the Gulf of Mexico subsurface, in GSAGS Transactions, v. L, pg. 669-678.

Willis B. J., 2005, Deposits of tide-influenced river deltas, in Giosan, L., and Bhattacharya, J.P., eds., River Deltas: Concepts, Models, and Examples: SEPM, Special Publication 83, pg. 87–129.

Willis, B.J., Bhattacharya, J.B., Gabel, S.L., and White, C.D., 1999, Architecture of a tide-influenced river delta in the Frontier Formation of central Wyoming, USA: Sedimentology, v. 46, pg. 667–688.
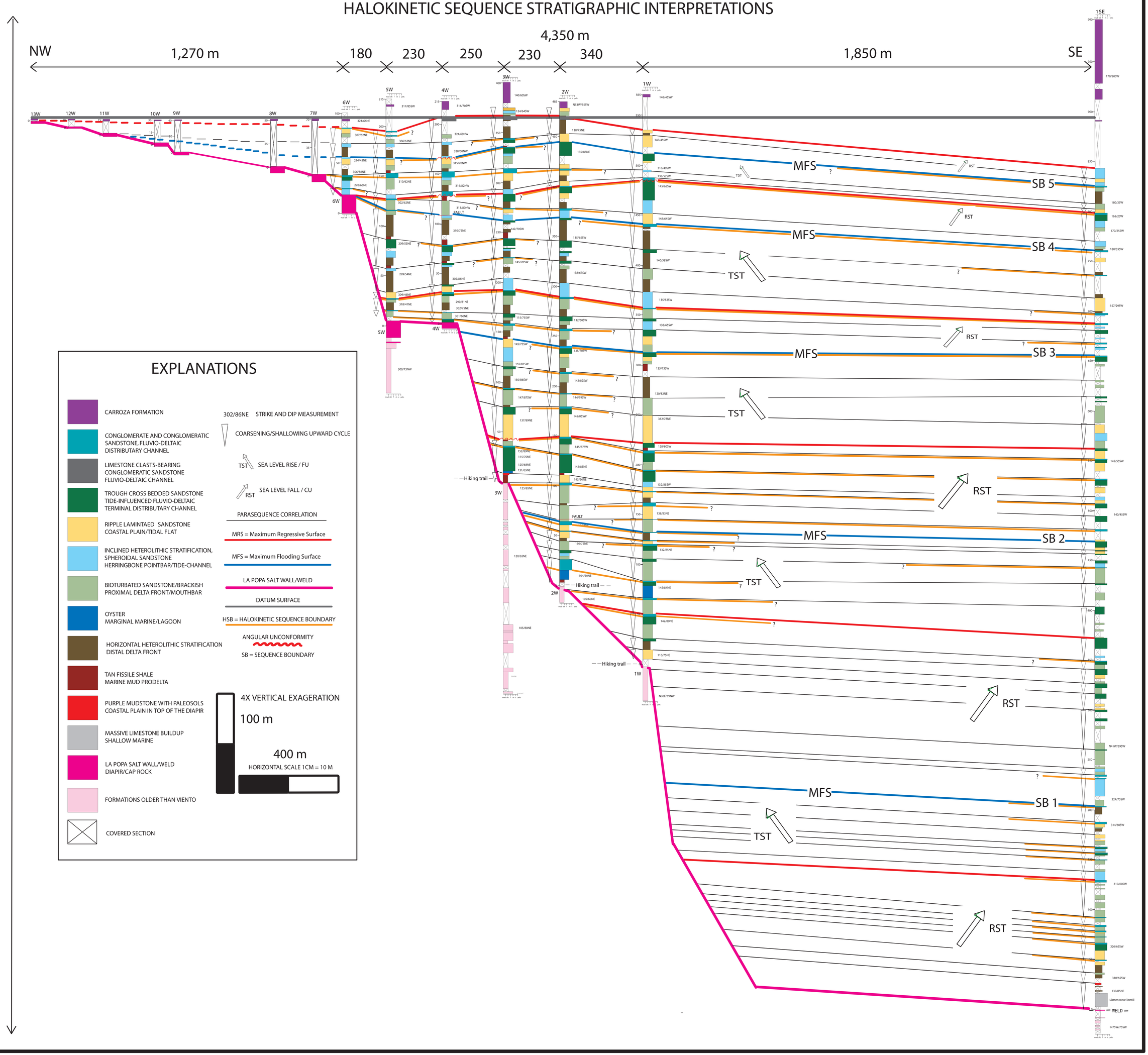
APPENDIX 1. VIENTO FORMATION MEASURED SECTIONS WITHIN THE BEND OF LA POPA SALT WALL/WELD, HALOKINETIC SEQUENCE STRATIGRAPHIC INTERPRETATIONS